Diogo Alexandre Fialho de Almeida

Mestrado em Engenharia Física

The role of electron transfer in DNA building blocks: evaluation of strand breaks and their implications

Dissertação para obtenção do Grau de Doutor em Engenharia Física

Orientador: Prof. Doutor Paulo Manuel Assis Loureiro Limão-Vieira, Professor Associado com Agregação, Faculdade de Ciências e Tecnologia da Universidade Nova de Lisboa

Júri:

Presidente: Prof. Doutor Fernando Pina
Arguente(s): Prof. Doutor Pedro Tavares
Prof. Doutor Oddur Ingólfsson

Vogais: Prof. Doutor António Varandas
Prof. Doutor Gustavo García
Prof. Doutor Antonio Aguillar
Prof. Doutor Paulo Limão-Vieira
Doutor Filipe Ferreira da Silva

FACULDADE DE CIÊNCIAS E TECNOLOGIA
UNIVERSIDADE NOVA DE LISBOA

Novembro 2013

Acknowledgements:

Prof. Dr. Paulo Limão-Vieira for his constant supervision, encouragement and availability throughout the course of this work, as well as for the opportunity to visit other international groups and attend several scientific meetings, from which I have learned a great deal.

Prof. Dr. Gustavo García for his invaluable support and expertise, Dr. Samuel Eden for his always friendly and available help and Dr. Filipe Ferreira da Silva for his candid and reassuring support through several stages of this thesis.

All of the remaining members of the Molecular Physics and applications research group, particularly Drª Susana Sério, Juscelino Ferreira. Prof. João Lourenço for his support and soothing advisement. Ana Cruz for the always available help and patience.

FCT/MCTES for the SFRH/BD/61645/2009 scholarship and to the several international collaboration networks EIPAM, ECCL, NANO-IBCT that over the years provided me with financial support for the several STSM's. To the Department of Physics of the New University of Lisbon and CEFITEC for providing me with the necessary working conditions.

Martina Fuss and Ana Sanz for their hospitality at the IFF, CSIC, Madrid, and Prof. Robert McCullough for his hospitality at the Centre for Plasma Physics at Queen's University Belfast.

On a more personal note, Rodrigo Antunes, Mauro Guerra, Rui Pinto, and Diana Guimarães for their much-valued and deeply thankful friendship and companionship throughout the last decade, as well as for the several unique episodes that will forever be remembered. Thumbs up, guys!

Cláudio Ribeiro and Julia Blanco for their very special and stimulating companionship and support. Shine on, you crazy diamonds.

Rita Ralha, Isa Matos (and the rest of the Matos family), Gonçalo Martins and Margarida Coelho for their much-appreciated friendship and patience, despite everything... José Samões and Rui Pedro for their availability and presence.

My family, in particular to Carla Simões, and other dear friends.

Finally, my dedicated parents, Maria João and Mário Almeida, for their unconditional and ever-present support. I lack the words to quantify the feeling of indebtness that I feel towards you.

Abstract:

Radiation-induced damage to biological systems, both direct and indirect processes, has increasingly come under scrutiny by the international scientific community due to recent findings that electrons are a very effective agent in damaging DNA/RNA. Indeed, much remains to be discovered regarding the exact physico-chemical processes that occur in the nascent stages of DNA/RNA damage by incident radiation. However, it is also known that electrons do not exist freely in the physiological medium, but rather solvated and/or pre-solvated states. This leads to the need for new techniques that can better explore the damaging role of "bound" electrons to DNA/RNA.

The work presented in this thesis consists on the study of electron transfer in collisions of atomic species with molecules of biological relevance. In order to study these processes, two experimental setups were used. One setup consists of a crossed beam experiment where a neutral potassium beam is created and made to collide with an effusive molecular target beam. The anionic products that stem from electron transfer in potassium atom to the molecular target collisions are then extracted and time-of-flight (TOF) mass analysed. In the second setup a beam of anionic species is formed and made to collide with a molecular target. Collisions with three different anionic beams were performed (H^-, O^- and OH^-), as well as with different simple organic molecules, by measuring the positive and negative ion fragmentation patterns with a quadrupole mass spectrometer (QMS). A comparison between these two collisional systems can greatly help to understand the underlying mechanisms of the electron transfer processes. Finally, studies of potassium collisions with sugar surrogates D-Ribose and THF were performed. These studies show very different fragmentation patterns from DEA, although in the case of THF, it is suggested that the initially accessed states are the same as in DEA.

With these studies was also possible to show for the first time collision induced site and bond selectivity breaking, where the electron is transferred into a given state of the acceptor molecule and the resulting fragmentation pathways are exclusive to the initial anionic state. Furthermore, the role of the potassium cation *post collision*was explored and indeed its presence is suggested to induce at least partial suppression of auto-detachment. The implications that ensue from this degradation are analysed in the light of the obtained fragmentation patterns.

Keywords: Electron transfer, Negative ion formation, time-of-flight mass spectrometry, atom-molecule collisions, DNA sugar unit.

Resumo:

Processos directos e indirectos de dano em sistemas biológicos causados por radiação incidente têm vindo gradualmente a ser apontados pela comunidade científica internacional como agentes altamente eficientes no que diz respeito à criação de quebras simples e duplas na estrutura do ADN/ARN. Em particular, electrões criados como produto secundário destes processos têm vindo a revelar-se especialmente eficazes nos porcessos de decomposição a nível molecular. No entanto, é sabido que no meio fisiológico, não existem electrões livres, mas sim tipicamente em estados (pré-)solvatados. Assim, o uso de novas técnicas no estudo da interacção de electrões provenientes de uma espécie dadora com o meio fisiológico, mais particularmente com o ADN/ARN, tem-se vindo a revelar de uma importância crítica nos últimos anos em especial no conhecimento dos mecanismos a nível molecular.

O trabalho apresentado nesta tese consiste no estudo de processos de transferência de electrão em colisões de espécies atómicas com moléculas de interesse biológico. De forma a estudar experimentalmente estes processos, foram usados dois sistemas experimentais. Um dos sistemas usa uma geometria de feixes cruzados onde um feixe de átomos neutros de potássio colide com um feixe efusivo da molécula alvo. Os produtos aniónicos que resultam da transferência de electrão que ocorre durante a colisão são então extraídos e analisados recorrendo a um espectrómetro de massa do tipo tempo de voo (TOF). No segundo sistema experimental é criado um feixe de espécies aniónicas e os produtos iónicos resultantes (aniónicos e catiónicos) são extraídos e analisados por um espectrómetro de massa tipo quadrupólo. A comparação destes dois sistemas de colisão pode dar respostas muito relevantes quanto aos mecanismos moleculares subjacentes ao processo de transferência de electrão.

No decorrer do trabalho apresentado nesta tese, deu-se especial ênfase ao estudo de processos dissociativos de selectividade quanto à posição e ligação química. Estes mecanismos foram pela primeira vez estudados por colisões átomo-molécula. Adicionalmente, este mesmo conjunto de medidas permitiu investigar o papel do potássio catiónico após este ter cedido o seu electrão no decorrer da colisão. De facto, a presença deste catião altera significativamente os decaímentos de fragmentação devido à sua capacidade de supressão (total ou parcial) de processos de auto-ionização do anião molecular. De seguida, procedeu-se ao estudo de colisões de espécie aniónicas com moléculas de interesse biológico. Por fim, as medidas relativas aos substitutos da unidade de açúcar do ADN/ARN, D-ribose e THF, mostram perfis de fragmentação significativamente diferentes quando comparados com os de captura electrónica dissociativa. As implicações que podem decorrer da degradação destes compostos foram analisadas à luz dos padrões de fragmentação obtidos.

Palavras-chave: Transferência de electrões, formação de iões negativos, espectrometria de tempo de voo, colisões átomo-molécula.

Contents

Acknowledgements: ..... **IV**

Abstract: ..... **VI**

Resumo: ..... **VIII**

Contents ..... **IX**

Figures ..... **XI**

Tables ..... **XIV**

Acronyms and symbols ..... **XV**

1. Introduction **1**

1.1. Radiation damage to biological tissue: **1**

1.2. Indirect DNA damage by electrons (dissociative electron attachment): **2**

1.3. DNA damage by electron transfer: **5**

2. Theory of electron transfer in Atom-molecule Collisions **9**

2.1. Atom-Atom collisions: **9**

2.2. Atom-molecule collisions: **15**

3. Experimental setups **19**

3.1 Neutral atom collisions experimental setup: **19**

3.1.1. Projectile beam: 21

3.1.2. Langmuir-Taylor surface detector: 22

3.1.3. Molecular target oven: 23

3.1.4. TOF mass spectrometer: 24

3.2. Anion-molecule collision experimental setup: **28**

3.2.1. Anion formation source: 28

3.2.2 Anion beam mass selection and focusing: 28

3.2.3 Interaction region and quadrupole mass spectrometer: 29

3.2.4 Vacuum system: 29

4. Site and bond selectivity in atom-molecule collisions: H^- abstraction and de-methylation of pyrimidine bases **30**

N-site de-methylation in pyrimidine bases as studied by low energy electrons and *ab initio* calculations **31**

4.1.1. Introduction: 31

4.1.2. Experimental setup: 33

4.1.3. Theoretical methods: 34

4.1.4. Results and discussion: 37

4.1.4. Conclusions: 45

Selective bond cleavage in potassium collisions with pyrimidine bases of DNA **50**

4.2.1. Introduction: 50

4.2.2. Experimental setup: 52

4.2.3. Discussion: 53

5. Anion collisions with simple organic molecules: negative and positive ion formation **58**

Mass spectrometry of anions and cations produced in 1-4 keV H^-, O^-, and OH^- collisions with nitromethane, water, ethanol, and methanol **59**

5.1.1. Introduction 59

5.1.2. Experimental set-up 62

5.1.5. Conclusions 75

6. Electron transfer to DNA/RNA sugar unit surrogates: THF vs D-Ribose 80
Dynamic of negative ions in potassium-D-Ribose collisions 81
6.1.1. Introduction: 81
6.1.2. Experimental details: 83
6.1.3. Results and Discussion: 84
6.1.4. Conclusions: 90
New fragmentation pathways in K-THF collisions as studied by electron transfer experiments: negative ion formation 95
6.2.1. Introduction: 95
6.2.2. Experiment: 97
6.2.3. Results and Discussion: 97
6.1.4. Conclusions: 101
7. Conclusions 108
7.1. Concluding remarks: **108**
7.2. Future work: **109**
References 112

Figures

Figure 1.1. Chronological schematic of DNA damage by incident radiation 1
Figure 1.2. Secondary electron energy distribution for ejected electrons in 20 keV electron collisions with water. The triangles represent solely second generation electrons and dots represent all generations. Taken from ref. [7]. 2
Figure 1.3. Thermalization of electrons after being created by interaction of ionizing radiation with the phyisiological environment.[XX] 3
Figure 2.1 Adiabatic and diabatic Potential Energy Surfaces for a general atom-atom collision. Dashed red line represents the diabatic ionic curve, dashed blue line is the diabatic covalent curve. The full lines represent the resulting adiabatic curves. Adapted from [24].....14
Figure 2.2. Schematic of atom-atom scattering with b representing the impact parameter, the shaded area representing the repulsive part of the nuclear potential. When the electron is not transferred at the first crossing, then the trajectory is named covalent. When the electron is transferred at the first crossing, the trajectory is named ionic. Adapted from[23]. 15
Figure 3. 2. Charge exchange beam formation. Taken from[24].....22
Figure 3.3. Picture of the solid sample oven. a) Molecular target oven; b) heating lamp; c) Stainless steel support and alignment system; d) radiation deflector. Taken from[24]. 23
Figure 3. 4. Photograph of the extraction system. a) Extraction region; b) Acceleration region; c) Einzel lens; d) XY Deflecting plates; e) Flight tube. Taken from[24]. 25
Figure 3. 5. Schematic of vacuum system. Taken from[24]..... 27
Figure 4.1 Structure and virtual orbitals of π* character as well as of σ* character along the N-CH_3 coordinate of the neutral 1meT and 3meU molecules obtained at the HF/6-31G* level of theory.....34
Figure 4. 2. Plot of the 3meU SVOEs for the second and third π* orbitals (red) as well as of the σ* orbital (blue), presented in Fig. 4.1, along the N-CH_3 stretching coordinate relative to the neutral ground state energy (black). VOEs and ground state energy have been obtained at the HF/6-31G* level of theory; scaling of VOEs has been done according to description in text. 35
Figure 4. 3 Plot of the 1meT SVOEs for the second and third π* orbitals (red) as well as of the σ* orbital (blue), presented in Fig. 4.1, along the N-CH_3 stretching coordinate relative to the neutral ground state energy (black). VOEs and ground state energy have been obtained at the HF/6-31G* level of theory; scaling of VOEs has been done according to description in text. 35
Figure 4. 4 Negative ion TOF mass spectra for potassium collisions with 3meU at 14, 14.5, 15.5, 30 and 50 eV in the lab frame. Arbitrary units result from the anionic signal divided by the potassium beam current and accumulation time. 38
Figure 4. 5 Negative ion TOF mass spectra for potassium collisions with 1meT at 14, 19 and 100 eV in the lab frame. Arbitrary units result from the anionic signal divided by the potassium beam current and accumulation time..... 39

Figure 4. 6 DEA resonance profiles for formation of a) $(3meU\text{-}CH_3)^-$, b) $(3meU\text{-}CH_4)^-$, c) $(1meT\text{-}CH_3)^-$ and d) $(1meT\text{-}CH_4)^-$. Measurements shown in a), b) and d) were derived utilizing the Nier type ion source (energy resolution ~1 eV) while for c) the electron monochromator was used (resolution ~0.1 eV). 43
Figure 4. 7 Molecular structure of thymine, uracil, 1-methyl- thymine (1-meT), 3-methyl-uracil (3-meU), and partly deuterated thymine (thymine-d_4). 51
Figure 4. 8. Time-of-flight mass spectrum showing the different anions formed in collisions of neutral potassium atoms with 1-methyl-thymine (1-meT) at 66.1 eV collision energy. 53
Figure 4. 9. H^-/D^- ion yield as a function of the collision energy. The vertical dotted lines indicate the mean values of the $H^-=D^-$ position of the centre of the different resonances for N1, N3, C6 , and CH_3 positions obtained in DEA studies (from Fig. 3 in Ref. [11]). (a) H^- formation from thymine methylated at the N1 position (1-meT) at 7.6, 9.0 and 66.1 eV; (b) H^- formation from uracil methylated at the N3 position (3-meU) at 5.3, 7.4, and 64.4 eV; (c) H^- and D^- formation from partly deuterated thymine (thymine-d4) at 7.4 and 64.9 eV. 54
Figure 5. 1 Mass spectra of cations produced in 1-4 keV H^- collisions with gas-phase nitromethane. The data has normalized such that the intensities of the $CH_3NO_2^+$ (parent cation) peaks are equal.....63
Figure 5. 2 Mass spectra of cations produced in 4 keV H^-, O^-, and OH^- collisions with gas-phase nitromethane. The data has been normalized such that the intensities of the $CH_3NO_2^+$ (parent cation) peaks are equal..... 64
Figure 5. 3 Mass spectra of cations produced in 4 keV O^- and OH^- collisions with gas-phase methanol. The data has been normalized such that the intensities of the CH_3OH^+ (parent cation) peaks are equal..... 66
Figure 5. 4 Mass spectra of cations produced in 4 keV H^-, O^-, and OH^- collisions with gas-phase ethanol. The data has been normalized such that the intensities of the $C_2H_5OH^+$ (parent cation) peaks are equal..... 67
Figure 5. 5 Mass spectra of cations produced in 4 keV H^-, O^-, and OH^- collisions with gas-phase water. The data has been normalized such that the intensities of the H_2O^+ (parent cation) peaks are equal. 68
Figure 5. 6 Mass spectra of anions produced in 1, 2 and 4 keV H^- collisions with gas-phase nitromethane. The data has been normalized to the parent anion (61 Th). 70
Figure 5. 7 Mass spectra of anions produced in 4 keV H^-, O^- and OH^- collisions with gas-phase nitromethane. The data has been normalized to the parent anion (61 Th). 71
Figure 5. 8 Mass spectra of anions produced in 4 keV O^- and OH^- collisions with gas-phase methanol. The data has been normalized to 1 Th. 72
Figure 5. 9 Mass spectra of anions produced in 4 keV O^- and OH^- collisions with gas-phase ethanol. The data has been normalized to 1 Th. 73

Figure 5. 10 Mass spectra of anions produced in 4 keV H^-, O^- and OH^- collisions with gas-phase water. The data has been normalized to 17 Th. 74
Figure 6. 1 Negative TOF mass spectra in potassium-D-Ribose collisions at: a) 50 eV; b) 75 eV; and c) at 100 eV collision energy in the lab frame. An insert with the dominant conformer is added[29].....85
Figure 6. 2 Branching ratios for the anions as a function of the collision energy. Error bars are within the data points and so not visible. 86
Figure 6. 3 Structure of gas-phase dominant C_s and C_2 conformers of THF, according to proposed geometries as in refs. [6,25]. 105
Figure 6. 4 TOF negative ions mass spectra from collisions of potassium atoms with THF at: a) 30 eV; b) 70 eV and c) 100 eV. An inset of a spectra at 20 eV is presented in a) in order to show the absence of the fragmentation channels at the corresponding available energy. 106
Figure 6. 5 Branching ratios (fragment anion yield / total anion yield) as a function of the collision energy in the lab frame. 107

Tables

Table 4. 1 Scaled virtual orbital energies (SVOEs) from HF/6-31G* calculations for the optimized neutral equilibrium molecules (see Fig. 1), in eV. 36

Table 4. 2. Available energies for the different collision energies in potassium molecule experiments. 36

Table 5. 1 Summary of anion-molecule collisions studied using product cation mass spectrometry. 62

Table 5. 2. Cations produced in the present collisions (1-4 keV H^- impact, 4 keV O^- impact, and 4 keV OH^- impact) compared with examples of previous electron impact and photoionisation data. It is noteworthy that for all impact energies and projectiles the same major peaks were observed. [E] Impact energy unspecified (typically ~70 eV); [m] Local maximum; * Only resolved for 4 keV anion impact; [#] Only resolved for O^- and OH^- impact; [†] Similar intensities 66

Table 5. 3Anionic fragmentation products for the several target molecules. The different projectiles do not yield different products. [m] Local maximum; * Only resolved for 4 keV anion impact; [#] Only resolved for O^- and OH^- impact; [†] Similar intensities; [a] Extrapolated 69

Table 6. 1 Assignment of TOF mass spectrum anions in collisions of potassium atoms with D-Ribose. Comparisons are made with the available DEA studies to deoxyribose and fructose molecules. M means parent.....86

Table 6. 2 Assignment of the anions produced by potassium impact on THF (C_4H_8O, m/z = 72). Comparisons are made with the available DEA studies. * Only observed at 30 and 100 eV; no signal was observed above the background level at 70 eV; [†] From ref. [33]; [‡] A possible water contribution from the background (ref. [33]). 107

Acronyms and symbols

1-MeT	1-methil-thymine
3-MeU	3-methil-uracil
a.m.u	Atomic mass units
a.u.	Arbitrary units
α	Experimental factor
b	Impact parameter
CE	Charge Exchange
CM	Centre of Mass
CTSR	Charge transfer to shape resonance
DBS	Dipole-bound state
DD	Direct detachment
DEA	Dissociative electron attachment
DFT	Density functional theory
DNA	Deoxyribonucleic acid
DR	D-Ribose
DSB	Double strand Breaks
E_{CM}	Energy in the centre of mass framework
EA	Molecular electron affinity
e-	Single electron
ΔE	Reaction energy
E_{effec}	Effective energy
E_{Lab}	Energy in the laboratory framework
E1;E2	Adiabatic potential curves
E_a	Available energy
EA	Electron affinity
EA_{ad}	Adiabatic electron affinity
EA_v	Vertical electron affinity
$E_{n,r}$	electronic energy levels
$E_{Threshold}$	Threshold energy
ETS	Electron Transmission Spectroscopy
FWHM	Full-Width Half-Maximum
H_{el}	Electronic Hamiltonian
H	Hamiltonian
h	Planck constant
$\hbar$	Reduced Planck constant

H_0	Hamiltonian for the internal motion
H_{11};H_{22}	Diabatic potential curves (diagonal coupling matrix elements)
H_{12};H_{21}	Diabatic coupling terms (non-diagonal coupling matrix elements)
HF	Hartree-Fock
I	Ionization potential
IE	Ionization energy
K_{hyper}	Hyperthermal potassium atom
K^+_{Hyper}	Hyperthermal potassium ion
K^+	Potassium cation
K_{Ther}	Thermal potassium atom
k	Electronic state
K	Potassium
KE	Kinetic energy
K_0	Neutral potassium
LEE	Low energy electrons
LUMO	Lowest unoccupied molecular orbital
M_{hyper}	Hyperthermal alkali atom
M^+_{Hyper}	Hyperthermal alkali ion
m_p	Projectile mass
m_t	Target mass
M_{Ther}	Thermal alkali atom
M^+	Thermal alkali ion
m/z	Mass to charge ratio
MP	Methylated pyrimidine base
MO	Molecular orbital
μ	Dipolar moment
NB	Nucleobase
p	Landau-Zener probability
PES	Potential energy surface
PID	Proportional integral derivative
Pt100	Platinum resistance thermometers
Ψ(r,R)	total wavefunction
QMS	Quadrupole mass spectrometer
π*	πantibonding orbital
R_{c1}	First crossing radius
R_{c2}	Second crossing radius
r	Electronic coordinates

R	Nuclear coordinates
ΔR	Characteristic length of the system
R(t)	nucleii classical trajectory
R_c	Crossing radius
RET	Rydberg Electron Transfer
RNA	Ribonucleic acid
R_o	Fixed internuclear distance
r	Vibrational coordinate of the diatomic molecule
SE	Secondary electron
SSB	Single strand breaks
σ*	σ antibonding orbital
Γ	Resonance width
τ	Autodetachment lifetime
T_n	Kinetic energy operator of the nucleii
T_e	Kinetic energy operator of the electrons
TEM	Tissue equivalent material
T	Thymine
t_{col}	Collision time
Th	Thomson (mass unit)
THF	Tetrahydrofuran
TNI	Temporary negative ion
TOF	Time of Flight
t_{vib}	Vibration period
U_0	Initial kinetic energy
U	Uracil
V	sum of all potentials between intervening particles in a system
VAE	Vertical attachment energy
v_{bohr}	Bohr velocity
V_{cov}	Covalent potential curve
V(q;R)	Interaction potential
V_{ion}	Ionic potential curve
υ	Radial velocity
v	Velocity
$V_{cov}(R,r)$	Covalent potential surface
$V_{ion}(R,r,a)$	Ionic potential surface
VOE	Virtual orbital energy
VUV	Vacuum ultraviolet

$\Phi_k(r;R)$	adiabatic electronic wavefunctions
$\Omega_k(R)$	diabatic electronic wavefunctions
VFR	Vibrational Feshbach Resonance

1. Introduction

1.1. Radiation damage to biological tissue:

During recent decades, cancer research has gradually increasedits focus on the study of the fundamental molecular mechanisms that govern the appearance of mutagenic pathologies[1].In particular, a great interest lies in determining the role of ionizing radiation as a genotoxic agent, and in what way these mutagenic effects occur at the cellular and molecular level. Indeed, it soon became clear that ionizing radiation, comprised by X-, γ-, β- rays, as well as electrons and ions from other sources, are quite efficient agents in damaging the DNA structure, by inducing single and double strand breaks in the DNA helix[2]. These molecular mechanisms occur during the initial instants of the interaction of the ionizing radiation and are precursors to the myriad of (bio-)chemical mechanisms that eventually result in mutagenesis and formation of cancer tissues. In Fig. 1, a representation of the different stages of DNA damage, starting at the time of irradiation and evolving up to a time scale of decades, is presented. The initial instants of irradiation (in the order of 10^{-16} s) are dominated by the occurrence of physical processes, namely excitation and ionization by the incident radiation. The products of these processes eventually lead to other physico-chemical processes that in turn damage the DNA molecule. From here on, a chain reaction of natural mechanisms and processes will eventually result in mutagenic effects in the living tissue, with the final consequences being felt even as far as decades later in the form of cancer and other health problems.

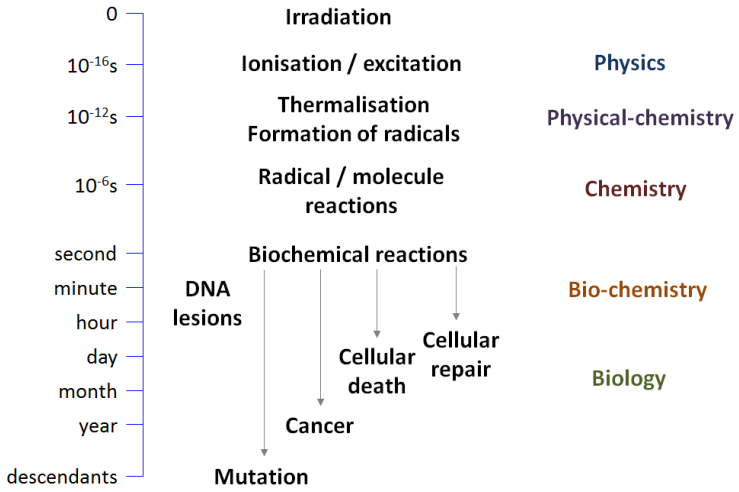

Figure 1.1.Chronological schematic of DNA damage by incident radiation

As such, a better understanding of the nascent molecular mechanisms that trigger this chain reaction is critical in order to avoid these health problems.

Initially, from a molecular point of view, it was thought that direct ionization and attack by OH radicals, created by water radiolysis ([3]and references therein), were the main culprits in creating single and double strand breaks in DNA[2]. However, recent studies on low-energy electron (LEE)

interactions with DNA have shown that the previously mentioned mechanisms are not alone in their role as DNA damaging agents, and more importantly, that their relative importance pales in comparison to the damaging capability of LEEs[4,5]. Indeed, these pioneering studies show that LEE's have a resonant-like behaviour in degrading these molecules[4] at energies lower than the ionisation threshold of such molecules (~10 eV), and even at sub-excitation energies(<3 eV)[6]. Furthermore, they demonstrate that processes of electron capture of the incident electrons to the molecular components of DNA are the main cause for the formation of single and double strand breaks in this energy range. This discovery presents itself as a major breakthrough in the way we view DNA damage by radiation damage since a whole new set of natural mechanisms that were largely ignored until now, have to be taken into account.

1.2. Indirect DNA damage by electrons (dissociative electron attachment):

It is now well established within the scientific community that the main product of living tissue irradiation with ionizing radiation are LEEs. Indeed,it is known that for each MeV of deposited energy in living tissue, approximately $5x10^4$ secondary electrons are formed[7]. Furthermore, strong evidences show that these electrons possess an energy distribution ranging from virtually 0 eV up to 20 eV, as can be seen in Fig. 2. A glance at this distribution shows that the majority of the secondary electrons will be created with energies below the typical ionization energies of the relevant molecules (~10 eV), thereby further supporting the claim that the physical processes undergone (or triggered) by these LEEs at sub-ionization energies are dominant above ionization processes.

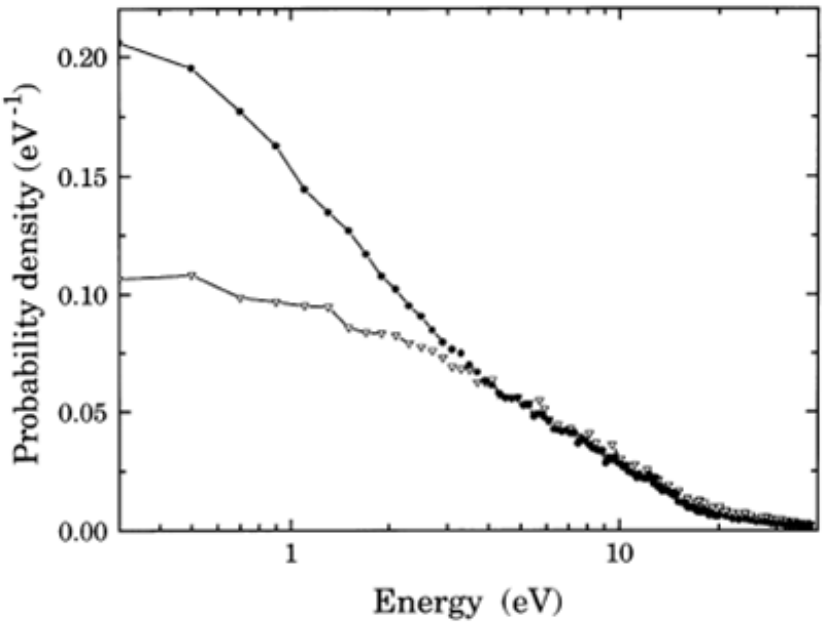

Figure 1.2. Secondary electron energy distribution for ejected electrons in 20 keV electron collisions with water. The triangles represent solely second generation electrons and dots represent all generations. Taken from ref. [7].

These electrons are initially created by high-energy radiation interacting with the physiological medium and producing secondary electrons, among other species. These secondary electrons will subsequently gradually lose their kinetic energy by undergoing a series of different processes until reaching near-zero eV energies and becoming solvated in the physiological environment. Fig. 3 shows a schematic of this electron thermalization phenomenon.

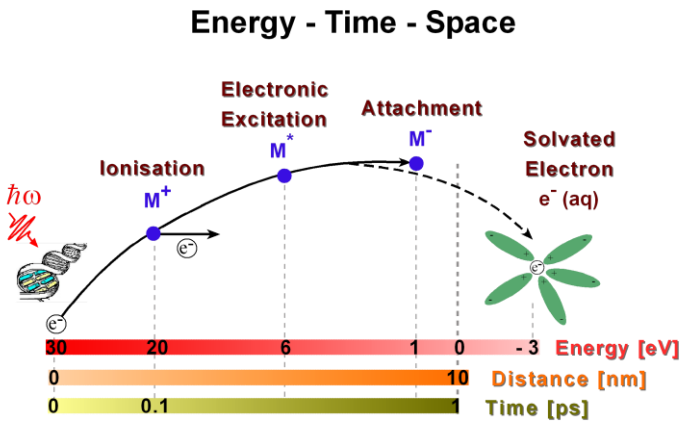

Figure 1.3. Thermalization of electrons after being created by interaction of ionizing radiation with the phyisiological environment [2].

Studies of electron interaction (near-0 to 20 eV) with Plasmid DNA show that electrons in these energy ranges are very efficient in inducing single and double strand breaks, as well as loss of helicity by the molecule. Given the resonant behaviour of the obtained profiles, DEA to the DNA constituents was proposed to be the main cause for damage of the DNA molecule. Following this seminal set of studies, several other DEA studies were performed, focusing mostly on biological relevant molecules, e.g., nucleobases, sugar units and amino-acids.

The mechanism of electron attachment consists of a resonant scattering of a low energy electron by a given molecule, resulting in a capture of the electron by said molecule and thus yielding a transient negative ion (TNI).In order for the capture to occur, the energy of the incident electron has to be the as that of the TNI. This mechanism can be seen as a resonant scattering, where the residence time of the electron in the vicinity of the molecule is much longer than its normal transit time. Furthermore, the scattering can be elastic, in which the energy of the incident electron is equal to the energy of the ejected electron, or inelastic, in which the energy of the incident electron is higher than the energy of the ejected electron. Regardless, this mechanism can be adequately understood in the context of Franck-Condon transitions, where the initial state is the neutral state and the final state is the anionic state that results from the capture of the incident electron. Indeed, in most cases the resulting molecular anion is unstable and can decay through one of the following pathways:

$$e^- + AB \rightarrow \left(AB^-\right)^* \rightarrow \left(AB\right)^- + h\upsilon \qquad (1.1)$$

$$\rightarrow (AB)^{*} + e^{-} \qquad (1.2)$$

$$\rightarrow A + B^{-} \qquad (1.3)$$

Where *e-* represents the incident electron and *AB*represents a generic molecule. Equation 1.1 represents a radiative stabilization of the TNI into a stable version of the molecular anion. This decay occurs along time scales (10^{-12} s) significantly higher than the ones considered in the latter processes and thus will, in most cases, not be able to compete with the other channels, unless some external influence "forces" the electron to remain attached to the molecular framework for long enough for this mechanism to occur.

Equation 1.2 represents auto-detachment, i.e., the extra electron will be ejected from the TNI.As was approached above, the auto-detachment can be both elastic and inelastic which, in the case of the latter, will leave the resulting molecular anion in an electronic or vibrational excited state.The auto-detachment lifetime of the TNI will greatly depend on energy of the resonant processes, as well as on the geometry of the TNI. According to one of Heisenberg's uncertainty principles, the relation between the auto-detachment lifetime and energy width of the final state is thus:

$$\Gamma \approx \frac{\hbar}{\tau} \qquad (1.4)$$

Where Γ is the energy width of the resonant anionic state, ħ is the Plank's constant andτ is the lifetime of the anionic state. One may, in effect,calculate the auto-detachment lifetime τ with this expression,only by knowing the width of the resonance Γ that allows the formation of that anionic state. This value can be obtained experimentally through some spectrometric and spectroscopic techniquesand theoretically by making use of electron scattering computations.

Equation 1.3 represents the fragmentation of the molecular anion into an anionic fragment and one (or more) neutral fragment(s). This mechanism is what is called dissociative electron attachment (DEA). In this process, the repulsive behaviour of the extra electron, which is generally captured into an otherwise unoccupied anti-bonding orbital, will result in the fragmentation of the molecular anion, leading to the formation of an anionic fragment and one (or more) neutral fragments. It competes with auto-detachment,which is mainly dependent on the lifetime of the resonant TNI state. Also, since this is a resonant process, only electrons with specific energies are captured and yield bond breaks. Furthermore, owing to the locality of the occupied orbitals, effects of site and bond selectivity, i.e., specific electron energies yielding specific fragmentation pathways, have recently been shown for a set of biological molecules[6,8–10]. Therefore, this mechanism is thought to be extremely effective in fragmenting the target molecule and the reason for this is twofold: for one, the presence of the extra electron will greatly change the intramolecular potentials in the molecule, but the capture of the extra

electron will also add energy to the molecule which also disrupts the cohesion of the molecule, resulting in bond breaking.

In the context of DNA damage, dissociative electron attachment to DNA subunits has been demonstrated to be an extremely effective agent in damaging DNA[5]. However, it is not only the direct role of electrons that bears discussing, but also the indirect role. Indeed, low energy electrons present in the physiological medium may be also highly efficient in creating free radicals, which in turn have also been shown as being highly efficient in damaging DNA. In particular, radicals like $OH^{\cdot}$ and $O^{\cdot}$, produced from degradation of water have been shown to very damaging to DNA. As such, the sole study of free electron interaction processes in biologically relevant molecules does not entirely encompass the full extent of the damage capability of electrons to DNA. Indeed, it is now well known that presence of free electrons in the physiological medium is very limited and that these damaging agents mostly manifest in bound or quasi-bound states, namely solvated in this medium[11].

1.3. DNA damage by electron transfer:

As was already stated, the discovery that secondary LEEs are the main agents in DNA damage led to a significant interest in studying the interactions of these secondary species with biologically relevant molecules. In particular, extensive studies of dissociative electron attachment to gas-phase biological molecules like the DNA nucleobases, as well as the sugar units have provided a significant knowledge on how the fragmentation pathways of these molecules when electron capture occurs. However, these studies are still quite far in their ability to precisely mimic these processes in the physiological environment. One of the main reasons pertains to the fact that, since DNA is embedded in a physiological medium, the created LEEs will not act as free electrons, but rather have to be treated as being in a bound or quasi-bound state, namely solvated in water. As such, studies of electron transfer of "bound" electrons to biological relevant molecules can be a good stepping stone in providing additional information not obtainable throughgas-phase DEA studies. In particular, studies of atom-molecule collisions approach theseshortcomings in several ways: 1) in this type of collisions, the electron is not in a free state, but rather is bound to its donor, which can be seen as a gross approximation to what in effect happens to electrons in the physiological environment; 2) the presence of the donor projectile post-electron transfer can (and will be shown to) significantly change the fragmentation pathways of the concerned molecules.In these collisions, an electron donor (A) will, upon reaching a given distance from the molecule (AB), transfer its valence electron to the molecular target, resulting in a cationic donor and a molecular anion:

$$A + BC \rightarrow A^{+} + \left(BC^{-}\right)^{*} \qquad (1.5)$$

This molecular anion will, much like the case of (1.1), be a transient negative ion and the A+ BC system can proceed through various reaction pathways, in which the following are the most common:

$$A + BC \rightarrow A^+ + \left(BC^-\right)^* \rightarrow A^+ + BC^- \quad \text{(Non-dissociative Ionisation)} \quad (1.6)$$

$$A^+ + B^- + C \quad \text{(Dissociative Ionisation)} \quad (1.7)$$

$$AB^+ + C^- \quad \text{(Associative Chemionisation)} \quad (1.8)$$

$$A^+ + B^+ + C^- + e^- \quad \text{(Dipolar Dissociation)} \quad (1.9)$$

Pathway (1.6) represents the case where the electron acceptor is able to form a parent anion, which can have lifetimes in the order of microseconds. This pathway generally involves major structural differences between the neutral and anionic geometries, in order to minimize the repulsive character of the extra electron. A few cases of this process are known, where CH_3NO_2 and SF_6 are two notable cases. It is interesting to note that, in the specific case of CH_3NO_2, the parent anion is obtained solely through electron transfer, which includes highly excited Rydberg atom donors [12]. Pathway (1.7) represents the fragmentation of the TNI, similarly to what happens in DEA. However, it is critical to note that, despite accessing the same initial resonances as in DEA, the TNI obtained in electron transfer may decay through different pathways, thereby potentially yielding different products. Such is the case of Nitromethane, where the formation of NO_2^- through DEA and electron transfer proceeds through accessing different initial anionic states. However, formation of the $CH_3NO_2^-$parent anion in electron transfer stems from initial access of the resonance through which NO_2^- is formed in DEA[13]. Apart from CH_3NO_2, no other electron transfer studies were performed where the parent anion was reported. Reaction (1.8) represents a capture of an element from the electron acceptor to the donor, it mostly comes in the form of proton transfer. This mechanism will occur mostly in conditions of reactive scattering, i.e., when the electron donor has near-zero eV kinetic energy and/or at below the threshold for ion-pair formation. Finally, (1.9) represents dipolar dissociation of the TNI, which has been observed in DEA (e.g. ref.[14]) but not discussed much in the context of electron transfer studies. It is worth noting that the electron transfer mechanism in atom-molecule collisions can be understood in two separate steps: initially, the valence electron of the donor projectile (A) is ionized, followed by a capture of the electron by the target molecule (BC). As such, from a thermodynamic point of view (at large atom-molecule distances),the endoergicity of the process is determined by the ionization energy of the donor projectile and the electron affinity of the molecular target, i.e.:

$$\Delta E = IE(A) - EA(BC)$$

Where ΔE represents the reaction energy, *IE(A)* the ionization energy of the donor projectile A and *EA(BC)* the electron affinity of the molecular target BC. If the ionisation energy is higher than the electron affinity, then the process is endothermic. Another point to be made lies in the nature of the electron affinity of the molecular target. The electron affinity of a molecule can be described either as the adiabatic electron affinity, which is the transition energy between the ground state of the neutral and anionic state, or as the vertical electron affinity, which is the Franck-Condon transition from the neutral to the anionic state. Owing to convenience of using a donor projectile with a low ionization energy, the choice fell upon alkali atoms, in particular potassium, which is the element used throughout the studies presented in this thesis.

Despite the possible analogies between electron transfer and DEA, the presence of an electron donor greatly affects the reaction pathways of the collision system. In particular, it has been shown that atom-molecule collisions can induce formation of a stable version of the parent anion[15]. Additionally, more recent measurements on electron transfer to DNA nucleobases highlight that ring breaking fragmentation pathways are much more prevalent than was initially assumed through DEA measurements[16]. Indeed, the presence of the cationic donor projectile post-collision is shown throughout the results of this thesis to greatly change the resulting fragmentation when comparing electron donation with free electron capture.

The main focus of this thesis consists of extending the already published studies on electron transfer to encompass the DNA sugar unit and possible substitutes, uridine, and also studying with greater care mechanisms of site and bond selectivity in pyrimidine nucleobases. Initially, through the use of a crossed molecular beam setup designed to study electron transfer in potassium-molecule collisions, sets of measurements of fragmentation patterns were performed for methylated versions of thymine and uracil with the main goal of studying site and bond selectivity from C-H against N-H sites[17]. Additionally, owing to the presence of the de-methylated parent anions in the mass spectra, further investigations on this fragment were performed, coupled with DEA measurements and supported byquantum chemical calculations[18]. Subsequently, in order to further expand these studies towards more complex molecules, deoxyriboseand its possible surrogate THF, were investigated in order to obtain additional information about the importance of the sugar unit as far as DNA damage is concerned.

It should be noted that, during the course of the work on atomic collisions presented in this thesis, some side-work was performed with other projectiles, mainly those with a different charge state. As part of an on-going attempt to better understand these collisional systems, mass spectrometric measurements on collisions of anions with simple organic molecules were performed at the Queen's University Belfast, under the supervision of Prof. Robert E. McCullough. In light of some of the conclusions presented in this study, it can be seen as an interesting complement to the research presented in chapter 5[19].

In the second chapter of this thesis, a discussion of the fundamental aspects of atom-molecule collision theory will be presented. The main focus of the chapter will not be to present a full formal treatment of the theories, but rather present the required information that is used in the latter chapters of the thesis. In the third chapter, a thorough description of the experimental setup in which the electron transfer measurements were performed, as well as the experiment in which the anion collision experiments were performed, will be presented. The subsequent chapters will each focus on the publications that followed from the several studies performed throughout the duration of the PhD. Finally, a last chapter will be presented where: 1) conclusions and remarks that result from comparing the several presented publications will be drawn; 2) a glimpse of several suggestions and future implementations and plans are discussed.

2. Theory of electron transfer in Atom-molecule Collisions

In this chapter, an brief description of some generic concepts of electron transfer in atom-molecule collisions will be made, starting with the simplest case of atom-atom collisions. The concepts presented for this case will be further extended to atom-molecule collisions, where the most common example will be for diatomic molecules. It is critical to note that, given the complexity of the molecules studied throughout the work described in this thesis, the concepts discussed in this chapter will serve as an intuitive "guiding hand", rather than models that can be used to precisely predict the behaviour of the studied collisions.

2.1. Atom-Atom collisions:

Collisions between two atoms can lead to two main processes. The first is elastic scattering, where the collision proceeds through a kinetic energy transfer from one atom to the other, yielding the same two atoms, albeit with different final kinetic energies. The second process is inelastic scattering, where the final electronic states of the colliding atoms can be different. The particular mechanism explored in this thesis is electron transfer, in which an electron is transferred from an atom to the other, with possible electronic excitation of the electron acceptor, i.e.:

$$A + B \rightarrow A^{+} + \left(B^{-}\right)^{*} \tag{2.1}$$

A represents the electron-donating atom and B the electron-acceptor atom. The * means electronic excited. As is obvious from (2.1), the collision yields an ion-pair, in which it is possible to leave the target (or electron acceptor) electronically excited. Considering the interaction between two particles, the system will obey the time-dependent Schrödinger equation[20]:

$$H\Psi\left(r,R\right) = i\hbar\left(\frac{d\Psi\left(r,R\right)}{dt}\right) \tag{2.2}$$

In which H is the Hamiltonian operator and Ψ the total wavefunction of the atom-atom system. R represents the nuclear coordinates and r represents the electronic coordinates. Furthermore, the Hamiltonian H can be divided in three different components:

$$H = T_n + T_e + V \tag{2.3}$$

Where T_n is the kinetic energy operator of the nuclei, T_e is the kinetic energy operator of the electrons and V is the potential sum between all of the intervening particles of the system. Given the sheer complexity inherent in considering all possible interactions encompassed in (2.3), the solution of (2.2) can only be achieved through approximations, the first being the Born-Oppenheimer approximation. This ubiquitously used approximation consists of separating the motion of the electrons from the motion of the nuclei. As such, it is possible to express the total wavefunction $\Psi(r,R)$ as a complete orthogonal set of adiabatic electronic functions that depend parametrically on the nuclear coordinates R, in effect separating this wavefunction into a nuclear and electronic wavefunction[20–23], according to (2.4).

$$\Psi(r,R) = \sum_k \Phi_k(r;R)\Omega_k(R) \tag{2.4}$$

Where $\Phi_k(r;R)$ is the adiabatic electronic wavefunctions and $\Omega_k(R)$ is the nuclear wave function associated with each electronic state. As such, the usefulness of this approximation is twofold; a) it allows for considering the motion of the nuclei as a classical trajectory R(t), in which the nuclei will move as a function of the final state of the electrons; b) as a gross approximation, for all intents and purposes, it is plausible to consider the nuclei fixed when studying the behaviour of the electrons. This then leads to ignore the influence of T_n and defining a new Hamiltonian:

$$H' = T_e + V \tag{2.5}$$

With which the following fixed-nuclei Schrödinger equation can be written[20,24]:

$$(T_e + V(r;R))\Phi(r;R) = E_{n,R}\Phi(r;R) \tag{2.6}$$

Where $\Phi_k(r;R)$ is the already mentioned adiabatic electronic wavefunction and $E_{n,R}$ are the corresponding electronic energy levels. The next step lies in considering that the nuclei move slowly, insofar as the Born-Oppenheimer approximation is not violated. In this context, one can assume that the electronic state will adiabatically accompany the motion of the nuclei. In other words, as long as R(t) does not vary rapidly, we can adapt (2.6) from a fixed-nuclei solution to a time-dependent solution, in which the trajectory of the nuclei will still remain a parametric variable and the Born-Oppenheimer approximation still holds[24].

$$(T_e + V(r;R))\Phi(r;R) = E_n(R)\Phi(r;R) \tag{2.7}$$

In other words, the main difference between (2.6) and (2.7) lies in, while the former describes a static situation (R is a fixed value), the latter describes a dynamic situation in which the nuclei coordinates change over time but always allow the electrons to reach their "equilibrium" positions. $E_n(R)$ will represent continuous functions, rather than $E_{n,R}$ which consists of sets of values.

Although $\Phi_k(r;R)$ is an eigenfunction of (2.3), it is not an eigenfunction of (2.5)[24]. However, through the use of perturbation theory[20], a set of eigenfunctions $\Theta_n(r;R)$ can be obtained through the use of $\Phi_k(r;R)$[20]. The total wavefunction $\Psi(r,R)$ can also be written as[20]:

$$\Psi(r,R)=\sum_n a_n\Theta_n(r,R)=\sum_n a_n\Phi_n(r,R)e^{-\frac{i}{\hbar}\int_0^t E_n(R)dt} \tag{2.8}$$

By forcing (2.8) to (2.2), the a_n coefficients can be calculated, thereby obtaining full knowledge of $\Psi(r,R)$ in the adiabatic framework[20]. Ignoring T_n and taking into account (2.7), one can obtain the following system of coupled equations:

$$a_n=\sum_j a_j v\left\langle \Phi_n\left|\frac{\partial}{\partial R}\right|\Phi_j\right\rangle e^{-\frac{i}{\hbar}\int_0^t (E_j-E_n)dt} \tag{2.9}$$

where,

$$v\left\langle \Phi_n\left|\frac{\partial}{\partial R}\right|\Phi_j\right\rangle \approx \frac{v}{\Delta R} \tag{2.10}$$

v is the nuclear radial velocity, ΔR is a characteristic length of the system, which can be seen as a measure of the non-adiabatic coupling between the adiabatic states[20,21,23,24]. By applying the Heisenberg uncertainty principle to this system, one can obtain:

$$\Delta E.\frac{\Delta R}{\hbar v}>>1 \tag{2.11}$$

if this condition is verified, it means that the adiabatic states are quasi-stationary and that $E_n(R)$ represents the adiabatic potential energy surfaces (PESs) that govern the motion of the nuclei[20,24]. However, when (2.11) does not hold, there is a strong non-adiabatic coupling and the

width between the energy levels is comparable to the energy uncertainty, thereby allowing for non-adiabatic transitions between adiabatic states. A class of these non-adiabatic transitions occur at a pseudo-crossing of adiabatic PES. In the context of atom-atom scattering, a transition from one adiabatic state to another will mean the transfer of an electron from one atom to the other, designated by ion-pair formation[20–24].

The former demonstration is the treatment of electron transfer in atom-atom collisions from an adiabatic point of view. Below, an approach through a diabatic framework will be presented. This approach, albeit through a different pathway, will arrive at similar conclusions as the adiabatic one. The collision system A + B can be characterized by two stationary states $|\varphi_i\rangle$ and $|\varphi_c\rangle$, the ionic and covalent states, respectively. These states arise from considering that the relative velocity of the two atoms is high enough to not allow enough time for any kind of interaction between them. As such, these states are eigenfunctions of the non-perturbed Hamiltonean H_0, of which the eigenvalues H_{11} and H_{22} are eigenvalues[20,24]. The lifetime of $|\varphi_i\rangle$ and $|\varphi_c\rangle$are supposed to be much larger than the collision time. This means that, in effect, when the system is in either of these states, it will remain so until acted upon. As such, only the following possibilities may hold:

$$A^+ + B^- \rightarrow A^+ + B^- \tag{2.12}$$

$$A + B \rightarrow A + B \tag{2.13}$$

Where (2.12) is the ionic curve, whose wavefunction is $|\varphi_i\rangle$ and (2.13) represents the covalent curve, described by $|\varphi_c\rangle$. As such, the Schrödinger equation for these two wavefunctions will be[20]:

$$H_0|\varphi_i\rangle = H_{11}|\varphi_i\rangle \tag{2.14}$$

$$H_0|\varphi_c\rangle = H_{22}|\varphi_c\rangle \tag{2.15}$$

However, if one considers the atoms as moving slowly, the interaction between the nuclei can be seen as a perturbation *W*, which can induce transitions between the non-perturbed states, which in effect is a transfer of a valence electron from one particle to the other. The perturbed Hamiltonean $H_a = H_0 + W$, will therefore be defined as[20]:

$$H_a|\theta_+\rangle = E_+|\theta_+\rangle \tag{2.16}$$

$$H_a|\theta_-\rangle = E_-|\theta_-\rangle \tag{2.17}$$

Where θ_+ and θ_- represent the possible eigenfunctions of the perturbed Hamiltonean H_a. Assuming that the W matrix only possesses non-diagonal terms, one can write H in the following way[20]:

$$[H]=[W]+[H_0]=\begin{bmatrix} H_{11} & H_{12} \\ H_{21} & H_{22} \end{bmatrix} \tag{2.18}$$

Where $<\theta_j|H|\theta_k> = H_{jk}$. In (2.18), H_{11} and H_{22} represent the diabatic energies and H_{12} and H_{21} the adiabatic coupling elements between the ionic and covalent diabatic states. However, [H] from (2.18) is diagonizable within the adiabatic bases of (2.16) and (2.17), which makes it possible to express these elements in terms of E_+ and E_-, in the following way[20]:

$$E_{\pm}=\frac{1}{2}\left(H_{11}+H_{22}\right)\pm\frac{1}{2}\sqrt{\left(H_{11}-H_{22}\right)^2+4H_{12}^2} \tag{2.19}$$

In summary, there are therefore two ways with which to describe the electron transfer process; from an diabatic point of view, the diabatic states presented in (2.14) and (2.15), correspond to the diabatic curves $H_{11}(r)$ and $H_{22}(r)$, in which adiabatic transitions (electron transfer) are induced by the H_{12} coupling term. On the other hand, from an adiabatic point of view, the PES correspond to the states described in (2.16) and (2.17), with $E_+(r)$ and $E_-(r)$ as their corresponding eigenstates, and non-adiabatic (i.e. diabatic) transitions between these states are induced by a so-called non-adiabatic coupling similar to the one described in (2.10). The coupling term H_{12}, which can be seen as a "measure" of the electron transfer probability, can be estimated from semi-empirical or even completely empirical approximations. A possible formalism that can be used to calculate the non-adiabatic (electron transfer) transition probability was initially developed as a solution to a general quantum mechanical problem by Landau, Zener and Stuckelberg[20,22]:

$$p=e^{-\left[\frac{2H_{12}(R_c)^2}{\hbar v\left|\frac{d}{dR}(H_{11}-H_{22})\right|_{R=R_c}}\right]} \tag{2.20}$$

where p is the probability of electron transfer. As can be seen, the main parameters are the H_{12} coupling term and the radial velocity v. To better illustrate how the adiabatic and diabatic frameworks can "overlap", a set of diabatic and adiabatic PESs are schematically represented in Fig. 2.1.

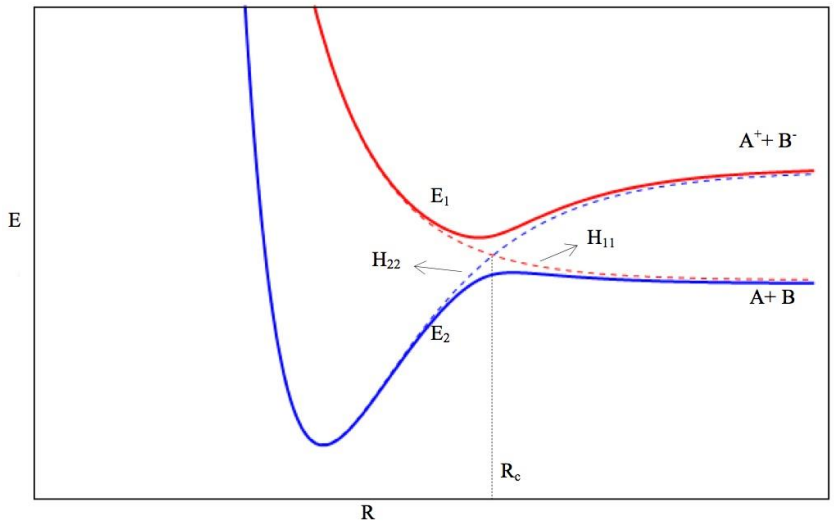

Figure 2.1Adiabatic and diabatic Potential Energy Surfaces for a general atom-atom collision. Dashed red line represents the diabatic ionic curve, dashed blue line is the diabatic covalent curve. The full lines represent the resulting adiabatic curves. Adapted from [24].

As can be seen, both the diabatic and adiabatic curves are similar for internuclear coordinates away from the crossing radius, where, for this particularcase an avoided crossing is observed. The asymptotic energy value between the covalent and ionic curves is given by:

$$\Delta E = I - EA \tag{2.21}$$

Where I is the ionization potential of the donor atom and EA is the electron affinity of the acceptor atom. If one makes the approximation of stating that the crossing radius R_c is large, then Van der Waals and induction forces can be disregarded, thereby making V_{cov} zero and V_{ion} a purely coulombic interaction. This leads to R_c being approximated to:

$$R_c = \frac{14.41}{IE - EA} \tag{2.22}$$

with R_c in Å and ΔE in eV.

Up until now, the discussion only pertained to the presence of a single crossing point. However, in a general atom-atom collision, for a given impact parameter *b*, two crossing radii will appear. Fig. 2.2 shows schematically this[23].

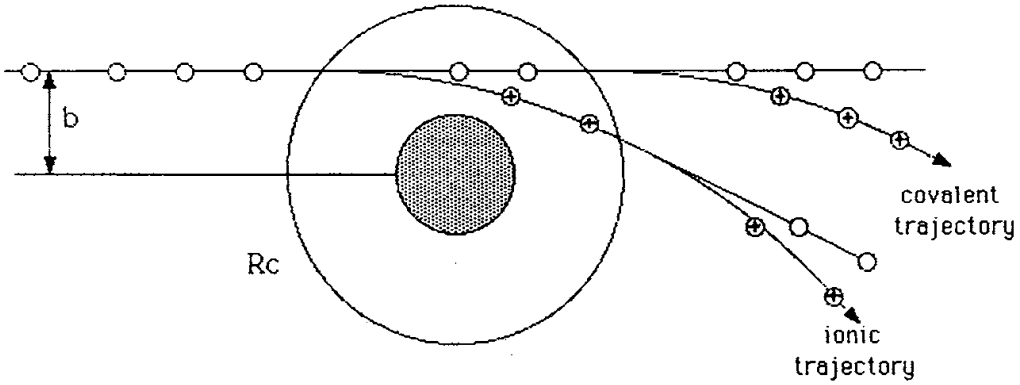

Figure 2.2. Schematic of atom-atom scattering with b representing the impact parameter, the shaded area representing the repulsive part of the nuclear potential. When the electron is not transferred at the first crossing, then the trajectory is known as covalent. When the electron is transferred at the first crossing, the trajectory is named ionic. Adapted from[23].

According to Fig. 2.2, if the impact parameter b is smaller than R_c, there will be then 4 possible processes. If the electron is transferred at the first crossing, then the coulombic interaction will create a significant deflection in the trajectory of the cation. Even if the electron is transferred back to the now-cationic electron donor (reneutralization) at the second crossing, the deflection will still be quite significant. In contrast, if there is no electron transfer at the first crossing, the trajectory of the electron donor will not be affected, regardless of a possible electron transfer at the second crossing. Both of thesepossibilities have been designated by covalent scattering, as can be seen in Fig. 2.1. At this point, it is worth noting that, for low radial velocities, the electron transfer probability is increased and as such, the ionic scattering, as described in Fig. 1, will tend to dominate relatively to covalent scattering. The probability of reneutralization will still be possible, however, as far as the work of this thesis is concerned, detection of neutral particles is not possible and as such, it is not possible to infer about this reaction pathway. A more thorough review on this subject can be obtained in ref.[23] and references therein. Furthermore, studies of potassium energy loss at different angles can provide information on whether the reaction channel is covalent or ionic (see e.g.[12,13]).

Until now, the presented formalism only holds for atom-atom collisions. However, some of the principles will still apply for atom-molecule collisions. Below a small discussion regarding this will be presented.

2.2. Atom-molecule collisions:

When attempting to incorporate the models discussed in section 2.1 to atom-molecule collisions, some general considerations have to be taken into account. Firstly, even for collisions between atoms and diatomic molecules, a multitude of new processes have to be taken into account, namely electronic, vibrational and rotational excitations of the electron acceptor (molecule). Furthermore, collision-induced dissociation and even chemical reaction processes can also occur. The

models considered above do not easily encompass these processes. Indeed, atom-molecule collisions can no longer be completely described by uni-dimensional potential energy curves.

Another consideration is that, in order to develop a fully encompassing model of atom-molecule collisions, multi-dimensional potential hypersurfaces have to be considered, in which the various nuclear coordinates of the molecule will have to be taken into account. For this purpose, some models for simple diatomic molecules were developed (discussed in ref. [23] and references therein). However, these models cannot be used in polyatomic molecules, owing to the sheer number of possible processes that can occur. Indeed, the aforementioned models are not applicable to the molecules that are studied throughout this thesis and as such, it is neither possible, nor convenient, to make use of them. Moreover, it is not the main aim of this thesis to provide precise information on the effect of these processes.

The main intent in this chapter is therefore to provide a more qualitative perspective of the electron transfer process in these collisional systems. However, through this perspective, it is possible to obtain some information about the general behaviour of these collisional systems by carefully analysing the data and complementing it with electron scattering techniques and quantum chemical calculations, namely those related to DEA. However in the subsequent chapters we will make a discussion highlighting the major differences between these for each set of the relevant molecules.

As was already discussed in the previous chapter, dissociative electron attachment, as is detailed in (1.1) consists of the capture of a free electron by the molecular target, after which, the resulting transient negative ion can proceed through different reaction pathways. This process can be tentatively compared to what occurs in atom-molecule collisions insofar as the electron in these collisions has two main major differences: 1) the electron is initially in a ‘bound’ state; 2) the resulting capture of the electron will also result in the formation of a cationic species in the close vicinity of the now-anionic molecular target. As will be shown, these differences will greatly influence the reaction and fragmentation pathways of the TNI when comparing DEA to electron transfer by atom-molecule collisions.

From a more generic point of view, the electron transfer process described in the previous section, can be described two main steps: 1) the ‘bound’ electron is ionized from the electron-donating projectile; 2) the electron is captured by the electron-accepting molecule. However, a corollary that can be made from this reasoning is that, as is now quite well established for DEA, electron capture by a molecule is a resonant process, and therefore only certain energy losses from the system can lead to electron transfer. Therefore, one can state that the energy loss of the atom-molecule system when electron transfer occurs is resonant. This means that, as long as the available energy of the atom-molecule system is enough for the anionic state of the molecule to be accessed, the initial anionic state will be formed. This available energy defined as the kinetic energy of the electron donor in reference to the centre-of-mass frame, taking into account the ionization energy of the electron donor, i.e.:

$$E_a = \frac{m_m}{m_m + m_K}.a.E_{lab} - IE \qquad (2.23)$$

Where E_a is the available energy (in eV) for the process to occur, m_K is the projectile's mass, m_M is the molecule's mass, E_{lab} is the kinetic energy of the projectile relative to the lab frame, α is an experimental correction factor and IE is the ionization energy of the donating projectile. It is critical to note two main points regarding this formula. The first point pertains to the implicit assumption (for the sake of simplicity) that the velocity of the acceptor molecule (which is at a thermal energy) is negligible in comparison to the velocity of the hyperthermal projectile beam.

The second point pertains to the experimental parameter that is taken into account in (2.23). This parameter stems from the non-linearity of the acceleration fields of the initially cationic projectile before it resonantly charge-exchanges. Studies on this effect have already been performed [25] and recent simulations also confirm this value. Furthermore, all studies assuming this formula appear to yield E_a values that are congruent with what is expected. This adimensional value (~0.90) does not appear to change appreciably with the applied accelerating potential.

Regarding (2.23), it implies that, as long as E_a is higher than the energy of the resonant anionic state that one wants to access, then it can be accessed. On the other hand, anionic resonant states with energies above E_a are not accessible. Through this rationale, measurements which demonstrated site and bond selectivity in pyrimidine bases yielding H^- formation were performed [17]. Additionally, by tuning the potassium kinetic energy to values where E_a is below the accessible resonant states, it has been shown in several biologically relevant molecules that indeed, the accessed resonances appear to be the same as in DEA, despite the fragment yields being different. This was shown for other methylated derivatives of pyrimidine bases [18]. It is worth noting that one can take this rationale one step further, i.e., by gradually increasing E_a, it is possible to indirectly derive resonance profiles similar to the ones obtained through DEA. This is true as long as the lowest covalent and anionic states in the collision complex are involved.

Another major mechanism that has been shown to be critical to the way the reaction pathways decay after electron transfer, is the presence of the electron-donating projectile in the vicinity of the resulting molecular anion. This temporary reaction complex has been shown in our studies to greatly influence as some fragmentation channels evolve. An already well-explored example is nitromethane (CH_3NO_2)[12,13], where through electron transfer with potassium atoms, it was shown that the presence of the potassium cation allows enough time for the $CH_3NO_2^-$ TNI to change into a stable geometry, significantly different from the neutral. This was in sharp contrast to DEA[13], where no parent anion was reported. Perhaps most interestingly, it was also shown that the initial accessed state in electron transfer that yielded the parent anion was also an accessed state in DEA, however, it yielded a different fragment (NO_2^-).

Throughout the course of this thesis, several other similar cases will be shown and discussed. However, it is not totally clear the exact way as to how the creation of this reaction pathway works. Indeed, the empirical rationale that was developed was that, after electron transfer, the system forms a chemical complex that interacts through a coulombic potential. This coulombic complex will affect the molecular anion in several ways, most notably by greatly suppressing the possibility of rejection of the extra electron from the molecular anion. In other words, during the lifetime of this temporary coulombic complex, the competition between auto-detachment and formation of an anion favours the latter, rather than the former, which is normally the case of DEA. The formation of the anionic species can either be through fragmentation, or through formation of the parent anion, as is the case of CH_3NO_2.

3. Experimental setups

The main focus of this chapter pertains to the characterization of the two experimental setups used throughout the main work performed during this thesis. The main core of the work was performed in the Atomic and Molecular Collisions Laboratory, CEFITEC, FCT/UNL in an experimental setup designed for time-of-flight (TOF) mass spectrometric studies of negative ions that are a result of electron transfer in neutral atom-molecule collisions, with specific emphasis on biologically relevant molecules. It is worth noting that most of the system's components were constructed and developed in our laboratory specifically devoted to this sort of collisions. In the next sub-chapters, each of these will be discussed.

Additionally, some research work was also performed in anion collisions with simple organic molecules. This work was performed in the Centre for Plasma Physics, Queen's University Belfast, under the supervision of Prof. Robert W. McCullough. The system used for these measurements was fully usable during the time at Queen's University Belfast so no experimental development was required.

We now discuss and present the main characteristics of both experimental setups.

3.1 Neutral atom collisions experimental setup:

A schematic of the experimental system is shown in Fig. 3.1. In order to ensure the necessary mean free path, ultimate base pressures of the order of 3×10^{-7} mbar (3×10^{-5} Pa) in the collision chamber were used. The crossed molecular beam apparatus can be divided into two main regions, which are set in two different vacuum chambers and accordingly differentially pumped. The first region consists on the hyperthermal neutral potassium beam creation, with a tuneable energy ranging from 15 to 300 eV. This is in a vacuum chamber with working pressures at approximately 5×10^{-7} mbar and communicates with the second vacuum chamber through a 1 cm wide aperture valve.

The second region comprises the extraction system of the time-of-flight (TOF) mass spectrometer, the molecular target oven and a Langmuir-Taylor detector for beam monitoring. Depending on the sample, typical working pressures are of the order of 6×10^{-6} mbar (6×10^{-5} Pa). In the second chamber are installed a set of heating lamps to both avoid condensation of samples and to allow for baking of the chamber. Below, each of these components will be discussed in more detail.

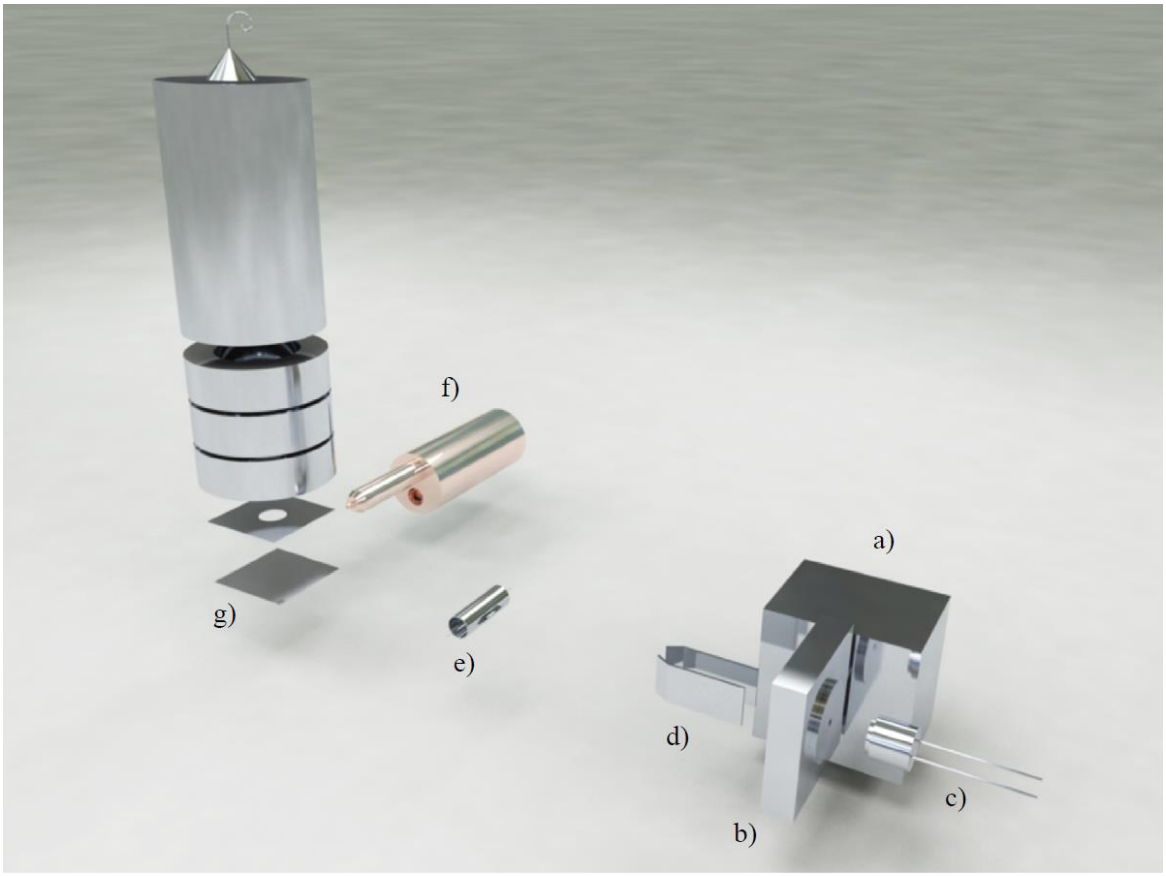

Figure 3.1.Overview of the electron transfer experimental system. a) potassium oven; b) charge exchange chamber; c) cationic potassium source; d) deflecting plates; e) Langmuir-Taylor detector; f) molecular target oven; g) TOF mass spectrometer. Adapted from[24].

3.1.1. Projectile beam:

In Fig. 3.1, a schematic of the beam creation system is depicted, where all the major components can be visualized. Additionally, Fig. 3.2 shows a schematic explaining the formation of the neutral potassium beam. The hyperthermal potassium beam is obtained through a resonant charge exchange process between hyperthermal cationic potassium atoms and thermal neutral potassium atoms, briefly according to the following equation:

$$K^{+}_{hyp} + K^{0}_{ther} \rightarrow K^{+}_{ther} + K^{0}_{hyp} \qquad (3.1)$$

Where K^{+}_{hyp} represents the initial hyperthermal potassium cation beam and K^{0}_{ther} the neutral potassium vapour in the charge exchange chamber (b in Fig. 3.2), while the products of the reaction are the desired K^{0}_{hyp} and the K^{+}_{ther}. Initially, a cationic potassium source creates a beam of K^{+} ions, which are then accelerated to the desired energy. This ion source is assembled as is shown in Fig. 3.2 in order to guarantee correct electrical and thermal isolation between the source and the rest of the metal body. More technical information can be found elsewhere[24].

Solid potassium is managed and inserted inside the charge exchange oven,. This oven will then be heated to approximately 160ºC (433 K) by two cartridge heaters and the temperature controlled by two PT100 resistors. The heating will create a potassium vapour, diffusing K^{0}_{ther} into the connected charge exchange chamber. The temperature of the charge exchange chamber is kept at a slightly higher temperature than the oven, in order to avoid condensation in the connection between the oven to the chamber.

The K^{+}_{hyp} that is created by the ion source will then pass through the charge exchange chamber (a) in Fig. 3.2), where it will resonantly charge exchange with the K^{0}_{ther} atoms inside it, yielding K^{0}_{hyp}. The K^{+}_{hyp} that do not charge exchange are deflected by the deflecting plates, thereby producing a beam of K^{0}_{hyp}. This charge exchange process has been shown to be resonant, i.e., no kinetic energy by the hyperthermal projectile is lost. However, space charge effects in the system may be present[25], which explains the experimental parameter α factored in equation (2.23) of the previous chapter. In Figure 3.2 below, a schematic of the charge exchange system is presented, in order to provide a more clear description.

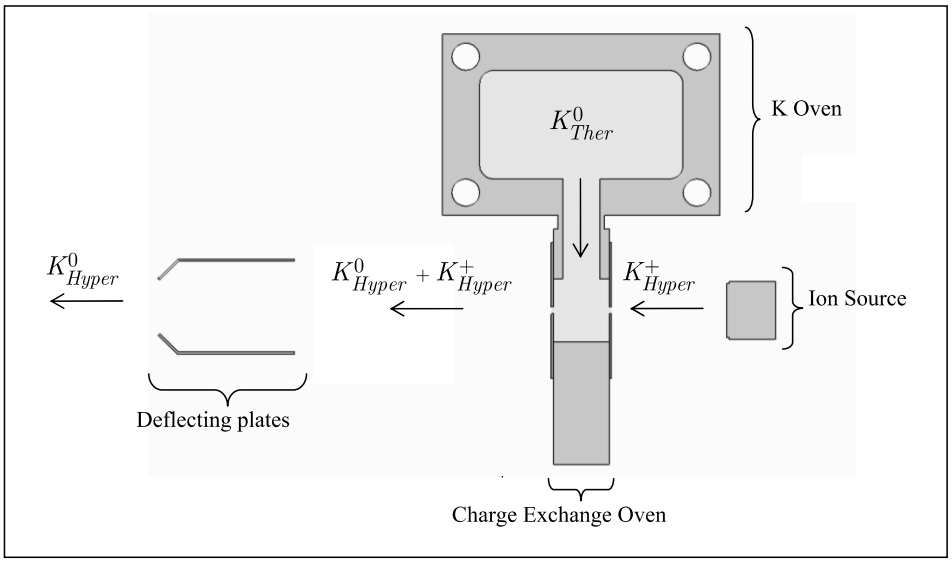

Figure 3. 2. Charge exchange beam formation. Taken from[24].

The deflecting plates basically consist of two parallel plates, in which a positive voltage is applied to one of them, while the other is either connected to ground, or to an electrometer. The deflecting plates is; 1) provide deflection of all unwanted charged particles; 2) by connecting one of the plates to an electrometer, a relative current of the K^+_{hyp} that did not charge exchange can be obtained. This value can be used to monitor if the ion source is working properly and to have an indication of the charge-exchange efficiency, which is related to the fact that if there is still enough potassium vapour in the charge exchange chamber. In order to ensure an effective deflection of the undesired K^+_{hyp}, the applied voltage to the deflecting plate is changed accordingly to the beam kinetic energy. Previous studies on optimal values have been already performed and are shown elsewhere[24].

3.1.2. Langmuir-Taylor surface detector:

The main purpose for this detector is to monitor the potassium neutral beam. It will allow for a relative measure of the beam in order to ascertain its stability for the same beam energy and relative intensity for different beam energies. The Langmuir-Taylor detector is essentially a high-purity iridium filament (>99%), surrounded by a stainless steel cylindrical collector. This collector has two wide holes along the beam axis and the filament is set slightly above the main section of the beam, in order to minimize tampering with it.

The working mechanism is by heating the Iridium filament, an electron cloud of electrons will be created with enough energy to ionize any particle that passes in the vicinity of the filament. These ionized particles will, owing to an applied positive voltage in the filament relative to ground, be repelled outwards and be detected in the surrounding cylindrical collector, which is directly connected

to an electrometer and referenced to ground potential. Currents of 0.63A are used to heat the filament and a voltage drop of +60 V is used to repel the ionized potassium atoms into the collector.

It is worth noting that it is possible to have K^0_{ther} reaching the filament. To account for this fact, the K^+_{hyp} voltage source is turned off and a current is measured, which then is subtracted to the current obtained with the power supply turned on. However, these are negligible, given their thermal velocities when exiting the charge exchange chamber.

3.1.3. Molecular target oven:

The molecular target oven is placed perpendicular to the axis of the potassium beam allowing the effusive molecular beam to collide in the collision region, which will be discussed in the next sub-section. The molecular target oven is composed of 3 main copper-made parts: 1) the outer body, attached to the support; 2) the sample holder, which is inserted at the back of the outer body and 3) the copper capillary tip. The oven is supported on a XY system to allow for a more fine alignment. The outer body is connected to a *Swagelock* entrance through a feedthrough to the outside of the chamber, which in turn is connected to a liquid and gas sample admission system to allow for non-solid samples. A picture of the oven can be seen in Fig. 3.3.

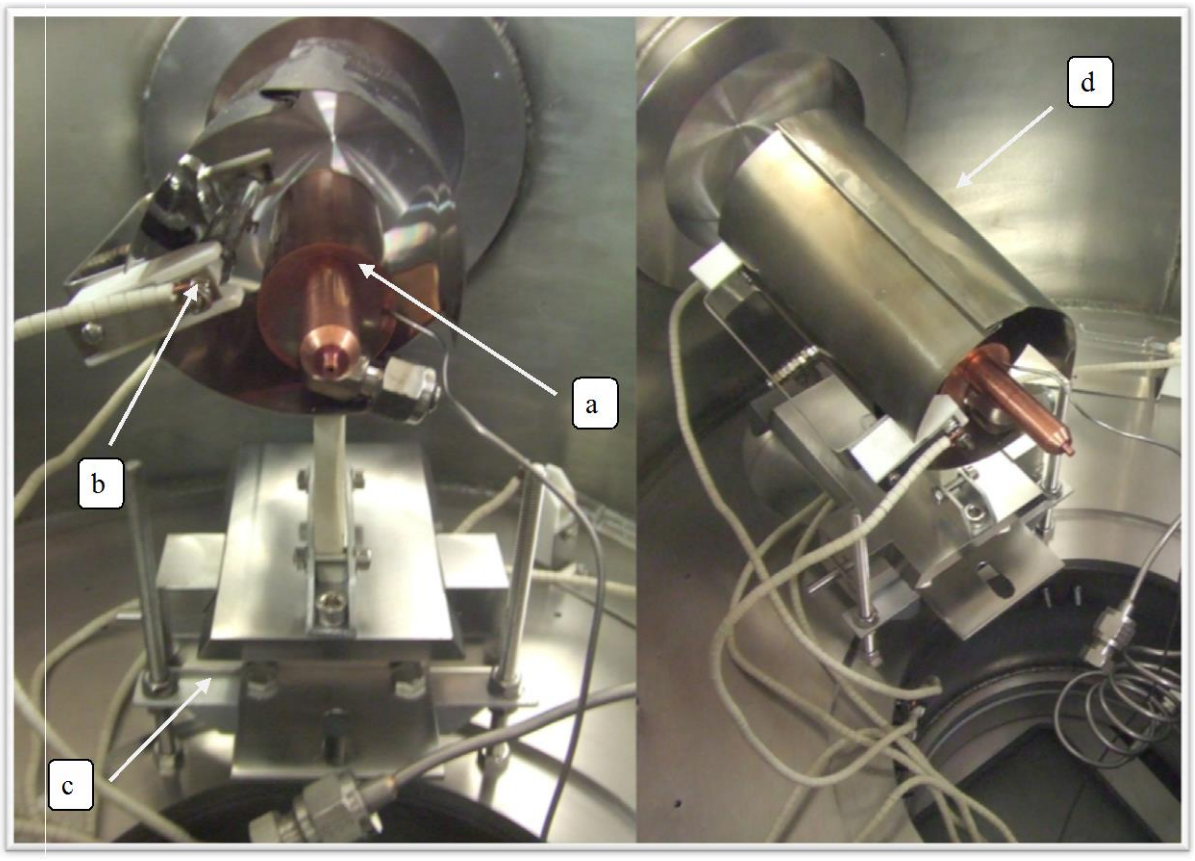

Figure 3.3.Picture of the solid sample oven. a) Molecular target oven; b) heating lamp; c) Stainless steel support and alignment system; d) radiation deflector.Taken from[24].

The oven is heated through a halogen bulb and surrounded by a stainless steel reflector, which increases the heating efficiency. The bulb's intensity is manually controlled by a Variac and the temperature of the outer body is measured by a K-type thermocouple.

The liquid and gas sample system is comprised of a sapphire valve for fine tuning of the admission pressure and a rotatory pump to pump the extra unwanted sample. In order to purify liquid samples, heat and thaw-pump cycles are used.

3.1.4. TOF mass spectrometer:

A time-of-flight TOF mass spectrometer is based on the simple principle that particles with different masses, subjected to the same force, obtain different velocities and thereby fly a given fixed distances in different time intervals. The simplest versions of a TOF mass spectrometer consist of an extraction region, where the initial electric force is applied to all charged particles, and a free field zone, particles with different mass, and hence different velocities, will arrive at the end of it at different times. There have, however, been extensive improvements to this simple concept, namely reflectron type TOF spectrometers, which greatly increase the resolution of the spectrometer. The configuration used in this experiment is a custom-made linear TOF spectrometer of a Wiley-McLaren geometry[26]. This, consists of a dual-stage linear TOF geometry, comprised by an extraction region (which will be the collision region), an acceleration region, a set of einzel lens system, a set of deflecting plates, a free-field region and a channeltron detector.

3.1.4.1. Extraction region:

The extraction region is where the neutral potassium and molecular beams are made to collide. On both incoming axis, collimating slits avoid the saturating of the extraction region with particles, as can be seen below in Fig. 3.4. It is composed of two electrodes with a mutual distance of 1.2cm, where the top has a 1cm grid. In order to extract the anionic species that are created by the collision of the two beams, a pulsed voltage signal is applied in the lower electrode consisting of a -400 V pulse embedded on top of a -3500V constant value.

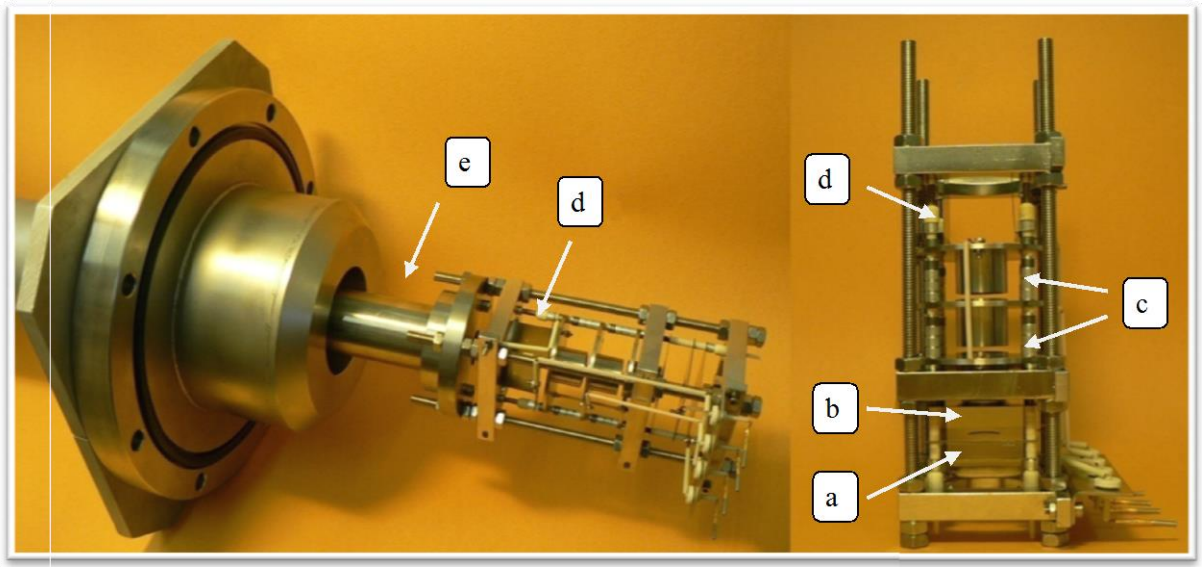

Figure 3. 4. Photograph of the extraction system. a) Extraction region; b) Acceleration region; c) Einzel lens; d) XY Deflecting plates; e) Flight tube.Taken from[24].

3.1.4.2. Acceleration region:

This region will apply a significant acceleration to all particles. When the -400V pulse is active, the anionic particles will be extracted into the accelerating region and then accelerated forward with a total energy of 3900 eV. On the other hand, if the -400V pulse is not on, the voltage difference between the two electrodes will be 0 and no particle extraction will occur. This mechanism will therefore act as the start signal for the TOF spectrometer. More details on this can be found elsewhere[24].

3.1.4.3. Einzel Lens system and deflecting plates:

In order to optimize the transmittance of the TOF mass spectrometer, an Einzel lens system and an XY set of deflecting plates were assembled after the acceleration region. The Einzel lens system is composed of three electrodes, where the first and the third are grounded and the voltage applied to the middle electrode will determine the focusing of the beam of the extracted anionic species. Several tests performed with a calibration molecule (CH_3NO_2) allowed to conclude that, for the set of extraction voltages, a voltage of -1500 V optimizes the transmittance of the TOF spectrometer.

A set of XY deflecting plates are also mounted after the Einzel lens system to provide the possibility to deflect the anionic species beam in order to also optimize the transmittance of the TOF spectrometer. After similar tests, it was found that there was no need for deflection of the beam and the plates were grounded in order to avoid charge accumulation.

3.1.5. Vacuum system:

The Potassium chamber (1) consists of a potassium oven, the charge exchange oven, the ion source and a pair of deflecting plates (described in the previous sub-sections). The vacuum conditions are guaranteed by a 1300 l/s pumping speed diffusion pump (5), which provides an ultimate pressure of 5×10^{-7}mbar (5×10^{-5}Pa). A liquid nitrogen trap will avoid migrations of diffusion pump oil into the chamber and undesired residues into the diffusion pump. The primary vacuum required by the diffusion pump is guaranteed by a two-stage rotary pump, with a pumping speed of 6 l/s that ensures an ultimate pressure around 3×10^{-2} mbar (3 Pa). A molecular sieve trap is placed to avoid contamination with rotary oil vapours.

The collision chamber (2) consists of the Langmuir-Taylor detector, the lamp baking system, the molecular target oven and the TOF mass spectrometer (described in the previous sub-sections). Similarly to the potassium chamber, the high-vacuum is achieved by a diffusion pump (13), with a pumping speed of 1550 l/s and an ultimate pressure of 5×10^{-7}mbar (5×10^{-5}Pa) and a liquid nitrogen trap. The TOF system is pumped differentially by a turbomolecular pump placed near the channeltron detector. Both the diffusion and turbo pumps are backed by a two-stage rotary pump (26), with a pumping speed of 6 l/s, providing an ultimate pressure of 1×10^{-2} mbar (1Pa). A molecular sieve trap is placed after the rotary pump to prevent the chamber and TOF spectrometer contamination with rotary oil vapours.

The potassium and the collision chamber are connected through a manual gate valve (24) that allows for changes in either chamber without tampering with the adjacent chamber. This is especially important in situations where one either has to clean the collision chamber or restock the potassium charge in the potassium oven.

The liquid and gas sample system is pumped differentially by a two-stage rotary pump (35). The whole system is protected against electric and water failures through a security system.

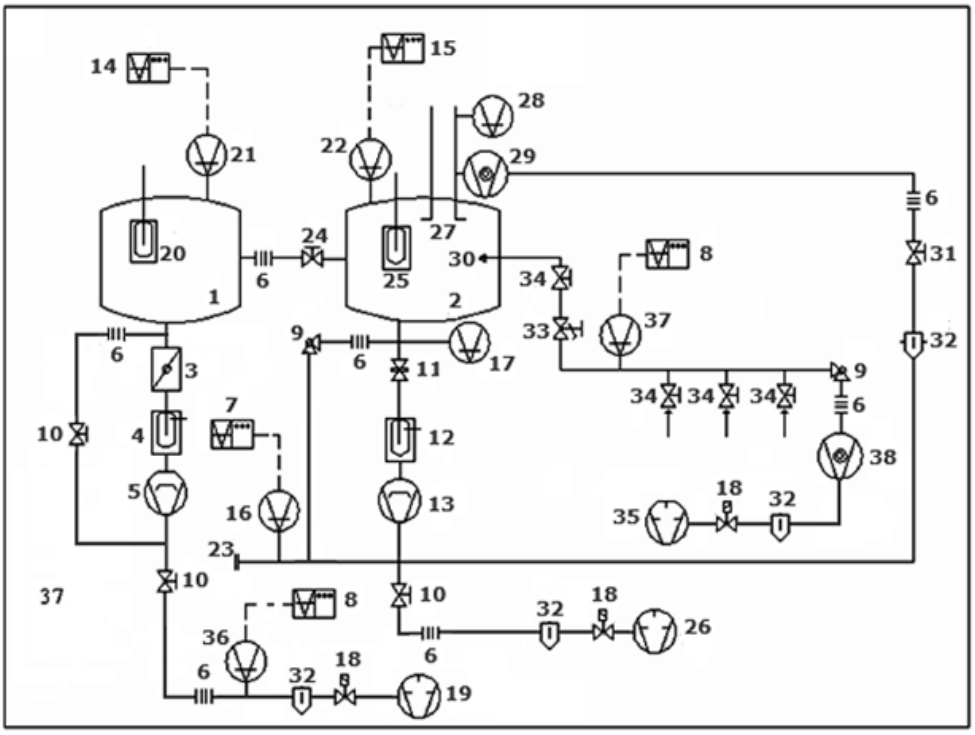

Figure 3. 5. Schematic of vacuum system.Taken from[24].

1. Potassium chamber
2. Collision chamber
3. Butterfly valve
4. Liquid nitrogen trap
5. Diffusion pump
6. Bellow
7. TIC instrumentation controller
8. Instrumentation controller
9. Vacuum valve
10. Speedivac manual valve
11. Gate valve
12. Liquid nitrogen trap
13. Diffusion pump
14. Penning controller
15. Penning controller
16. Pirani vacuum gauge
17. Penning vacuum gauge
18. Speedivac solenoid valve
19. Two-stage rotary pump
20. Liquid nitrogen trap
21. Penning vacuum gauge
22. Penning vacuum gauge
23. Blank connecting flange
24. Inter-chambers manual gate valve
25. Liquid nitrogen trap
26. Two-stage rotary pump.
27. TOF Mass spectrometer
28. Penning vacuum gauge
29. Varian turbomolecular high-vacuum pump
30. Swagelok Male Elbow
31. Manual valve

32. Molecular sieve trap
33. Precision leak valve – sapphire valve.
34. Swagelock manual valves
35. Two-stage rotary pump
36. Pirani vacuum gauge
37. Pirani vacuum gauge
38. Turbomolecular high-vacuum pump

3.2. Anion-molecule collision experimental setup:

The experimental setup that is described below was used to study positive and negative ion fragmentation patterns that result from collisions of anions in the keV region with a set of simple organic molecules. The studies were performed at Queen's University Belfast. This setup can be separated into several components: 1) anion formation source; 2) anion beam mass selection and focusing; 3) collision region and quadrupole spectrometer and 4) vacuum system.

3.2.1. Anion formation source:

The anion beam is produced in a PS-120 Negative Ion Caesium Sputter Source from Peabody Scientific^{TM}, operating between 1 and 4keV. The source is adaptable to various types of negative ions. The operation of the source consists of heating Cesium in an oven, with the resulting vapour migrating into the source region. This region contains the ionizer assembly which will ionize the Cesium. The resulting cations, owing to a voltage applied to the chamber and ionizer will be repelled towards an insulated holder assembly at a voltage negative in respect to the ionizer. Cesium ions are therefore formed by surface ionization and are then attracted to the sputter targets because of the potential difference between the ionizer and target holder. The resulting sputtering by the Cesium ions will create a significant amount of negative ions of the sputtered surface. These negative ions can be extracted up to 30 keV. To obtain different anion beams, the target holder can be taken out and a new target can be inserted.

3.2.2Anion beam mass selection and focusing:

The beam emerging from the source may contain several types of different anions and requires a constant focus by electrostatic lens systems. By using a 90º double focusing magnet, the beam can be momentum analysed and therefore, mass selection of the beam can be performed. Before and after the magnet, sets of electrostatic lenses ensure a correct focusing of the anionic beam. Depending on the anionic species, typical ion currents can range up to 40 nA.

3.2.3Interaction region and quadrupole mass spectrometer:

Further to the anionic beam, an effusive molecular beam is formed through the use of a sample admission system. This effusive beam is created in a perpendicular axis to the anionic beam and they are made to collide in the collision region. The collision region is composed of an extraction electrode and a subsequent set of einzel lens systems to improve the extraction efficiency of the formed anionic and cationic products. An extraction voltage of 25 $V.cm^{-1}$ ensures any unwanted deflection of the anionic beam into the quadrupole mass spectrometer, used for mass analysis.

3.2.4Vacuum system:

In order to improve the beam's mean free path, the anionic beam pathway is sectioned in several intermediate chambers, each with its independent turbomolecular pump and pneumatic valves were used between each of these sections. Sets of turbomolecular pumps are used throughout the entire anionic beam pathway, ensuring average working pressures in the order of 5×10^{-7} mbar (5×10^{-5}Pa). Furthermore, the quadrupole mass spectrometer is differentially pumped to avoid damage to its components. The working pressure in the interaction chamber was in the order of the 5×10^{-6} mbar (5×10^{-4}Pa).

Chapter 4

4. Site and bond selectivity in atom-molecule collisions: H^- abstraction and de-methylation of pyrimidine bases

The main emphasis of this chapter lies on an attempt to better understand the fundamental underlying molecular mechanisms triggered by electron transfer in atom-molecule collisions in biologically relevant molecules. As such, studies of electron transfer from potassium atoms to pyrimidine bases and methylated derivatives were performed.

In the first study, a particular attention was given to the de-methylation of these pyrimidine derivatives, which was unreported neither in DEA studies, nor in atom-molecule collision experiments. Given this discrepancy between DEA and electron transfer, DEA measurements were performed and compared with electron transfer studies. Together with the support of theoretical calculations, fragmentation pathways for these de-methylation channels, both in DEA and in electron transfer, were proposed, and the differences between the results obtained in these two techniques were discussed.

In the second study, the sole focus lies on studying site and bond selectivity in atom-molecule collisions. Indeed, such mechanisms were already shown in the context of DEA but no such studies were ever performed in the context of atomic collisions. As is shown, H^- abstraction caused by electron transfer is site and bond selective by tuning the kinetic energy of the electron donor beam.

N-site de-methylation in pyrimidine bases as studied by low energy electrons and *ab initio* calculations

D. Almeida [1], D. Kinzel [2], F. Ferreira da Silva [1], B. Puschnigg [3], D. Gschliesser [3], P. Scheier [3], S. Denifl [3,*], G. García [4,5], L. González[2] and P. Limão-Vieira[1,*]

[1] Laboratório de Colisões Atómicas e Moleculares, CEFITEC, Departamento de Física, Faculdade de Ciências e Tecnologia, Universidade Nova de Lisboa, 2829-516 Caparica, Portugal
[2]Institut für Theoretische Chemie, Universität Wien, Währinger Strasse 17, A-1090 Wien, Austria
[3]Institut für Ionenphysik und Angewandte Physik and Center of Molecular Biosciences Innsbruck, Universität Innsbruck, Technikerstr. 25, A-6020 Innsbruck, Austria
[4] Instituto de Física Fundamental, Consejo Superior de Investigaciones Científicas, Serrano 113-bis, 28006 Madrid, Spain
[5] Departamento de Física de los Materiales, UNED, Senda del Rey 9, 28040 Madrid, Spain

Published in Phys. Chem. Chem. Phys. **15**, 11431-11440 (2013)

Abstract

Electron transfer and dissociative electron attachment to 3-methyluracil (3meU) and 1-methylthymine (1meT) yielding anion formation have been investigated in atom-molecule collision and electron attachment experiments, respectively. The former has been studied in the collision energy range 14-100 eV whereas the latter in the 0-15 eV incident electron energy range. In the present studies, emphasis is given to the reaction channel resulting in the loss of the methyl group from the N-sites with the extra charge sitting on the pyrimidine ring. This particular reaction channel has neither been approached in the context of dissociative electron attachment nor in atom-molecule collisions yet. Quantum chemical calculations have been performed in order to provide some insight into the dissociation mechanism involved along the N-CH_3 bond reaction coordinate. The calculations provide support to the values derived from the electron transfer measurements, allowing for a better understanding of the role of the potassium cation as a stabilising agent in the collision complex. The present comparative study gives insight into the dynamics of the decaying transient anion and more precisely, into the competition between dissociation and auto-detachment.

4.1.1. Introduction:

In the context of radiation damage to biologically relevant systems, gas-phase dissociative electron attachment (DEA) studies have thoroughly shown that radiation-induced damage to DNA, along with its ensuing long-term biological consequences, can be attributed to underlying fundamental physical and chemical degradation mechanisms. These processes occur during the initial stages of the

interaction between the radiation and the molecules that constitute the biological environment [1,2]. Along the ionisation track, for each 1 MeV of incident primary radiation an estimated amount of ~5×10^4 low energy electrons (< 20 eV) are produced [3]. These electrons are indeed the most abundant secondary species formed in the interaction of radiation with the biological environment. Subsequent electron capture processes produce considerable damage in isolated nucleobases [4-8], nucleosides [9-11] and even DNA adsorbed on surfaces[1,2,12]. Studying molecular constituents of DNA in the gas-phase, while still a very distant picture from what effectively happens in the physiological environment, can act as a stepping stone towards constructing increasingly encompassing models that are able to explain and predict the real extent of the damage that (non-)ionising radiation imposes upon biological environments. Within this context, the study of methylated variations of thymine and uracil may be perceived as a first step in studying how nucleobase moieties behave when in a molecular DNA framework, rather than in an isolated state. Therefore, the study of these molecules may be considered as one step in expanding the studies from isolated bases to more biologically relevant attuned molecules.

Another major issue regarding the study of ionising radiation effects pertains to the more exact nature of the electron capture process, either originating from a free or bound electron, by the (bio) molecular target. Indeed, most of the electron-induced dissociation studies have been performed by interaction with free electrons. However, while electrons are indeed a major secondary product of ionising radiation, these result from the ionisation of atoms and molecules or are released from their solvated and/or pre-solvated stages within the physiological environment [13,14]. As such, the study of electron transfer processes in atomic collisions with these molecular targets can provide valuable information since the presence of the electron donor can greatly affect the chemical pathways of the reaction.

The present studies focus on the fragmentation channel leading to the loss of a methyl radical triggered by electron transfer in neutral atom-molecule interactions and DEA experiments, briefly represented as:

$$K + MP \rightarrow [K^+(MP^-)]^* \rightarrow K^+ + (MP\text{-}CH_3)^- + CH_3$$
$$e^- + MP \rightarrow (MP^-)^* \rightarrow (MP\text{-}CH_3)^- + CH_3$$

where K stands for a potassium atom and MP a methylated pyrimidine that is either 3-methyluracil (3meU) or 1-methylthymine (1meT). The threshold of anion formation can be obtained from the analysis of mass spectra collected at different collision energies around a particular appearance energy and the possible pathways yielding such fragment negative ion, are proposed by taking advantage of the information provided with the help of the theoretical computations. As far as authors are aware, the mass spectrometric detection of the demethylated anion has never been reported for the presently studied molecules.

Due to the nature of the electron transfer process, and in contrast to free electron attachment studies, the energy of the transferred electron is not precisely fixed and much less known. Generally speaking, the "available" energy for the transferred electron is dictated by the collision energy in the centre-of-mass frame, meaning that it may be anywhere between ~0 eV and that provided by the collision, as long as that energy matches the energy of a particular unoccupied molecular orbital of the target. As such, any resonance above this value is inaccessible. This may hold at collision energies where only the lowest neutral and ionic states are involved [15], which has been recently reported for selective site- and bond-cleavage in potassium collisions with pyrimidine bases of DNA [16].

4.1.2. Experimental setup:

The experimental set-up used in the present studies has already been reported for other pyrimidine related targets [17,18]. Briefly, in the Lisbon laboratory, a hyperthermal neutral potassium beam was formed by accelerating K^+ ions from a source and forcing them to pass through an oven where they resonantly charge exchange with thermal potassium atoms, thereby yielding a neutral hyperthermal potassium beam with an estimated energy resolution of ± 0.5 eV and currents in the order of the pA range for lower energy beams (typically 1pA for 20 eV collision energy). The neutral beam encountered an effusive molecular target in the collision region and upon electron transfer the fragment anions produced were extracted into a Time-of-Flight (TOF) spectrometer and mass analysed. Before reaching the collision area, the neutral potassium beam was monitored by a Langmuir-Taylor ionisation detector, before and after the collection of each mass spectrum. Mass calibration was carried out on the basis of the well-known anionic species formed after potassium collisions with nitromethane molecule [19]. The extraction region and the TOF system were heated to approximately 393 K throughout measurements in order to prevent any sample condensation and thence charge accumulation on the electrodes. The spectra collected at each collision energy showing the recorded anionic signals, were obtained by subtracting the background signal from the sample signal.

In the Innsbruck experiment, a molecular effusive beam of 1-methylthymine and 3-methyluracil molecules was formed by vaporization of the powder in an electrically heated oven kept in vacuum. The effusive beam of isolated molecules was crossed with an electron beam either in a standard Nier-type ion source [20] or in the collision chamber of an electron monochromator[5]. For the former ion source, the electron current used was about 10 μA with a resolution of about 1 eV (FWHM). Anions formed were accelerated by 6 kV into the mass spectrometer. After passing a first field-free-region (FF1), anions were analysed by their momentum in a magnetic sector and entered a second field-free-region (FF2). Subsequently anions were analysed by their kinetic energy in an electric sector. The mass and energy analysed anions were detected finally by a channeltron type secondary electron multiplier. In the monochromator setup, the electron current was about 15 nA with

a resolution of about 100 meV. Anions formed were extracted by a weak electric field into a quadrupole mass spectrometer and detected by a channeltron type secondary electron multiplier. The temperature used to evaporate the molecules in the oven was about 330 K (sector field mass spectrometer) and 370 K (electron monochromator), respectively.

The 3-methyluracil (3meU) and 1-methylthymine (1meT) solid samples used in the present experiments were purchased from Sigma-Aldrich with a minimum purity of ≥99%. They were used as delivered. The samples were heated to 400 K in the Lisbon experiment. In order to test for thermal decomposition products in the target beam, mass spectra were recorded at higher temperatures (up to 440 K) at the highest collision energy, i.e. 100 eV for 1meT and 50 eV for 3meU. The ratios between the main fragmentation products appeared unaltered. However at lower temperatures we were limited by the number density of vapored molecules, which unable any reasonable mass spectra collection.

4.1.3. Theoretical methods:

The theoretical computations and results presented in this paper are aimed at describing possible pathways that lead to the demethylated negative ion fragments, upon electron attachment to the target molecules, 1meT and 3meU. To this purpose, estimates of the relevant temporary anion states need to be considered. As shown in a series of studies by the group of Burrow *et al.* [21], such anion states and the associated vertical attachment energies (VAE) can be predicted in terms of the Koopmans' theorem [22] by calculating the virtual orbital energies (VOE) of the neutral ground state molecule [21,23]. However, VOEs are known to be incorrect in an absolute sense. Hence, empirical scaling functions have been established for certain kind of orbitals (i.e. π^* and σ^* virtual orbitals) to agree with experimental VAE measurements in a group of related compounds, yielding the scaled VOEs (SVOE) for these type of orbitals [24,25].

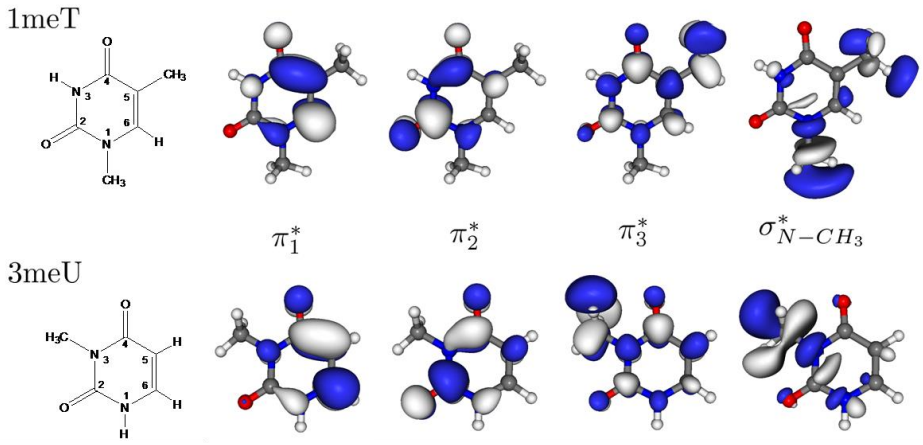

Figure 4.1Structure and virtual orbitals of π* character as well as of σ* character along the N-CH_3 coordinate of the neutral 1meT and 3meU molecules obtained at the HF/6-31G* level of theory.

Thus, following the protocol of Burrow *et al*. [21], 1meT and 3meU have been optimized in their neutral electronic and vibrational ground state at the Hartree-Fock level of theory using the double zeta basis set 6-31G(d). The structure and virtual orbitals that are of interest during the demethylation process in 3meU and 1meT, respectively, are depicted in Fig. 4.1 and their SVOEs are listed in Table 4.1. In Figs. 4.2 and 4.3, the potential energy curves (PECs) of these same orbitals are plotted along the N-CH_3 stretching coordinate. The SVOE for the π^*_1-π^*_3 orbitals are then calculated in electron volts (eV) according to $SVOE_{\pi^*} = 0.753\ VOE - 1.968$[26], whereas the scaled $\sigma^*_{N\text{-}CH3}$ orbital energy has been obtained as $SVOE_{\sigma^*} = 0.9\ VOE - 2.55$[27].

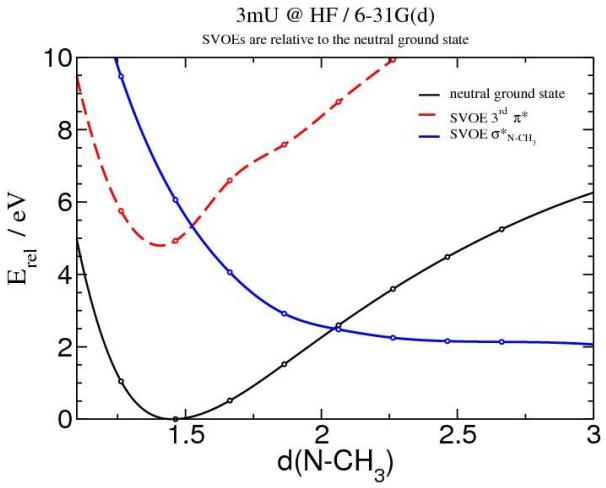

Figure 4. 2. Plot of the 3meU SVOEs for the second and third π* orbitals (red) as well as of the σ* orbital (blue), presented in Fig. 4.1, along the N-CH_3 stretching coordinate relative to the neutral ground state energy (black). VOEs and ground state energy have been obtained at the HF/6-31G* level of theory; scaling of VOEs has been done according to description in text.

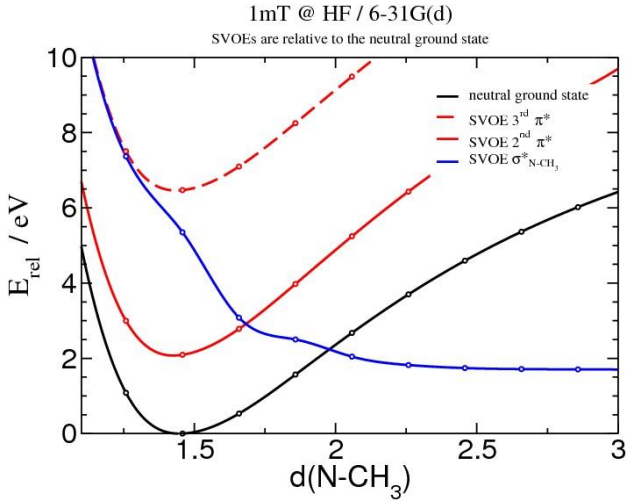

Figure 4. 3 Plot of the 1meT SVOEs for the second and third π* orbitals (red) as well as of the σ* orbital (blue), presented in Fig. 4.1, along the N-CH_3 stretching coordinate relative to the neutral ground state energy (black). VOEs and ground state energy have been obtained at the HF/6-31G* level of theory; scaling of VOEs has been done according to description in text.

In order to estimate possible pathways during the demethylation of both 1meT and 3meU, the SVOEs for the π* and σ* orbitals have been computed along the demethylation coordinate, that is the 1N-CH_3 distance and the 3N-CH_3 bond distance for 3meU and 1meT, respectively (see Figs. 4.2 and 4.3), relative to the neutral ground state energy. For both molecules, a one-dimensional grid of 11 points using different N-C distances between 1.058 Å and 3.058 Å for 1meT (1.063 Å and 3.063 Å for 3meU) with a step size of 0.2 Å have been calculated at the HF/6-31G(d) level of theory. The rest of the molecule's framework has been kept frozen at the optimized geometry. For each point on the resulting unrelaxed grid, the relevant wave function characters for the π^*_1-π^*_3 and $\sigma^*_{N\text{-}CH3}$ orbitals have been followed, and SVOEs have been obtained according to the estimation procedure described above. The calculated values, relative to the ground state energy, have been connected using a cubic spline to give a final grid of 1024 points along the dissociation coordinate. Hence, within the Koopmans' theorem, the resulting curves can be considered as an estimation for the diabatic π^* and σ^* anion states for the target molecules.

Compound	π_1*	π_2*	π_3*	σ*(N-CH_3)
3meU	0.40	1.94	5.39	6.06
1meT	0.48	1.91	5.58	5.35

Table 4. 1 Scaled virtual orbital energies (SVOEs) from HF/6-31G* calculations for the optimized neutral equilibrium molecules (see Fig. 1), in eV.

	Available energy (eV)	
Collision energy in the lab frame (eV)	3meU	1meT
14.0	5.2	5.5
14.5	5.5	-
15.5	6.2	-
19.0	-	9.0
30.0	16.0	-
50.0	29.6	-
100.0	-	66.1

Table 4. 2. Available energies for the different collision energies in potassium molecule experiments.

However, it has to be noted that the scaling functions used have been established to agree with experimental VAEs, which are a measure of the electron attachment energy into a virtual orbital around the ground state minimum geometry. Here, we are considering a significant distortion from

that minimum, and hence we cannot be sure if the scaling function is still correct for long N-C distances as it is well known that the computational error of the Hartree-Fock method increases during the description of dissociation processes. Nevertheless, we believe that the obtained curves serve well for a quantitative interpretation of the initial electron attachment (around the ground state minimum) and a qualitative good estimation for the dissociation pathways. All calculations on 1meT and 3meU have been carried out using the GAUSSIAN09 program package[28].

4.1.4. Results and discussion:

4.1.4.1 Electron transfer in potassium-molecule collisions:

De-methylated 3-methyluracil $(3meU\text{-}CH_3)^-$

Fig. 4.4 shows the section ranging from m/z 100 to 130 of a complete TOF mass spectrum (not shown here) of the negative ions formed in the collision of potassium atoms with 3meU. In order to infer on the role of the resonances and the collision dynamics, a set of measurements solely dedicated to studying the $(3meU\text{-}CH_3)^-$ formation were performed, varying the collision energy from 14 eV (5.2 eV available energy) up to 50 eV, vastly above the threshold yielding this anion (see Table 4.2 for the list of available energies for the different K + MP systems). The dominant fragments are the dehydrogenated parent anion (m/z 125), the de-methylated parent anion (m/z 111) and CNO^- (m/z 42). However, of these three fragments, only the dehydrogenated parent anion is present for all collision energies. This is not surprising, given that the formation of this fragment has been assigned to initial access of a π^* state at ~1.8 eV [21], which is lower than 5.2 eV, corresponding to the available energy for K+3meU system (14 eV in the lab frame). In contrast, since CNO^- and $(3meU\text{-}CH_3)^-$ yields are significantly lower for 14 eV, it stands to reason that the threshold for formation of both these channels may lie close to the corresponding available energy (i.e. 5.2 eV). Indeed, the 14 eV mass spectra in Fig. 4.4 shows the presence of $(3meU\text{-}H)^-$ but no traces of $(3meU\text{-}CH_3)^-$ which is not discernible from the background baseline. However, for 14.5 eV collision energy (~5.5 eV available energy), formation of $(3meU\text{-}CH_3)^-$ is accessible. This means that $(3meU\text{-}CH_3)^-$ threshold lies between 5.2 and 5.5 eV. Furthermore, it is interesting to note that, for increasing energies, $(3meU\text{-}CH_3)^-$ formation increases, which is rationalized in terms of available energy enabling an increase access to the full width of the resonance profile. In other words, for an available energy of 9 eV, all of the resonance width may become accessible, whereas for 6 eV only a fraction of the resonance is attainable. Deriving the threshold from the branching ratios turns out to be not possible since, much like $(3meU\text{-}CH_3)^-$ and CNO^- formation are both open at similar thresholds. As such, the branching ratios will not provide the correct information.

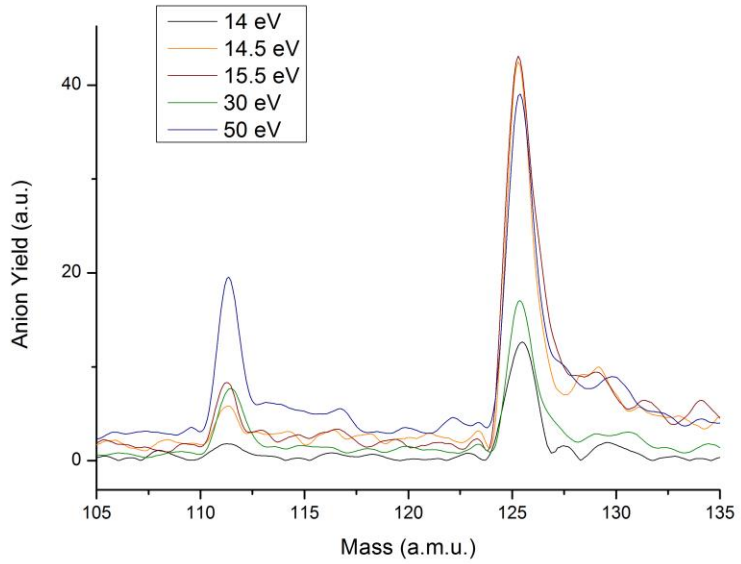

Figure 4. 4 Negative ion TOF mass spectra for potassium collisions with 3meU at 14, 14.5, 15.5, 30 and 50 eV in the lab frame. Arbitrary units result from the anionic signal divided by the potassium beam current and accumulation time.

A sole study of the experimental data presented herein is, by itself, not able to provide any insight to which mechanism(s) is (are) responsible in the formation of this fragment anion. Theoretical computations of the LUMOs in the ground state were performed in order to help finding the electron densities that ultimately lead to bond breaking upon electron capture. In particular, some of the computed LUMOs were also plotted along the 3N-CH_3 coordinate, as presented in Fig. 4.2. At this point, it is worth stressing that these LUMOs were calculated taking into account solely the neutral ground state of the molecule, i.e. no electronic excited or anion states were considered. As such, no information regarding core-excited resonances can be obtained through the present computations.

From Fig. 4.2, a vertical transition to the third π* state leads to a transition from the neutral ground state of roughly the same energy as the one obtained in ion-pair formation measurements, which supports accessing a shape resonance. Furthermore, resorting to Fig. 4.2, a highly antibonding σ* state may be achieved at an energy of ~5.8 eV, which crosses with the aforementioned π* state. This crossing lends support to the proposed pathway of an initial capture to the π* state and subsequent intramolecular electron transfer to the σ* state, leading most likely to dissociation along the N_3-CH_3 bond, which results in the formation of a demethylated anion $(3meU\text{-}CH_3)^-$ and a neutral methyl group. This assumption holds as long as the nuclear wavepacket (on the π* configuration) survives long enough to diabatically couple with the repulsive σ* state. Another mechanism is the direct access to this σ* state. This alternative implies a slightly higher value in vertical electron affinity than the previous pathway and owing to technical reasons, the beam resolution is not enough to unambiguously state which of these pathways is actually accessed.

De-methylated 1-methylthymine $(1meT\text{-}CH_3)^-$

Fig. 4.5 shows the negative ion formation ranging from m/z 105 to 150 from a TOF mass spectrum (not shown here) recorded for 14, 19 and 100 eV potassium collision energies with 1-methylthymine (1meT) in the lab frame. In Table 4.2 a list of the corresponding available energies is presented. In contrast to 3-methyluracil, the demethylated fragment can result from abstraction of the methyl group either from the 1N or the 5C positions.

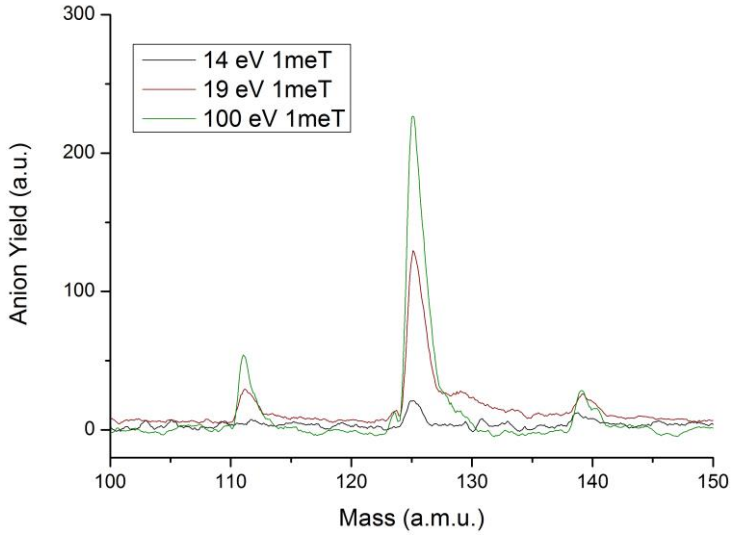

Figure 4. 5 Negative ion TOF mass spectra for potassium collisions with 1meT at 14, 19 and 100 eV in the lab frame. Arbitrary units result from the anionic signal divided by the potassium beam current and accumulation time.

In a recent work on potassium-thymine collisions [17], we observed the demethylated parent anion, albeit with a much lower intensity in comparison with the dehydrogenated parent anion. In 1meT, this fragment is greatly enhanced when compared with the dehydrogenated parent anion, therefore indicating that the majority of the yield stems from CH_3 abstraction from the 1N position. A close inspection of Fig. 4.5 shows that while at 14 eV there is only a weak evidence of the demethylated parent anion, as the energy is increased its relative yield becomes higher. This indicates that the threshold for formation of this fragment lies very close to 14 eV, which corresponds to ~5.5 eV available energy in the centre-of-mass of the 1meT + K system. From a different point of view, the mechanism yielding such anion formation can be rationalised in terms of the accessible LUMOs (Fig. 1). As such, and following the same procedure as for 3meU, plotted in Fig. 4.3 are the accessible π^* and σ^* states, the latter being dissociative along the 1N-CH_3 bond. A close observation of this figure, and taking into account the fragmentation yields in Fig. 5, leads to two possible mechanisms regarding $(1meT\text{-}CH_3)^-$ formation: a) the electron is initially transferred to the π_3^* state and subsequently to the

σ* state, which then results in dissociation; or b) direct initial transfer to the σ* state and subsequent dissociation. As in the case of 3meU, the closeness of the vertical transition energies for both states does not allow us to precise which pathway is actually followed, although it is very likely that both should end up in a dissociation through the σ* state.

Finally, formation of the demethylated parent anion in 1meT could initially be considered to progress along the same pathway as H abstraction from the 1N site in thymine. As has already been shown in free electron attachment studies, H abstraction from the 1N position in thymine (and uracil) proceeds through a Vibrational Feshbach Resonance (VFR) of the dipole-bound anion state, followed by a tunnelling through the potential barrier formed by an avoided crossing between the dipole-bound anion and the lowest dissociative σ* valence state [21,23]. However, methyl abstraction from 1meT through this mechanism is most likely not possible to occur. Due to the presence of the methyl group, the aforementioned σ* is greatly suppressed along the 1N-CH_3 coordinate thereby inhibiting this fragmentation pathway. In addition, the higher mass of the methyl group, in comparison to the hydrogen atom, will lead to much less efficient tunnelling, as was shown recently in the case of deuteration [29]. Regardless, this is in agreement with the relative quite small yield of the demethylated parent anion appearing below 14 eV collision energy (~5.5 eV available energy). Worth mentioning that such assignment may also accommodate the loss of CH_4. However, the calibrations performed for the mass assignments point out systematically to the loss of a CH_3. This would benefit in the future from isotopic labelling. One final issue regarding Fig. 4.5 pertains to the presence of a mass peak assigned to m/z 110 which, due to its broadness and the modest resolution of the TOF mass spectrometer, could also be attributed to m/z 111. Notwithstanding, we do not discard the possibility that this peak may accommodate both anions. Assignment of m/z 111 will most likely consist in the abstraction of C_2H_5, whereas for m/z 110 to C_2H_6 loss. Assuming that these neutral hydrocarbon species are formed from the loss of both methyl groups, m/z 110 would therefore correspond to the abstraction of these two groups, whilst m/z 111 would require a considerable internal rearrangement in the precursor TNI. A more thorough set of calibrations were performed, which tended to point out to the abstraction of C_2H_6.

Another alternative assignment would lead m/z 110 and m/z 111 to $COH_2$and COH abstraction, respectively. However, in a previous potassium electron transfer study to thymine[17], we notice a small contribution that corresponds to abstraction of the methyl group from the C5 position (m/z 111), which in the present experiment is an indicative that the feature at m/z 110/111 is due to the loss of two methyl groups.

Regardless, since the present calculations are far beyond the scope of this contribution, such assignment would benefit from further investigation. As far as neutral species are concerned, we have no information on their molecular structure.

4.1.4.2 Dissociative Electron Attachment (DEA) measurements:

In addition to the potassium-molecule collisions experiments performed in the Lisbon laboratory, dissociative electron attachment (DEA) experiments to 1meT and 3meU were performed in the Innsbruck laboratory regarding the loss of a CH_3 group. Remarkably, also one mass below $(MP\text{-}CH_3)^-$ abundant ion signal is observed, i.e. CH_4 abstraction from both 1-meT and 3-meU occurs upon free electron capture. In previous DEA experiments with thymine, the loss of CH_3 and CH_4 was not observed within the detection limit of the setups used [30] and for 1meT and 3meU this reaction channel was not yet reported. The corresponding anion yields as a function of the incident electron energy investigated here for 1meT and 3meU are presented in Fig. 4.6.

Anion formation $(3meU\text{-}CH_3)^-$ & $(3meU\text{-}CH_4)^-$

The anion efficiency curve of $(3meU\text{-}CH_3)^-$ (m/z 111) is shown in Figure 4.6a) measured with the Nier type ion source (energy resolution ~1 eV). Three resonances are observed; the first and most abundant one at ~1.8 eV and two more at ~4 eV and 10.5 eV. The first resonance at 1.8 eV we ascribe to an impurity of the 3meU sample by uracil. DEA studies for uracil have shown that H abstraction from the N_3 site involves a shape resonance at 1.8 eV[31], consisting of an initial occupation of the second π* orbital, followed by an intramolecular electron transfer to the second σ* orbital, which is known to be highly dissociative along the 3N-H stretching coordinate [21,23,31]. We have measured the ion yield shown in Figure 4.6a) also with an energy resolution of about 100 meV utilizing the electron monochromator which allows resolving a sharp vibrational Feshbach resonance observed at 1 eV for uracil and the intensity of the 1.8 eV resonance matches perfectly with that of uracil (U) (not shown). Based on the assumption of the same DEA cross sections for $(U\text{-}H)^-$ and $(3meU\text{-}H)^-$ [31] at 1.8 eV, we obtain a sample contamination of about 0.7% with uracil. The assignment of the 1.8 eV resonance to an impurity is further supported by the PEC's for 3meU shown in Figure 4.2. The thermodynamic threshold for $(3meU\text{-}H)^-$ formation (corresponding to the energy difference between the minimum of the potential energy curve for the neutral ground and the asymptote of the anionic $\sigma^*_{N\text{-}CH3}$ potential energy curve) is about 2.1 eV and hence considerably above the experimental resonance position. Therefore, only the two resonances at higher energies (~4 eV and 10.5 eV) can be ascribed to form upon electron attachment to 3meU. The 4eV resonance can be identified by means of the present SVOE calculations: since population of the third π* orbital requires electrons with a kinetic energy of more than ~5.3 eV (i.e., 1.3 eV above the DEA resonance maximum), we rather ascribe the dissociation to a direct decomposition process via the purely repulsive second σ* orbital. It should be noted that the corresponding SVOE at equilibrium distance is about 6 eV. However, this value would correspond to a DEA peak position with neglecting of any autodetachment from the temporary negative ion during dissociation. When including autodetachment, the DEA resonance will

considerably shift to lower energies [32]. At this point it is critical to note that the accuracy of the calculation of the SVOEs has not been tested thoroughly from an experimental point of view, and as such, these calculations are used in order to provide a tentative assignment between the resonances and the occupied states. The second resonance likely involves a core excited resonance or Rydberg excitation. The lowest electronically excited state of neutral thymine in the gas phase was found at about 3.60 eV and was ascribed to a $\pi \rightarrow \pi^*$ transition [33]. As mentioned above, core excited resonance are not included in the present calculations.

Regarding loss of CH_4, a broad asymmetric resonance is observed, with a threshold at about 4.0 eV, centred at ~7.0 eV and with a yield almost one order of magnitude lower than CH_3 abstraction (see Figure 4.6b). The formation of $(3meU\text{-}CH_4)^-$ requires breaking the N–CH_3 bond and a loss of a hydrogen atom. The resonance maximum is 3 eV lower than the high-energy resonance for CH_3 loss, i.e. a different electronic state of the temporary anion is likely involved. We note that the resonance position is very close to the most abundant peak in the anion yield of CNO^- formed upon DEA to thymine [30]. In the case of electron capture by a pyrimidine base, CNO^- is formed in a two-fold cleavage of the ring and a loss of at least one hydrogen atom from the nitrogen sites. Upon methylation of the N3 position, CNO^- becomes considerable quenched relative to single hydrogen loss: the ratio $(M\text{-}H)^-/CNO^-$ changes to about 12:1 compared to 5:1 for standard thymine [4]. Moreover, the resonance at about 6.8 eV is completely quenched for 3meT [34]. It is likely that both anions, $(M\text{-}CH_4)^-$ and CNO^-, are formed through the same electronic state of the temporary negative ion (TNI) state which is at this electron energy likely a core excited state of the TNI initiating a complex decomposition process including possible molecular rearrangement of the precursor ion.

Concerning the dissociation dynamics, we point out that the H abstraction is about a factor of 4 faster than CH_3, i.e. formation of $(3meU\text{-}CH_4)^-$ can be viewed as a sequential dissociation process, where initially an H is abstracted, followed by the methyl group. Indeed, this fact is supported by a previous study of DEA to thymine embedded in helium droplets, performed in the Innsbruck laboratory, showing that H abstraction is a dissociation intermediate of all other fragments [35]. Fast evaporative cooling in the helium droplet thereby allowed freezing of slow decomposition reactions while $(M\text{-}H)^-$ is formed exclusively due to a fast decomposition along a purely repulsive state of the TNI.

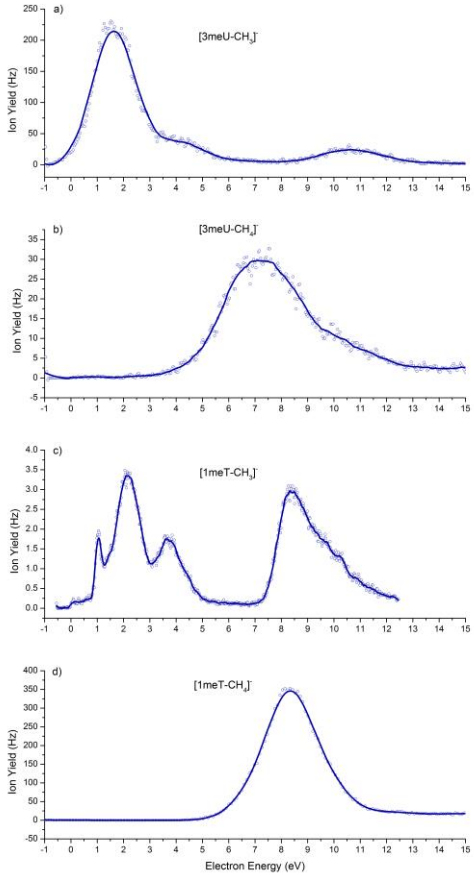

Figure 4. 6 DEA resonance profiles for formation of a) $(3meU\text{-}CH_3)^-$, b) $(3meU\text{-}CH_4)^-$, c) $(1meT\text{-}CH_3)^-$ and d) $(1meT\text{-}CH_4)^-$. Measurements shown in a), b) and d) were derived utilizing the Nier type ion source (energy resolution ~1 eV) while for c) the electron monochromator was used (resolution ~0.1 eV).

$(1meT\text{-}CH_3)^-$ & $(1meT\text{-}CH_4)^-$

The anion efficiency curves for $(1meT\text{-}CH_3)^-$, m/z 125, & $(1meT\text{-}CH_4)^-$, m/z 124, dissociation channels are shown in Figs. 4.6c) and 4.6d). The anion efficiency curve for loss of CH_4 consists only of a single resonance centred at ~8.2 eV. We refer again to the ion yield of CNO^- from thymine which shows a resonance at the same energy [30]. The resonance at ~8.2 eV becomes completely suppressed in the CNO^- ion yield when thymine is methylated at 1N position [34]. Instead $(1meT\text{-}CH_4)^-$ is particularly intense at this resonance energy which follows that after initial H-loss further ligand loss is favoured against ring cleavage. Remarkably, the loss of H + CH_3 in the 1meT anion is more intense than H + H loss in the thymine anion (the difference is a factor of ~16 relative to the corresponding dehydrogenated anion). In the case of twofold hydrogen loss from thymine, the main resonance at high electron energies was found to be at ~7.3 eV. Measurements with partially deuterated thymine showed that this resonance is formed by hydrogen loss from N_1 and N_3 [36]. In case of simple (isolated) bond

cleavage reactions, one would expect a red-shift of the peak position as well as a lower DEA cross section due to increased autodetachment for the loss of H + CH_3. Since both are not observed, we ascribe $(1meT\text{-}CH_4)^-$ to be formed in a complex decomposition process including electronically excited states that are likely to be involved. Methylation alters strongly the relative abundance of the decomposition products formed by this resonant state of the precursor anion.

In contrast to $(1meT\text{-}CH_4)^-$ and the 3meU molecule, $(1meT\text{-}CH_3)^-$ is not formed in a resonance at higher electron energies; and the ion yield relative to $(1meT\text{-}CH_4)^-$ is much weaker than in the case of 3meU. The apparent resonance at ~8.2 eV (see Fig. 4.6c) can be ascribed to ^{13}C isotope contribution of $(1meT\text{-}CH_4)^-$ since the abundance is in perfect agreement with the calculated one. Further, $(1meT\text{-}CH_3)^-$ shows low energy resonances at about 1, 2.1 and 3.7 eV. Based on the calculations of the potential energy diagram for the N-CH_3 reaction coordinate in Fig. 3, we may assign the resonances in the following way. The first resonance at about 1 eV arises likely from an impurity since the thermodynamic threshold for production of $(1meT\text{-}CH_3)^-$ is ~1.7 eV (see Fig. 4.5) and thus above this resonance. The narrow resonance may indicate spurious contamination of the sample with standard thymine (T), since $(T\text{-}H)^-$ with the same nominal mass like $(1meT\text{-}CH_3)^-$ is formed (like uracil) in an intense VFR at 1eV [21]. In DEA to thymine $(T\text{-}H)^-$ has also a resonance at ~ 1.8 eV with about half of intensity of the 1 eV peak. Therefore and in contrast to 3meU, about 70% of the ion yield at the resonance close to 2 eV can be ascribed to result from demethylation of 1meT. The SVOE of the π_2^* orbital is at 1.92 eV, i.e. within the accuracy of experiment and calculations, we assign the dissociation process to initial occupation of the π_2^* orbital (see Fig. 4.3) which couples with the repulsive $\sigma^*_{N\text{-}CH3}$ orbital. The initial occupation of this orbital can be assumed to have a significant overlap with the $\sigma^*_{N\text{-}CH3}$ orbital responsible for the bond break. We note that the thermodynamic threshold for dissociation via $\sigma^*_{N\text{-}CH3}$ orbital is 1.7 eV which allows appearance of this resonance, which is likely not the case for 3meU with a threshold of 2.1 eV. The slightly less abundant peak at 3.9 eV may be explained analogously to the 3meU case, i.e. direct dissociative electron capture into the $\sigma^*_{N\text{-}CH3}$ orbital since the π_3^* orbital is only accessible above 5.6 eV.

4.1.4.3.Dissociative Electron Attachment vs ion-pair formation:

An issue that is interesting to discuss pertains to the difference between the fragmentation obtained through ion-pair formation and DEA experiments. It is therefore important to highlight a major difference between both set of experiments. This difference revolves around the intrinsic property of the potassium cation post-collision to suppress electron ejection from the temporary negative ion [17]. Indeed, this autodetachment suppression mechanism not available in DEA has been shown to play an important role in electron transfer experiments with nitromethane, as well as in thymine and uracil. In the case of nitromethane, the formation of the parent anion was observed upon electron transfer which is only possible by a suppression of the rejection of the extra electron for a

time long enough to allow the reaction channel beyond a point where a transition back to the neutral ground state is no longer possible. In contrast, no parent anion was detectable in free electron capture by nitromethane. In thymine and uracil, CNO^- formation in potassium collisions is the dominant channel [17], in contrast to DEA studies where CNO^- only makes up approximately 25% of the total anion yield [4.8]. It was recently proposed that, since the lifetimes of the resonances responsible for this channel are significantly finite, a successful competition with autodetachment is required. This is accomplished by the presence of the potassium cation [17]. For the case of a metastable transient negative ion, there must be enough time for intramolecular energy distribution through the different available degrees of freedom, yielding a different fragmentation pattern.

For the presently studied methylated compounds we derive that in electron transfer reactions: i) no CH_4 abstraction fragment is obtained; ii) the demethylated parent anion is obtained and, given that the energy threshold for CH_3 abstraction channel lies at ~5.2 eV, it is very possible that this dissociation pathway consists of an initial electron transfer to one of the σ* or π* orbitals presented in Fig. 4.1. On the other hand, in DEA no resonance with a threshold at 5 eV is observed while CH_3 abstraction is obtained in a resonance close to 4 eV. The latter energetic difference in the ion yields of DEA and electron transfer is a direct consequence of the substantially lower autodetachment rate due to the presence of the potassium cation in the collision complex. For example, the ratio of demethylated/dehydrogenated parent anion (the latter being less affected by autodetachment) amounts in DEA to about 0.6 % for 1meT and about 0.1 % for 3meU while in electron transfer these ratios do not hold. Thus the present results show a remarkable modification on the dissociation process due to potassium (K^+) acting as a stabilizing agent. Compared to an isolated temporary negative ion formed by free electron capture, the anion in the vicinity of a potassium ion favours dissociation rather than autodetachment. We also note that the above mentioned nitromethane case is related to a (metastable) state of the parent anion and CNO^-formation in thymine and uracil represents a rather slow complex dissociation process including rearrangement. In contrast, the demethylation channel studied here is a simple bond cleavage reaction occurring on (much) faster timescale than rearrangement reactions or stabilization of the parent anion. For simple bond cleavage reactions, one may expect *a priori*, that autodetachment play a less important role than in the case of time consuming reactions which is however not necessarily the case as shown here.

In addition, the presence of the potassium cation post-collision changes the structure of the molecular anion that may also lead to the difference in the formation of $(MP\text{-}CH_4)^-$ completely absent as product from electron transfer collisions. As mentioned above this anion is formed at the same resonance energy as CNO^- which remains an abundant product in electron transfer collisions while in DEA the channel is quenched.

4.1.4. Conclusions:

In the work presented here we have investigated negative ion formation in N-site methylated pyrimidine derivatives (3meU and 1meT) through atom-molecule collisions, in particular the anionic fragment that results from abstraction of a methyl group from 3meU and 1meT. Additionally, DEA experiments were also performed, with an emphasis on obtaining the ion yields resulting from the CH_3 and CH_4 abstraction in both 3meU and 1meT. The interpretation of the experimental data $(MP\text{-}CH_3)^-$ was complemented with quantum chemical calculations that allowed for the assignment of some of the obtained resonances to the possible initial occupation of σ^* and π^* orbitals under the assumption that no electronic excitation occurs. This objective was only partially achieved due to the small energy differences of these orbitals inside the Frank-Condon region and the limited energy resolution of the neutral potassium beam. However, generally speaking, the proposed pathways seem to be reasonable to explain the observed fragmentation.

We may also compare the present results for 1meT with the nucleoside thymidine where the nucleobase and sugar moiety are linked at the 1N site by the glycosidic bond. A previous DEA study to thymidine indeed reported the glycosidic bond cleavage [9]. The resulting ion yield of the negatively charged thymine moiety showed lower-energy resonances below 3 eV as well as two resonances at 6.6 eV and 7.8 eV. While the lower-energy resonances (< 3 eV) were mostly shown to result from DEA to the thermal decomposed products (with the exception of a small contribution at virtually no energy which was ascribed to an impurity [9]), the higher energy features are indeed due to DEA to the pristine molecule [9]. Since here we observe for $(1meT\text{-}CH_3)^-$ only low energy resonances and no high energy resonance, the DEA channel leading to the 1N-C bond cleavage becomes substantially modified when going from the methylated nucleobase to thymidine. This indicates the limitation of the present molecules as model compounds for nucleosides at least for DEA. In contrast, a recent study on esterification of aminoacids has shown that methylation in the carboxyl group, in comparison to esterification with larger alkyl groups, does not seem to greatly change the negative fragment ion formation [37].

Finally, one can argue that, given the ability of electron transfer processes to strongly lower autodetachment rates and therefore enhance fragmentation channels, these processes may have a more damaging effect on biological molecules than DEA. In the latter case autodetached electrons will, at most, leave the molecule in a non-dissociative vibrationally excited state.

Acknowledgments

DA and FFS acknowledge the Portuguese Foundation for Science and Technology (FCT-MEC) for post-graduate and post-doctoral scholarships SFRH/BD/61645/2009 and SFRH/BPD/68979/2010, respectively. DA acknowledges the valuable discussions with Dr. Rodrigo Antunes and Eng. Gonçalo Martins. PL-V, FFS and DA acknowledge the strategic grant PEst-OE/FIS/UI0068/2011 and PTDC/FIS/ATO/1832/2012. PL-V and GG acknowledge the support from the Portuguese-Spanish joint collaboration through the bilateral Project HP 2006-0042. This work also

forms part of EU/ESF COST Actions The Chemical Cosmos CM0805 and Nanoscale Insights into Ion Beam Cancer Therapy (Nano-IBCT) MP1002. This work was partially supported by the Fonds zur Förderung der wissenschaftlichen Forschung (FWF, P22665), Wien.

References

[1]. B. Boudaïffa, P. Cloutier, D. Hunting, M. A. Huels, and L. Sanche, Science, 287, 1999(2000).

[2]. F. Martin, P. Burrow, Z. Cai, P. Cloutier, D. Hunting, and L. Sanche, Phys. Rev. Lett., 93, 6–9(2004).

[3]. V. Cobut, Y. Frongillo, J. P. Patau, and T. Goulet, Radiat. Phys. Chem., 3, 229–243(1998).

[4]. S. Denifl, S. Ptasinska, M. Cingel, S. Matejcik, P. Scheier, and T. D. Märk, J. Chem. Phys., 377, 74–80(2003).

[5]. S. Denifl, P. Sulzer, D. Huber, F. Zappa, M. Probst, T. D. Märk, P. Scheier, N. Injan, J. Limtrakul, R. Abouaf, and H. Dunet, Angew. Chem., Int. Ed. Engl., 46, 5238–41(2007).

[6]. I. Baccarelli, I. Bald, F. a. Gianturco, E. Illenberger, and J. Kopyra, Phys. Rep., 508, 1–44(2007).

[7]. E. Alizadeh and L. Sanche, Chem. Rev., 112, 5578-5602(2012).

[8]. S. Denifl, S. Ptasińska, G. Hanel, B. Gstir, M. Probst, P. Scheier, and T. D. Märk, J. Chem. Phys., 120, 6557–65(2004).

[9]. S. Ptasińska, S. Denifl, S. Gohlke, P. Scheier, E. Illenberger, and T. D. Märk, Angew. Chem., Int. Ed. Engl., 45, 1893–6(2006).

[10]. H. Abdoul-Carime, S. Gohlke, E. Fischbach, J. Scheike, and E. Illenberger, Chem. Phys. Lett., 387, 267–270(2004).

[11]. S. Denifl, P. Candori, S. Ptasińska, P. Limão-Vieira, V. Grill, T. D. Märk, and P. Scheier, Eur. Phys. J. D, 35, 391–398(2005).

[12]. S. V. K. Kumar, T. Pota, D. Peri, A. D. Dongre, and B. J. Rao, J. Chem. Phys., 137, 045101(2012).

[13]. L. Sanche, Nature, 461, 358(2009).

[14]. C. Wang, J. Nguyen, and Q. Lu, J. Am. Chem. Soc., 131, 11320–2(2009).

[15]. A. W. Kleyn and A. M. C. Moutinho, J. Phys. B: At. Mol. Opt. Phys., 4075, R1(2001).

[16]. D. Almeida, F. Ferreira da Silva, G. Garcia, and P. Limão-Vieira, Phys. Rev. Lett, 110, 023201(2013).

[17]. D. Almeida, R. Antunes, G. Martins, S. Eden, F. Ferreira da Silva, Y. Nunes, G. Garcia, and P. Limão-Vieira, Phys. Chem. Chem. Phys., 13, 15657–65(2011).

[18]. F. Ferreira da Silva, D. Almeida, R. Antunes, G. Martins, Y. Nunes, S. Eden, G. Garcia, and P. Limão-Vieira, Phys. Chem. Chem. Phys., 13, 21621–9(2011).

[19]. R. Antunes, D. Almeida, G. Martins, N. J. Mason, G. Garcia, M. J. P. Maneira, Y. Nunes, and P. Limão-Vieira, Phys. Chem. Chem. Phys., 12, 12513–9(2010).

[20]. D. Huber, M. Beikircher, S. Denifl, F. Zappa, S. Matejcik, A. Bacher, V. Grill, T. D. Märk, and P. Scheier, J. Chem. Phys., 125, 084304(2006).

[21]. P. D. Burrow, G. A. Gallup, A. M. Scheer, S. Denifl, S. Ptasinska, T. Märk, and P. Scheier, J. Chem. Phys., 124, 124310(2006).

[22]. T. Koopmans, Physica, 1, 104–113(1934).

[23]. A. M. Scheer, K. Aflatooni, G. Gallup, and P. Burrow, Phys. Rev. Lett., 92, 3–6(2004).

[24]. D. Chen and G. A. Gallup, J. Chem. Phys., 93, 8893(1990).

[25]. N. Heinrich, W. Koch, and G. Frenking, Chem. Phys. Lett., 124, 20-25(1986).

[26]. K. Aflatooni, G. A. Gallup, and P. D. Burrow, J. Chem. Phys., 132, 094306(2010).

[27]. K. Aflatooni and P. D. Burrow, J. Chem. Phys., 113, 1455(2000).

[28]. M. J. Frisch, G. W. Trucks, H. B. Schlegel, G. E. Scuseria, M. A. Robb, J. R. Cheeseman, G. Scalmani, V. Barone, B. Mennucci, G. A. Petersson, H. Nakatsuji, M. Caricato, X. Li, H. P. Hratchian, A. F. Izmaylov, J. Bloino, G. Zheng, and D. J. Sonnenb, Gaussian 09, Revision A.1, (2009).

[29]. S. Denifl, P. Sulzer, F. Zappa, S. Moser, B. Kräutler, O. Echt, D. K. Bohme, T. D. Märk, and P. Scheier, Int. J. Mass Spectrom., 277, 296–299(2008).

[30]. S. Denifl, S. Ptasińska, M. Probst, and J. Hrus, J. Phys. Chem. A, 6562–6569(2004).

[31]. S. Ptasinska, S. Denifl, P. Scheier, E. Illenberger, and T. D. Märk, Angew. Chem., Int. Ed. Engl., 44, 6941–6943(2005).

[32]. V. Vizcaino, B. Puschnigg, S. E. Huber, M. Probst, I. I. Fabrikant, G. A. Gallup, E. Illenberger, P. Scheier, and S. Denifl, New J. Phys., 14, 043017(2012).

[33]. R. Abouaf, J. Pommier, and H. Dunet, Chem. Phys. Lett., 381, 486–494(2003).

[34.]F. Ferreira da Silva, C. Matias, D. Almeida, G. Garcia, O. Ingolfsson, H. D. Flosadottir, B. Omarsson, S. Patsinska, B. Puschnigg, P. Scheier, P. Limão-Vieira, S. Denifl, J. Am. Soc. Mass Spectrom., (2013).

[35]. S. Denifl, F. Zappa, A. Mauracher, F. F. da Silva, A. Bacher, O. Echt, T. D. Märk, D. K. Bohme, and P. Scheier, Chem. Phys. Chem., 9, 1387–1389(2008).

[36]. S. Ptasińska, S. Denifl, B. Mróz, M. Probst, V. Grill, E. Illenberger, P. Scheier, and T. D. Märk, J. Chem. Phys., 123, 124302(2005).

[37]. Y. V. Vasil'ev, B. J. Figard, D. F. Barofsky, and M. L. Deinzer, Int. J. Mass Spectrom., 268, 106–121(2007).

Selective bond cleavage in potassium collisions with pyrimidine bases of DNA

D. Almeida [†], F. Ferreira da Silva [†], G. García [‡] and P. Limão-Vieira [†,*]

[†] Laboratório de Colisões Atómicas e Moleculares, CEFITEC, Departamento de Física, Faculdade de Ciências e Tecnologia, Universidade Nova de Lisboa, 2829-516 Caparica, Portugal
[‡] Instituto de Física Fundamental, Consejo Superior de Investigaciones Científicas, Serrano 113-bis, 28006 Madrid, Spain

Published in Phys. Rev. Lett. **110**, 023201 (2013).

Abstract.

Electron transfer in alkali-molecule collisions to gas phase thymine and uracil yielding H– formation is selectively controlled in the energy range between 5.3 and 66.1 eV. By tuning the collision energy, electron transfer from the alkali to partly deuterated thymine, methylated thymine at the N1 and methylated uracil at the N3 positions, H^- loss proceeds not only through the breaking of the (C–H) against (N–H) bonds but also through N1 against N3 sites. Such selectivity, as far as bond and site are concerned, is here reported for the first time by electron transfer induced dissociation experiments in alkali-molecule collisions.

4.2.1. Introduction:

Many investigations during the past century have been devoted to the understanding of the alterations induced by high energy radiation in biological systems, particularly within living cells and the DNA/RNA molecule. The biological effects of such radiation are now known to be essentially produced by the secondary species generated along the radiation track and their subsequent reactions within irradiated cells [1]. These species can cause mutagenic, genotoxic and other potentially lethal DNA lesions [2], such as base and sugar modifications, base release, single strand breaks (SSB), and cluster lesions, which includes a combination of two single modifications, e.g. double strand breaks (DSB) and cross-links. Secondary electrons (SE) are the most abundant of the secondary species produced by the primary interaction [1,2]. The vast majority of these SE are created with energies below 20 eV [1], producing therefore large quantities of highly reactive radicals, cations and anions. These species are found to be more efficient producing degradation than the primary radiation, i.e. they are more reactive. As such, studying chemical reactions for biomolecular systems is relevant to understand radiation induced damage at the molecular level with the uttermost need to develop more efficient radiation therapies.

Molecular reaction dynamics and chemical reactivity have been considerably explored by

different approaches [3], where laser probing techniques have gained a particular relevance during the last decades. Controlling and inducing selectivity of chemical reactions in molecular collisions have been achieved by mode-selective excitation in ultrafast laser pulses [4], by quantum molecular dynamics of photoexcited molecules [5], and in the case of unimolecular reactions through coherent quantum manipulation [6,7]. A tunable soft x ray to stimulate chemical reactions or to selectively break large organic molecules was considered further to site-specific fragmentation of small molecules such as carbon oxide and acetone [8]. Core-electron excitation inducing selective chemical bond scission due to its special localization and selectivity was also used on thin films of organic polymers by soft x rays interactions [9]. Additionally, such reaction control and selectivity have been achieved in inelastic electron tunnelling microscopy [10] and in the gas-phase by site- and bond-specific dissociation through low energy electron interactions [11-14]. Moreover, functional group dependence in dissociative electron attachment (DEA) process leading to site-selective fragmentation of molecules and the possibility of making use of electron energy as a parameter for control chemical reactions, have been reported [15]. Steric effects were shown to enhance reactive scattering in molecular beams with oriented molecules [16], whereas, at room temperature with random molecular orientation, regarding ion-pair formation, such site- and bond-selective dissociation by tuning the proper collision energy has never been reported.

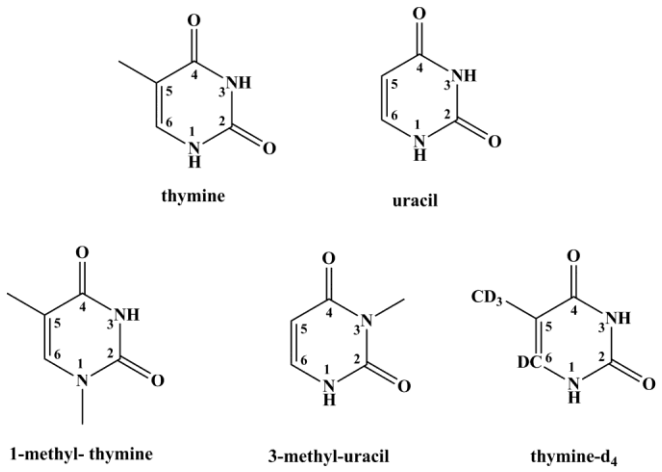

Figure 4. 7 Molecular structure of thymine, uracil, 1-methyl- thymine (1-meT), 3-methyl-uracil (3-meU), and partly deuterated thymine (thymine-d_4).

Similar site selectivity can be expected in any other bi-molecular collisions, including anions [17,18] and neutrals [19], and these processes play certainly an important role in low- temperature plasmas [20] as well as to the chemistry of the upper planetary atmospheres [21].

This also has consequences regarding fast neutral metal atoms being formed when cosmic ray metal ions are neutralized in planetary atmospheres where they subsequently may form anions [21]. Though, many elementary collisional processes depend upon electron transfer mechanisms. In atom-molecule collisions where an electron transfer occurs, a negative ion is formed as part of an

intermediate step or as a final product. The electron transfer process happens when electrons follow adiabatically the nuclear motion in the vicinity of the crossing of the stationary non-perturbed states [22], i.e. the covalent and the ionic diabatic states (from the crossing of the covalent and the ionic diabatic potential surfaces). For simplicity, let us consider a diatomic molecule, although for polyatomics hyperdimensional surfaces must be similarly considered. The ionic surface lies above the covalent surface, the endoergicity at large atom-molecule distances being:

$$\Delta E = IE(K) - EA(AB) \quad (1)$$

where K stands for the potassium atom and AB a molecule. However due to the coulombic interaction there is a crossing point for which both stationary non-adiabatic potential energy surfaces have the same value [22]. During the collision process and near that crossing (R_c), there can be a perturbation of the stationary states induced by the projectile/target nuclear motion leading to an adiabatic coupling. This leads after the collision path to the formation of a positive ion K+ and a molecular temporary negative ion - TNI - allowing access to parent molecular states, which are not accessible in free electron attachment experiments [23,24].

4.2.2. Experimental setup:

The experiments were performed in a crossed atom-molecule beam arrangement consisting of a potassium source, an oven and a time-of-flight (TOF) mass analyser [25]. The components were housed in two high-vacuum chambers at a base pressure of 10^{-5} Pa. A neutral potassium beam at an energy resolution of ~ 0.5 eV (FWHM) generated from a charge exchange chamber intersected orthogonally with an effusive molecular beam consisting of pyrimidine molecules. Atomic K^+ ions, obtained from a potassium ionic source, were accelerated through a chamber containing potassium vapour where they resonantly charge exchanged to form a beam of neutral K fast atoms. The energy of the resultant K neutral beam was established by the initial acceleration of the ions. After charge exchange, the ions that have not been neutralised were removed by electrostatic fields, the resulting neutral K molecular beam was now comprised of two components, a ‘hyperthermal’ beam and an ‘effusive thermal energy’ beam. Since the electron transfer process is endoergic, the thermal beam does not contribute to the formation of anions. The hyperthermal alkali beam entered a high vacuum chamber where was monitored by an iridium surface ionisation detector of the Langmuir–Taylor type. This detector sampled the beam intensity but did not interfere with the beam passing to the collision region. It operates in a temperature regime that only allows detection of the fast beam. The biomolecular target beams were produced in a hot gas cell (oven) and admitted to vacuum by an effusive source through a 1 mm diameter orifice where they were crossed with the neutral hyperthermal potassium beam. At a temperature of about 390 K (measured by a platinum resistance –

Pt100) the density of intact molecules was high enough to yield a reasonable negative-ion signal. The negative ions produced in the collision were extracted by a ~ 250 V/cm pulsed electrostatic field towards the entrance of a TOF where they were analysed and detected in a single-pulse counting mode. The spectra collected at each collision energy showing the recorded anionic signals, were obtained by subtracting the background signal from the sample signal. In potassium-pyrimidine collision studies (Fig. 4.7), the total energy available in the centre-of-mass frame, including potassium ionisation energy (4.34 eV), varies from ~5 up to 66 eV. 1-methyl-thymine (1-meT), 3- methyl-uracil (3-meU) and partly deuterated thymine (thymine-d4) were obtained from Sigma Aldrich with a stated purity 98%, respectively. The samples were used as delivered. Time-of- flight mass spectra of the different anions formed in collisions of neutral potassium atoms with the pyrimidine molecules have been obtained, and a typical TOF mass spectrum of 1- methyl-thymine (1-meT) at 66.1 eV collision energy is depicted in Fig. 4.8.

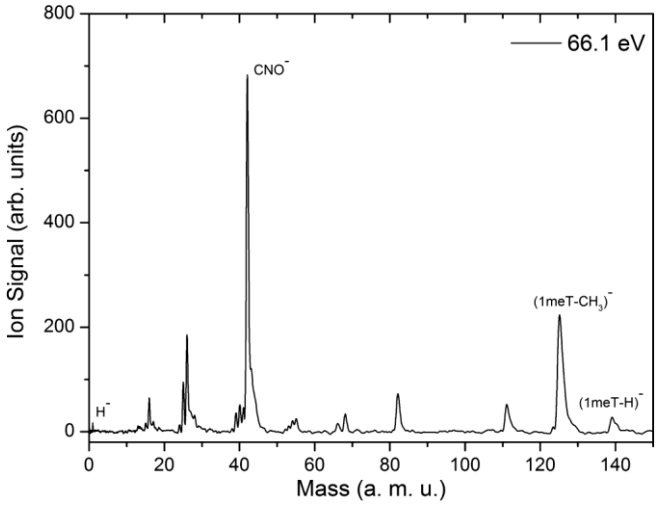

Figure 4. 8. Time-of-flight mass spectrum showing the different anions formed in collisions of neutral potassium atoms with 1-methyl-thymine (1-meT) at 66.1 eV collision energy.

4.2.3. Discussion:

In this Letter we are focusing our attention to the H^-yield only. However, this anion is a product from many other molecules such as water and hydrocarbons that are present in the HV chamber, and in the case of the former, even as moisture in the sample. Thus the spectra in the figures showing the recorded anionic signals were obtained by subtracting the background signal from the sample signal. The ion yields (relative intensity as a function of the collision energy) of $H^-$from 1-meT are shown in Fig. 4.9(a) at three different collision energies. Methylation at the N1 position completely supresses H^- formation in the low-energy collisions, i.e. at 7.6 eV, whereas at higher energies (9.0 and 66.1 eV), H^- loss mainly originates from the N3 and the carbon positions. However at the available energy of 9.0 eV, accessing the resonance yielding $H^-$from CH_3 is energetically unfavourable [11]. Therefore we

must conclude that at this energy (9.0 eV), the signal is mainly originating from the N3 position. In Figure 4.9(b) we show the H^-yield measured upon potassium collisions with uracil methylated at the N3 position (3-meU). Here we clearly see a distinct signal of H^-loss at 5.3 and 7.4 eV, in contrast to the strong suppression of the H^-signal in 1-meT at 7.6 eV. These findings indicate that H^-loss from the N1 position is contributing to such signal. The signal observed at 66.4 eV is now comprising the contributions from N3, C6 and CH_3. In order to support these unprecedented results, we have obtained the $H^-$and D^-yields from thymine deuterated at the C positions (thymine-d4) and the results are shown in Figure 4.9(c). It is obvious that D^-loss from the C positions is restricted to collision energies above 7.4 eV, while H^-loss from the N sites essentially occurs from the N1 position. This is in clear agreement with the resonance position in the dissociative electron attachment studies [11] even at the present moderate collision energy resolution. Further to these findings in the potassium-pyrimidine collisions, we can also add that H^-loss from the C positions is essentially due to C6, which is particularly relevant in the case of 1- meT.

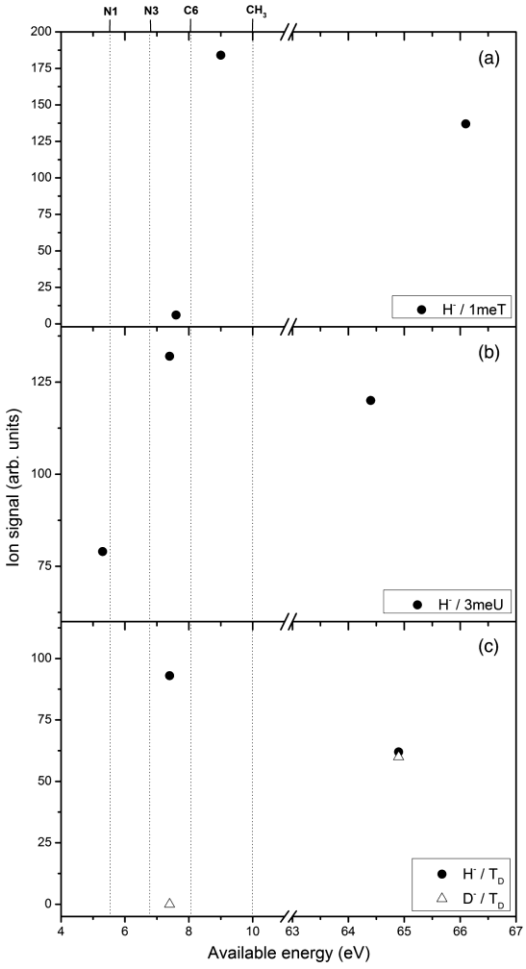

Figure 4. 9.H^-/D^- ion yield as a function of the collision energy. The vertical dotted lines indicate the mean values of the $H^-=D^-$ position of the centre of the different resonances for N1, N3, C6 , and CH_3 positions obtained in DEA studies (from Fig. 3 in Ref. [11]). (a) H^- formation from thymine methylated at the N1 position (1-meT) at 7.6, 9.0 and 66.1 eV; (b) H^- formation from uracil methylated at the N3 position (3-meU) at 5.3, 7.4, and 64.4 eV; (c) H^- and D^- formation from partly deuterated thymine (thymine-d4) at 7.4 and 64.9 eV.

In DEA to thymine the minimum electron energy required to break a particular bond (N1-H, N3-H, C6-H and CH2-H) lies between 4 to 5 eV [26], so bond- and site-selectivity [12] to gas phase methylated and deuterated pyrimidines yielding H^-formation, does not result from any particular energy constraints [11]. Since energy constraints cannot explain site selectivity, the electronic structure of the associated transient precursor ions accessed by electrons of different energies (either shape or core excited resonances) has been suggested as the main responsible for such achievement. The dissociation mechanism in the potassium collisions yielding a neutral dehydrogenated molecule and H^-loss, can be regarded as a pseudo- diatomic behaviour. In this context, we recall equation (1) and for large potassium-molecule values the van der Waals and induction forces can be neglected and consequently the covalent potential is zero and the ionic potential is purely coulombic. If this approximation holds, R_c is given by 14.41/ΔE (Å) [23], when ΔE is expressed in eV. Taking the adiabatic electron affinities of 1-meT, 3-meU and thymine-d4, as (0.025 ± 0.010) eV [27], (0.035 ± 0.010) eV [27] and (0.069 ± 0.007) eV [28], the values for R_c are found for the three molecular targets at ~ 3.3 Å. The corresponding total cross sections for ion-pair formation will be of the order of πR_{c2}, which is much larger than the corresponding gas kinetic cross sections.

Contributions to ion-pair formation through electron transfer to excited states of molecular negative ions have been observed in other polyatomic molecules, such as benzene and fluorobenzene [24]. In the case of thymine and uracil [29], the dehydrogenated parent anion fraction (not shown here) is attributed to excited states and at low collision velocities accounts for ~ 10-20% of the total cross section. The velocity dependence is shown that above 2×104 $ms^{-}1$ (> 40 eV), the contribution of the excited states is negligible. This is a remarkable finding since similar behaviour was observed in diatomics [23] and this result can be used here for the present molecular targets. Therefore if an excited state of the negative ion is involved, such contribution may be reached via smaller crossing distance. To reach such a crossing no electron transfer should occur at the first crossing and the excitation may occur at the inner crossing. When the collision energy is increased the diabatic probabilities controlling the electron transfer process at the first crossing as well as the inner crossing increase and the effect of these excited states will be reduced.

Charge transfer deposited on gas-phase thymine and uracil by electron harpooning mechanism in atom-molecule collisions [29], induces the loss of hydrogen, which exclusively takes place from the N positions. The bond selectivity can also be made site selective by proper adjustment of the collision energy. While at 5.3 eV collision energy results in the loss of hydrogen from N1 in 3-methyl-uracil, the reaction can be suppressed from N3 by tuning the collision energy to 7.6 eV as is in 1-methyl-thymine. Moreover D^- formation from thymine deuterated in the C positions is suppressed at 7.4 eV showing that H^- formation in 3-methyl-uracil proceeds only through the N1 position. Here we find that energy and charge transfer are completely inactivated when the N1-H bond is replaced by N1-CH_3. These findings open a new achievement in controlling chemical reactions that may have particular relevance for the investigation of early molecular processes in the nascent stages of DNA damage by

secondary electrons, especially those related to strand breaks. Such charge transfer processes may also play an important role in low-temperature plasmas as well as in the regions of planetary atmospheres.

Acknowledgements:

DA and FFS acknowledge the Portuguese Foundation for Science and Technology (FCT- MEC) for a post-graduate scholarship SFRH/BD/61645/2009 and post-doctoral grant SFRH/BPD/68979/2010, respectively. We also acknowledge partial funding from the Portuguese research grant PEst-OE/FIS/UI0068/2011 through FCT-MEC, and from the Spanish Ministerio de Economía y Competitividad (Project No. FIS 2009-10245). Some of this work forms part of the EU/ESF COST Actions Nano-IBCT – MP1002 and The Chemical Cosmos – CM0805. Authors are extremely grateful to Professor Eugen Illenberger from the Free University Berlin, Germany, for fruitful and lively discussions.

References:

[1]. B. Boudaïffa, P. Cloutier,D. Hunting, M. A. Huels, and L. Sanche, Science **287**, 1658 (2000).

[2]. C. von Sonntag, Free-Radical-Induced DNA Damage and Its Repair, Springer (2005).

[3]. R. D. Levine, and R. B. Bernstein, Molecular reaction dynamics and chemical reactivity (Oxford Univ. Press, New York, 1987).

[4]. E. D. Potter, J. L. Herek, S. Pedersen, Q. Liu, and A. H. Zewail, Nature **355**, 66 (1992).

[5] H. Rabitz, R. de Vivie-Riedle, M. Motzkus, K. Kompa, Science **288**, 824 (2000).

[6] H. H. Fielding, and M. A. Robb,. Phys. Chem. Chem. Phys. **12**, 15569 (2010).

[7] L. Ratschbacher, C. Zipkes, C. Sias, and M. Köhl, Nature Phys. **8**, 649(2012).

[8] W. Eberhardt, T. K. Sham, R. Carr, S. Krummacher, M. Strongin, S. L. Weng, and D. Wesner, Phys. Rev. Lett. **50**, 1038 (1983).

[9]. S.Wada, R. Sumii, K. Isari, S. Waki, E. O. Salo, T. Sekiguchi, T. Sekitani, and K. Tanaka, Surf. Sci. **528**, 242 (2003).

[10]. P. A. Sloan, and R. E. Palmer, Nature. **434**, 367 (2005).

[11]. S. Ptasińska, S. Denifl, V. Grill, T. D. Märk, E. Illenberger, and P. Scheier, Phys. Rev. Lett. **95**, 093201 (2005).

[12]. H. Abdoul-Carime, S. Gohlke, and E. Illenberger, Phys. Rev. Lett. **92**, 168103 (2004).

[13]. V. S. Prabhudesai, A. H. Kelkar, D. Nandi, and E. Krishnakumar, Phys. Rev. Lett. **95** 143202, (2005).

[14]. I. Bald, J. Kopyra, and E. Illenberger, Angew. Chem. Int. Ed. **45**, 4851(2006).

[15]. R. Balog, and E. Illenberger, Phys. Rev. Lett. **91**, 213201 (2003).

[16]. P. R. Brooks, Science. **193**, 11 (1976).

[17]. V. Vuitton, P. Lavvas, R. V. Yelle, M. Galand, A. Wellbrock, G. R. Lewis, A. J. Coates, and J.-E. Wahlund, Planet. Space Sci. **57**, 1558 (2009).

[18]. D. Almeida, R. Antunes, G. Martins, G. Garcia, R. W. McCullough, S. Eden, and P. Limão-Vieira, Int. J. Mass Spectrom. **311**, 7 (2012).

[19]. F. Gobet, S. Eden, B. Coupier, J. Tabet, B. Farizon, M. Farizon, M. J. Gaillard, S. Ouaskit, M. Carré, and T. D. Märk, Chem. Phys. Lett. **421**, 68(2006).

[20]. H. Tanaka, and M. Inokuti, Adv. Atom. Mol. Opt. Phys. **43**, 1 (2000).

[21]. M. Larsson, W. D. Geppert, and G. Nyman, Rep. Prog. Phys. **75**, 066901 (2012).

[22]. A. W. Kleyn, J. Los, and E. A. Gislason, Phys. Rep. **90**, 1 (1982).

[23]. A. W. Kleyn, and A. M. C. Moutinho, J. Phys. B: At. Mol. Opt. Phys. **34**, R1 (2001).

[24]. P. Limão-Vieira, A. M. C. Moutinho, J. and Los, J. Chem. Phys. **124**, 054306 (2006).

[25]. R. Antunes, D Almeida, G Martins, N. J. Mason, G. García, M. P. J. Maneira, Y. Nunes, and P. Limão-Vieira, Phys. Chem. Chem. Phys. **12**, 12513 (2010).

[26]. S. Denifl, S. Ptasińska, M. Probst, J. Hrušák, P. Scheier, and T. D. Märk, J. Phys. Chem. A **108**, 6562 (2004).

[27]. C. Desfrancois, H. Abdoul-Carime, S. Carles, V. Périquet, J. P. Schermann, D. M. A. Smith, and L. Adamowicz, J. Chem. Phys. **110**, 11876 (1999).

[28]. J. H. Hendricks, S. A. Lyapustina, H. L. de Clercq, J. T. Snodgrass, and K. H. Bowen, J. Chem. Phys. **104**, 7788 (1996).

[29]. D. Almeida, R. Antunes, G. Martins, S. Eden, F. Ferreira da Silva, Y. Nunes, G. Garcia, and P. Limão-Vieira, Phys. Chem. Chem. Phys. **13**, 15657 (2011).

Chapter 5

5. Anion collisions with simple organic molecules: negative and positive ion formation.

In this chapter, the main focus lies in the study of the fragmentation patterns that result from collisions of several anionic species with simple organic molecules. The negative ion fragmentation patterns are particularly important to compare with neutral atom-molecule collision measurements, since both measurements imply a electron transfer mechanism. The studies presented here include several molecular targets such as nitromethane (CH_3NO_2) water (H_2O), methanol (CH_3OH) and ethanol (C_2H_5OH). By comparing the anionic fragmentation patterns with DEA and cationic with ionisation measurements, fragmentation pathways have been proposed.

Mass spectrometry of anions and cations produced in 1-4 keV H^-, O^-, and OH^- collisions with nitromethane, water, ethanol, and methanol

D. Almeida [1], R. Antunes [1], G. Martins [1], G. Garcia [2,3],
R. W. McCullough [4], S. Eden [5,6*] and P. Limão-Vieira[1,5*]

[1] Laboratório de Colisões Atómicas e Moleculares, CEFITEC, Departamento de Física, FCT - Universidade Nova de Lisboa, P-2829-516 Caparica, Portugal
[2] Departamento de Física de los Materiales, UNED, Senda del Rey 9, 28040 Madrid, Spain
[3] Instituto de Física Fundamental, Consejo Superior de Investigaciones Científicas, Serrano 113-bis, 28006 Madrid, Spain
[4]Queens University Belfast, School of Mathematics & Physics, Centre for Plasma Physics, Belfast BT7 1NN, Co. Antrim North Ireland
[5] Department of Physical Sciences, Open University, Walton Hall, Milton Keynes MK7 6AA, UK
[6] Also of Institut de Physique Nucléaire de Lyon, IN2P3-CNRS et Université Claude Bernard Lyon 1, 43, boulevard du 11 Novembre 1918, 69622 Villeurbanne Cedex, France

Published in Int. J. Mass Spectrom., **311**, 7-16 (2011)

Abstract

Interactions between 1–4 keV anions (H^-, O^-, and OH^-) and gas-phase molecules (nitromethane, water, ethanol, and methanol) have been studied using quadrupole mass spectrometry of the product anions and cations. The low collision velocities (0.07-0.40 v_{Bohr}) provide favourable conditions for electron transfer from the anion projectile to the neutral target molecule yielding negative ion formation, while strong competition with cation formation is also observed. Relative production of fragment cations increases with H^- impact energy and with projectile mass when energy is constant. Considered together, these results suggest a momentum dependence on collisional energy deposition. As far as negative ion production is concerned, comparisons with previous free electron attachment studies are drawn as a starting point for the interpretation of the anion fragmentation channels. For nitromethane and water, the present anion fragmentation patterns are substantially different to the free electron attachment data. Conversely the fragmentation channels of ethanol and methanol anions only show clear dependence on the electron attachment / transfer process in terms of the relative anion yields.

5.1.1. Introduction

The importance of negative ion chemistry in the upper atmosphere is of recent interest amongst the astrochemistry community. It is now well established that negative ions exist in the upper atmosphere of Titan [1], produced by mechanisms such as three-body (dissociative) electron attachment. Indeed, Titan's upper atmosphere is composed of several types of organic molecules,

which are believed to be the building blocks of other, more complicated, biological molecules (Ref. 1 and references therein). As such, the study of anion collisions with simple organic molecules may provide some insight to the negative ion chemistry in relevant atmospheric systems. Some of the molecules studied herein (water, methanol and ethanol) are some of the more fundamental organic molecules and as such, their study may provide some insight on interactions of other more complex astrochemically relevant organic molecules. Furthermore, within the scope of astrochemistry, the study of anion collisions with H^-, O^- and OH^- as projectiles is quite critical since it is known that these anions are quite abundant in the upper earth's atmosphere, albeit at much lower (thermal) energies. Still, the difference in projectile's kinetic energy between our study and the astrophysical environment does not detract from the value of this work since the fundamental mechanisms surrounding both systems will mostly be the same.

From a more fundamental point of view, the potential role of the neutral atom as a stabilizing third body *post* electron transfer from the incident anion is of particular interest. Despite the fact that the collision energies of the projectiles in this study are far above the ones in alkali atom-molecule collisions, comparisons with the latter [2-4], and also with free electron attachment experiments can enhance our understanding of such stabilization effects on the mass spectrum of anions due to the target molecule. Regardless of the electron capture mechanism, electron transfer from the projectile to the acceptor molecule results in a transient negative ion (TNI), which can decay via electron autodetachment or fragmentation of the anion. As far as we are aware, no previous experimental or theoretical studies pertaining to the fragmentation patterns in collisions with anion projectiles have been carried out in the present range (0.07-0.40 v_{Bohr}). Moreover, the present work provides the first data for anion (or indeed cation) production in anion collisions with molecules of greater complexity than N_2 and H_2. Most of the literature regarding anion-molecule collisions at a velocity range of $0.1 < v/v_{Bohr} < 0.4$ pertains to the study of electron detachment post-collision [5-9]. Two main mechanisms are responsible for this; direct detachment (DD) and charge transfer to shape resonance (CTSR). The first process involves electron detachment from the collision complex without any formation of a temporary negative ion (TNI), for example:

$$X^- + AB \rightarrow X + AB + e^- \qquad \text{(DD)}$$

Where X^- represents the anion projectile and AB represents a molecular target. The second process involves charge transfer of the electron from the anion to the molecule, thereby creating a short-lived TNI. Due to the low lifetimes of the TNI, the electron is subsequently ejected.

$$X^- + AB \rightarrow X + (AB^-)^{\#} \rightarrow X + AB^{\#} + e^- \text{(CTSR)}$$

$(AB^-)^{\#}$ represents the TNI resulting from the electron transfer, which can be electronically and / or rovibrationally excited, while $AB^{\#}$ represents the neutral (excited) molecular target. Whereas the equation does not show X in an excited state, we do not disregard that possibility.

Previous studies of these collision systems [5-10] mostly focus on discrimination between DD and CTSR. Hence it has been shown that DD results in very low energy loss by the projectile (≤1 eV) while CTSR is characterized by higher energy losses (around 3-4 eV). Furthermore, these studies show that, while at lower projectile collision energies (up to ~100 eV, i.e., $v/v_{Bohr} \approx 0.063$) direct detachment dominates[7], CTSR becomes increasingly significant at gradually higher energies [7] (i.e., $v/v_{Bohr} > 0.2$). Conversely, fragmentation processes have received little attention. The lifetime of the TNI has to be sufficiently long for fragmentation channels to be able to compete with electron detachment through CTSR. The role of collisional excitation in TNI formation in anion-molecule collisions has not been investigated in the literature.

In the present work, the anion mass spectra will be largely based on comparisons with free electron attachment studies. Similarities with free electron attachment results are expected in the case of electron transfer from H^- since its *extra* electron is relatively loosely bound (0.75 eV [11]) and hence may be considered to approximate a free electron [7,8]. For this model to be valid, the collision velocity has to be much higher than the electron velocity in the projectile frame. In the case of H^-, this is achieved for collision energies much higher than 1.5 keV [8]. In the presented study, the highest collision was 4 keV and therefore the application of this model has to be made carefully. However, a classical picture can be used for collision energies in this energy range [8]. As is explained in the studies of references [5,7,8], the electron can be considered to have a broad energy distribution between $\upsilon_e - \upsilon_i$ and $\upsilon_e + \upsilon_i$, where υ_e is the velocity of the H^- system and υ_i is the velocity of the bound electron in the ion frame. As such, for a 1 keV H^- collision energy, an analogy can be made with free electrons with an impact energy distribution between 0.02 eV and 2.56 eV. Due to higher ion mass and also higher binding energies of the extra electron, the model is not useful to analyse the present O^- and OH^- impact results.

In table 5.1 the ion velocities for the several projectiles used in this study are presented. The velocity values are presented in Bohr velocity units and are obtained through:

$$\frac{v}{v_0} \approx 6.325\sqrt{E} \qquad (1)$$

Where v/v_0 is the velocity of the ion relative to the Bohr velocity and E is the energy per mass unit in MeV/a.m.u.. As is the case for anionic products, the literature surrounding cation production in collisions with anion projectiles is quite scarce. For velocities significantly higher than the Bohr velocity of the electron ($v >> v_{Bohr}$), cross section measurements for single and double ionisation of He and Ar by 0.5-2 MeV H^-impact (4.5-8.9 v_{Bohr}) have been performed [12]. Further experiments have

probed target ionisation, projectile scattering, and projectile electron loss in 1 MeV H^-collisions with He atoms [13]. At intermediate velocities ($v \approx v_{Bohr}$), single and double ionisation of He, Ar, N_2, and H_2 targets has been analyzed following collisions with anion projectiles (B^-, F^-, C^-, and O^-) [14-16]. These studies indicate the dissociative ionisation is dominant for low impact parameters (more *direct* collisions generally with higher momentum transfer), whereas non-dissociative ionisation (i.e., formation of the parent cation) dominates at higher impact parameters.

Ion	Binding energy of attached electron (eV)[11]	Ionisation energy of neutral (eV)[11]	Kinetic energy (keV)	Anion velocity (v_{Bohr})	Target molecules
H^-	0.75	13.60	1	0.20	CH_3NO_2
			2	0.28	CH_3NO_2, H_2O
			4	0.40	CH_3NO_2, H_2O, CH_3OH, C_2H_5OH
O^-	1.46	13.62	2	0.07	H_2O
			4	0.10	CH_3NO_2, H_2O, CH_3OH, C_2H_5OH
OH^-	1.92	13.02	2	0.07	H_2O
			4	0.10	CH_3NO_2, H_2O, CH_3OH, C_2H_5OH

Table 5. 1 Summary of anion-molecule collisions studied using product cation mass spectrometry.

At lower impact velocities ($v << v_{Bohr}$), electron loss from H^- projectiles with electronic excitation of the resultant H^o has been studied in 1-5 keV (0.20-0.45 v_{Bohr}) collisions with rare gas atoms and N_2 molecules [17]. Minimal H^- impact energy dependence was observed in the cross sections for excitation to H(3*d*), H(3*s*), H(4*s*), and H(5*s*) states. Furthermore, Geddes et al. [18] measured cross sections for the formation of excited (n = 2 or 3) hydrogen atoms in 3-25 keV (0.35-1.00 v_{Bohr}) H^- ions with H, H_2, He, Ne, Ar and N_2. Stone and Morgan [19] recorded cross sections for hydrogen excitation to highly excited states ($12 \leq n \leq 28$) in 2.8-60 keV (0.33-1.55 v_{Bohr}) H^- collisions with H, H_2, and Ar. Significantly, the cross sections for electron loss by H^-show contrasting trends in 0.1-10 keV (0.06-0.63 v_{Bohr}) [20] collisions with H and H_2. With increasing H^- impact velocity, the electron loss cross sections decrease for collisions with H whereas they increase to an apparent maximum at ~0.6 v_{Bohr} for H_2.

5.1.2. Experimental set-up

The experimental set-up used in this study consisted of a cross beam technique, where gas phase molecules interact with anion projectiles. The anion beam was produced in a PS-120 Negative Ion Caesium Sputter Source from Peabody Scientific™, operating between 1-4 keV. The beam emerging from the source was focused by an electrostatic lens system and momentum analysed by a 90 degree double focusing magnet. After further focusing and collimation, the beam was directed into the interaction chamber where it crossed an effusive beam of gas phase molecules derived from liquid samples. A cycle of freeze-thawing steps was carried out on the liquid samples to remove any dissolved gases and ensure a pure gas target.Cationic or anionic fragments were extracted from the

interaction region into an orthogonal quadrupole mass spectrometer. Notwithstanding the relatively low m/q resolution, clear distinctions can be made throughout the presented spectra and specific issues regarding this matter are discussed more thoroughly in the corresponding section. Anion currents were measured in a Faraday cup after the collision region.The low background pressure of 10^{-7} mbar in the interaction chamber resulted in a negligible background contribution to the mass spectra. The target pressures used ensured single collision conditions in the interaction region and negligible secondary collisions of the fragment ions. Ion extraction voltages of approximately 25 Vcm^{-1} were applied in order to prevent any deflection of the anionic beam into the differentially pumped quadrupole mass spectrometer. The mass spectra were normalized to both total extraction times and beam currents.

5.1.3. Results and discussion

5.1.3.1. Cation formation

Nitromethane (CH_3NO_2)

Generally speaking, the same main *groups* of cations were observed for the various ionisation methods (anion impact, fast electron impact, and photoionisation). In particular, the local maxima for each group in the present data agree with those in the previous work. The absence of some weak features in the present data can be explained by relatively low signal-to-noise ratios. Additionally, a general overview of the spectra shows that for all impact energies and projectiles, the major peaks are always the same for the corresponding target molecule.

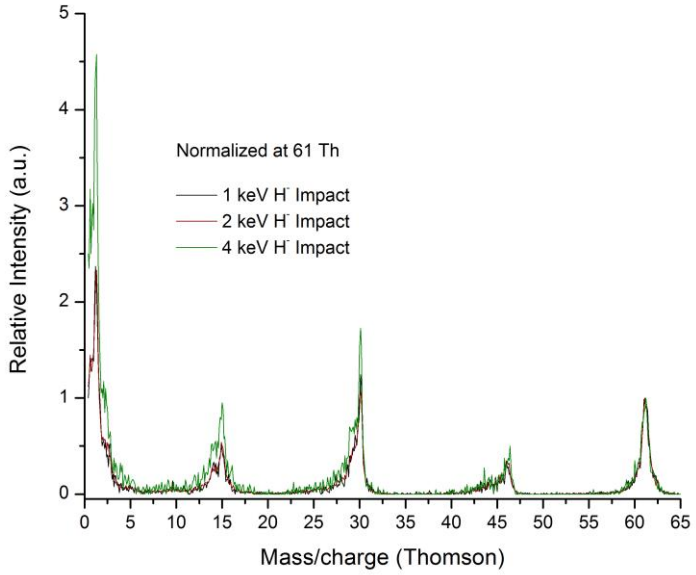

Figure 5. 1 Mass spectra of cations produced in 1-4 keV H^- collisions with gas-phase nitromethane. The data has normalized such that the intensities of the $CH_3NO_2^+$ (parent cation) peaks are equal.

Fig. 5.1 shows mass spectra at different H^- projectile energies (1, 2 and 4 keV), while Fig. 5.2 compares spectra for different projectiles. The yields in both figures are normalized to the parent cation, therefore creating a clearer picture of the relative amount of dissociative ionisation versus the parent cation production. Indeed, it is clear from Fig. 5.1 that for higher projectile energies, the relative amount of fragmentation is higher. This indicates increased statistical fragmentation associated with greater energy deposition. Indeed, the relative production of fragment cations is markedly greater for 4 keV H^- impact, with new resolved peaks visible at 45 and 29 Th. This suggests energy transfer distributions that are similar at 1 and 2 keV but distinctly higher at 4 keV.

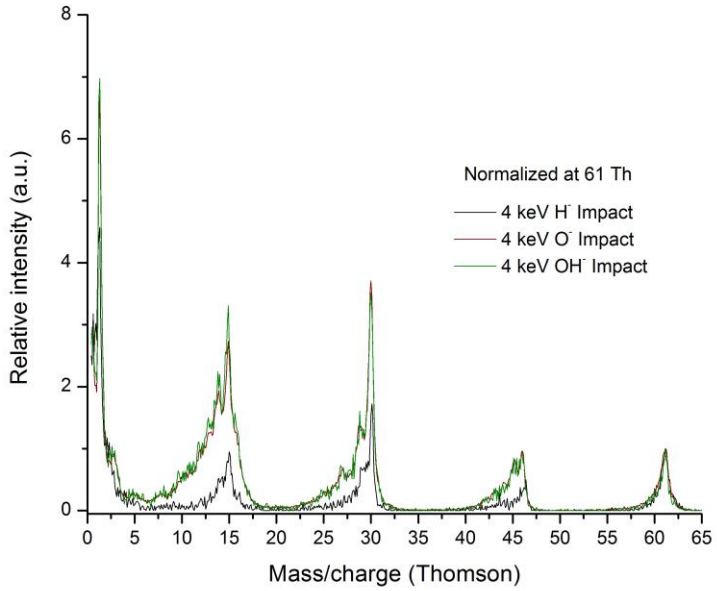

Figure 5. 2 Mass spectra of cations produced in 4 keV H^-, O^-, and OH^- collisions with gas-phase nitromethane. The data has been normalized such that the intensities of the $CH_3NO_2^+$ (parent cation) peaks are equal.

Fig. 5.2 shows that the ratio of fragment cation production / $CH_3NO_2^+$ production is much greater for 4 keV O^- and OH^- impact than for H^- impact. However at impact kinetic energies (KE) that are significantly greater than the thresholds for the various ionisation pathways, collision velocity is generally recognized as a more significant parameter than projectile KE for the interpretation of ionisation results (notably in relation to energy deposition and branching ratios for dissociative ionisation/total ionisation). Hence the reason for the observed differences in the present nitromethane mass spectra produced by H^- impact (1-4 keV, 0.20-0.40 v_{Bohr}) and by O^- and OH^- impact (4 keV, 0.010 v_{Bohr}) is not totally clear; the velocities are different as well as the projectiles. As H^- has the weakest outermost electron binding energy (0.75 eV), reduced fragmentation by H^- impact appears to be broadly consistent with the generalized association of smaller impact parameters (more *direct* collisions, smaller cross sections) with greater energy deposition and hence increased fragmentation [14,15,21,22]. Similarly, Fig. 5.2 shows a subtle increase in fragmentation for OH^- impact compared with O^- (binding energies of the outermost electrons in the respective anions: 1.92 and 1.46 eV). More

generally, however, both Fig. 5.1 and 5.2 are consistent with a possible relation between increased projectile momentum and increased relative production of fragment ions.

	Present work	**Electron impact [11E]**	**288.3 eV photoionisation[40]**	**Proposed assignments and appearance energies (eV)**
Methanol CH_3OH	32	32	32	CH_3OH^+ (10.84[11])
	31 [m]	31 [m]	31 [m]	CH_3O^+ (11.649[41])
	30	30	30	CH_2O^+ (12.05[42])
	29	29	29	CHO^+ (13.06[42])
		28	28	CO^+ (13.7[43])
			18	H_2O^+
	17		17	OH^+ or CH_4^+
			16	O^+
	15 [m]	15 [m]	15 [m]	CH_3^+ (13.82[42])
	14 [#]	14	14	CH_2^+ (14.05[42])
			13	CH^+
			12	C^+
			3	H_3^+
			2	H_2^+
	1 [m]		1 [m]	H^+

	Resolved cation masses (m/q)			**Proposed assignments and appearance energies (eV)**
	Present work	**Electron impact[11E]**	**375 nm (3.31 eV) multi-photon ionisation[44]**	
Nitro-methane CH_3NO_2	61 [m]	61 [m]	61 [m]	$CH_3NO_2^+$ (11.08[11, 23])
		60	60	$CH_2NO_2^+$ (11.8[45])
	46 [m]	46 [m]	46 [m]	NO_2^+ (12.1[45])
	45 *	45	45	CH_3NO^+
		44	44	CH_2NO^+ (11.75[45])
		43	43	$CHNO^+$
		42	42	CNO^+
		31	31	NOH^+
	30 [m]	30 [m]	30 [m]	NO^+ (11.75[45])
	29 *	29	29	CHO^+ / CH_3N^+
		28	28	CO^+ / CH_2N^+
		27	27	CHN^+
		26		CN^+
		16	16	O^+ (14.50[46])
	15 [m]	15 [m]	15 [m]	CH_3^+ (12.6[47])
	14	14	14	N^+ / CH_2^+
		13	13	CH^+
		12	12	C^+ (22.83[46])
			2	H_2^+
	1		1	H^+

	Present work	**Electron impact [11E]**	**292 eV photoionisation[40]**	**Proposed assignments and appearance energies (eV)**
Ethanol C_2H_5OH	46	46	46 [m]	$C_2H_5OH^+$ (10.48[11])
	45 [m]	45 [m]	45	$C_2H_5O^+$ (10.801[48])
	44 [#]		44	$C_2H_4O^+$ (10.45[49])
	43 [#]	43	43	$C_2H_3O^+$ (14.5[43])
	42	42	42	$C_2H_2O^+$
			41	C_2HO^+
			40	C_2O^+
			32	CH_4O^+
	31 [m]	31 [m]	31 [m]	CH_3O^+ (11.25[50])
	30 [#]	30	30	CH_2O^+ (11.70[51])
	29 [#]	29	29	CHO^+ or $C_2H_5^+$
	28 [#]	28	28	$C_2H_4^+$ (12.0[50])
	27 [#]		27	$C_2H_3^+$ (14.7[43])
	26 [#]	26	26	$C_2H_2^+$
		25	25	C_2H^+
	19 [#]	19	19	H_3O^+ (13.8[52])
			18	H_2O^+
			17	OH^+
			16	O^+
	15 [m †]	15 [m]	15 [m]	CH_3^+ (14.70[53])

	14 [m †]	14	14	CH_2^+
		13	13	CH^+
			12	C^+
			2	H_2^+
	1 [m]		1	H^+ (21.0[54])
	Present work	**Electron impact[37E]**	**21.23 eV photoionisation[55]**	**Proposed assignments and appearance energies (eV)**
Water H_2O	18	18 [m]	18 [m]	H_2O^+ (13.5)
	17	17	17	OH^+ (17.5)
	16	16	16	O^+ (25)
		16		O^{++} (90)
		2		H_2^+ (30)
	1	1		H^+ (20)

Table 5. 2. Cations produced in the present collisions (1-4 keV H^- impact, 4 keV O^- impact, and 4 keV OH^- impact) compared with examples of previous electron impact and photoionisation data. It is noteworthy that for all impact energies and projectiles the same major peaks were observed. [E] Impact energy unspecified (typically ~70 eV); [m] Local maximum; * Only resolved for 4 keV anion impact; [#] Only resolved for O^- and OH^- impact; [†] Similar intensities

Methanol (CH_3OH), Ethanol (C_2H_5OH) and Water (H_2O)

Fig. 5.3 shows mass spectra of methanol (CH_3OH) as a function of incident O^- and OH^-, while the observed cationic fragments are listed in Table 5.2. Apart from H^+ formation, the dominant fragments are the dehydrogenated parent cation and its parent precursor. It is interesting to note that a comparison with electron ionisation spectra [23] provides a very similar picture. As is the case of nitromethane, collisions of heavier projectiles at the same KE (hence higher momentum) favour dissociative ionisation in detriment of non-dissociative ionisation, consistent with the interpretation mentioned above.

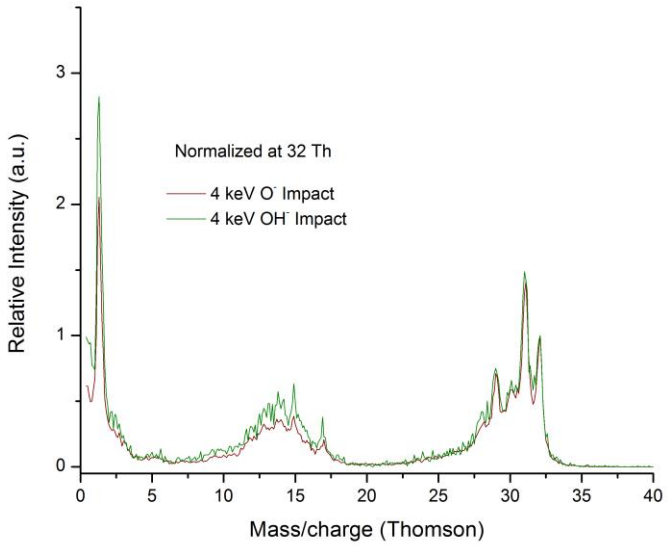

Figure 5. 3 Mass spectra of cations produced in 4 keV O^- and OH^- collisions with gas-phase methanol. The data has been normalized such that the intensities of the CH_3OH^+ (parent cation) peaks are equal.

Mass spectra for 4 keV H^-, O^- and OH^- impact on ethanol (C_2H_5OH) are presented in Fig. 5.4 and the identified cationic fragments are summarized in Table 5.2. As observed for methanol, the fragmentation pattern closely resembles the electron impact ionisation data [23]. Moreover, the ratio of fragment cation production / $C_2H_5OH^+$ production increases gradually with projectile mass (i.e. H^- to OH^-). Once more it would appear that the key parameter to consider is the momentum of the projectile rather than its energy [14,15,21,22].

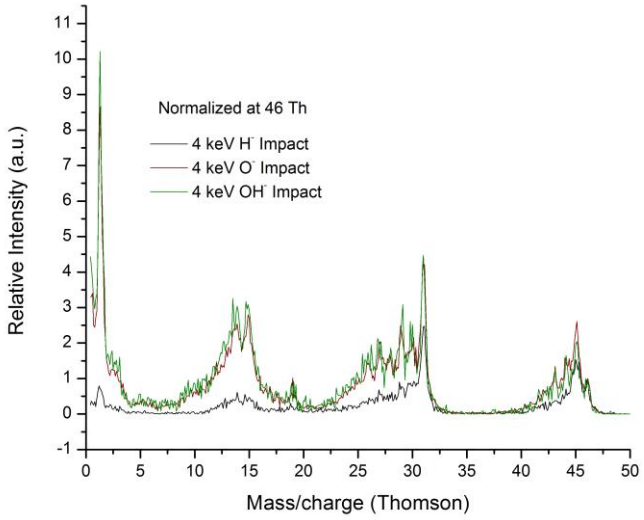

Figure 5. 4 Mass spectra of cations produced in 4 keV H^-, O^-, and OH^- collisions with gas-phase ethanol. The data has been normalized such that the intensities of the $C_2H_5OH^+$ (parent cation) peaks are equal.

Finally, Fig. 5.5 presents mass spectra of cations produced in 4 keV H^-, O^- and OH^- collisions with water. As observed in the equivalent data for nitromethane, ethanol, and methanol, no significant difference exists between O^- and OH^- collisions, whereas for H^- collisions it is clear that the relative H^+ yield is significantly lower.

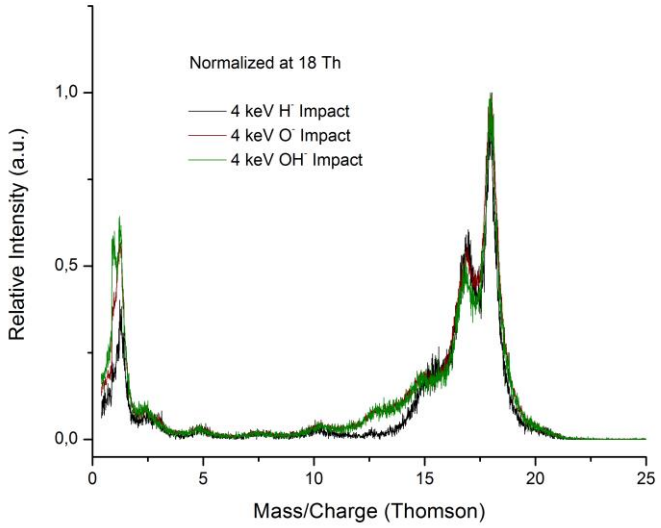

Figure 5. 5 Mass spectra of cations produced in 4 keV H^-, O^-, and OH^- collisions with gas-phase water. The data has been normalized such that the intensities of the H_2O^+ (parent cation) peaks are equal.

5.1.4.2. Anion formation

Nitromethane (CH_3NO_2)

Nitromethane anion formation has been studied in the gas-phase by free electron attachment [24,25], in alkali atom collisions [2] and in Rydberg electron transfer studies [26]. Of the molecules studied, nitromethane is the only one with a sufficiently large dipole moment (above the critical value of ~ 2.5 D [27]) to bound an extra electron in a stable dipole-bound state, potentially playing a significant role in the collisions dynamics. In free electron attachment studies, the dominant fragment was NO_2^- and no parent anion ($CH_3NO_2^-$) was observed. This is reasonable due to the small positive electron affinity of CH_3NO_2. In the present study, we observed the parent anion $CH_3NO_2^-$ as the dominant fragmentation pathway for all collision energies (Fig. 5.6) and for all the different electron donors (H^-, O^- and OH^-, Fig. 5.7). The other, less intense, detected fragments were NO_2^- and H^-. As a comparison, results obtained in alkali atom collision experiments have shown that the main fragment was reported to be NO_2^- but, in contrast to free electron attachment studies, the creation of the parent anion $CH_3NO_2^-$ was observed. As stated before, within the set of molecules investigated in this work, nitromethane stands out due to the presence of a stable dipole-bound anionic state [28], which has been shown both experimentally and theoretically to provide a doorway into valence states of the molecular parent anion [26,29]. This initial dipole-bound molecular anion possesses a significantly different geometry than its neutral counterpart (a symmetric bend of the oxygen atoms in the $–NO_2$ group resulting in a tetrahedral shape [30]).

Water H_2O	**Present work**	**Free electron attachment [38]**	**Proposed assignments**
	17	17	OH-
	16	16	O^-
	1	1	H^-

Methanol CH_3OH	**Present work**	**Free electron attachment [33, 36]**	**Proposed assignments**
	32^m		CH_3O^-
	31	31	OH^-
	17^a	17	OH^-
	16	16	O^-
	14		CH_2^-
	1	1	H^-

Nitromethane CH_3NO_2	**Resolved anion masses (m/q)**			**Proposed assignments**
	Present work	**Free electron attachment [24, 25]**	**Alkali atom collisions [2]**	
	61^m		61	$CH_3NO_2^-$
	60	60	60	$CH_2NO_2^-$
		59		$CHNO_2^-$
		47		$^{15}NO_2^-$
	46	46^m	46^m	NO_2^-
	45^a			CH_3NO^-
		44		CH_2NO^-
		42	42	CNO^-
		32		$H2NO^-$
		30	30	NO^-
		26	26	CN^-
		18		$^{18}O^-$
		17	17	OH^-
	16	16	16	O^-
		15		CH_3^-
		14		CH_2^-
		13		CH^-
	1	1	1	H^-

Ethanol C_2H_5OH	**Present work**	**Free electron attachment [34]**	**Proposed assignments**
	45	45	$CH_3CH_2O^-$
	44		$C_2H_4O^-$
	43		$C_2H_3O^-$
	32		CH_3OH^-
	17	17	OH^-
	16	16	O^-
	15		CH_3^-
	14		CH_2^-
	1	1	H^-

Table 5. 3Anionic fragmentation products for the several target molecules. The different projectiles do not yield different products. [m] Local maximum; * Only resolved for 4 keV anion impact; [#] Only resolved for O^- and OH^- impact; [†] Similar intensities; [a] Extrapolated

Similarly to both alkali atom collisions and Rydberg electron transfer, nitromethane parent anion formation by negative ion impact is expected to proceed through a transition to a low vibrational state of a $^2B_1$ anionic state, whereas this does not occur in free electron attachment interactions [31,32]. From a different point of view, this mechanism may rely on an interaction of the projectile donor and the molecule, modifying the relative position or shape of the potential surfaces and thereby changing the dissociation pathway. Owing to the high dipole moment of nitromethane, the presence of H, O or OH in the collision complex may be rationalised as a third body "forcing" the electron to remain in the

dipole-bound state long enough for the molecule to adiabatically proceed into its anionic geometry, thereby transferring by intramolecular relaxation the electron into one of its valence orbitals (in the anionic geometry). This is in contrast with free electrons where, even if the electron is initially captured into the dipole-bound state, its lifetime is not long enough to compete with necessary molecular deformation from the neutral to the anionic geometry, yielding considerable auto-detachment.

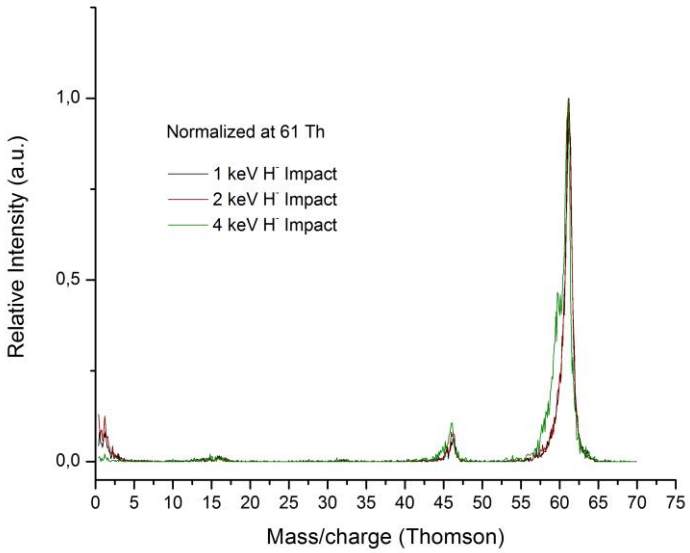

Figure 5. 6 Mass spectra of anions produced in 1, 2 and 4 keV H^- collisions with gas-phase nitromethane. The data has been normalized to the parent anion (61 Th).

In free electron attachment studies, the creation of NO_2^- arises from a vertical transition of 0.6 eV from the neutral ground state of the molecule to an $^2B_1$ (π^*) symmetry state of the anionic molecule[2]. At this stage, due to an avoided crossing between this state and a dissociative $^2A_1$ (σ^*) anionic state, tunnelling can occur through the formed barrier, thereby yielding NO_2^-. Another possibility for the formation of NO_2^- would be a direct transition to this $^2A_1$ (σ^*) anionic state. However, a vertical transition to this orbital would lie inside the curve of the neutral state, thereby most likely resulting in auto-detachment. By contrast, in alkali atom collision studies, NO_2^- is attributed to an initial transition to the aforementioned $^2A_1$ (σ^*) dissociative state, mainly through an ionic scattering. The presence of the alkali cation allows the temporary negative anion (TNI) to relax into a geometry below the neutral state, thereby precluding auto-detachment and allowing for the dissociation of the TNI into NO_2^- [31,32].

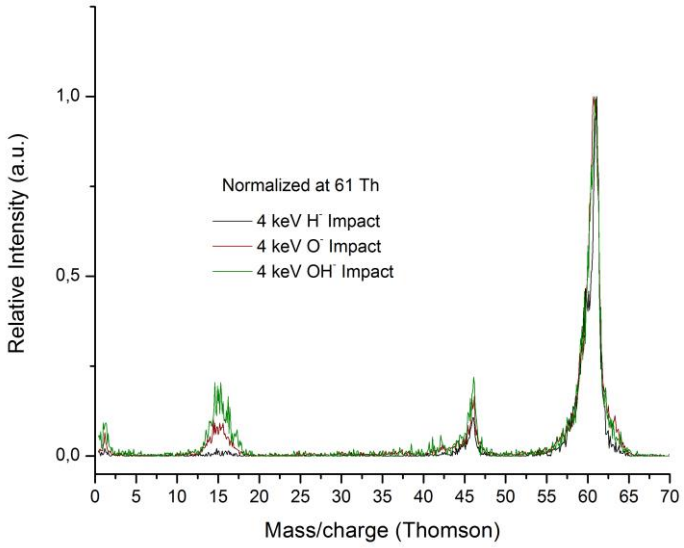

Figure 5. 7 Mass spectra of anions produced in 4 keV H^-, O^- and OH^- collisions with gas-phase nitromethane. The data has been normalized to the parent anion (61 Th).

When compared with free electron attachment and K impact, the present data show very low yields of NO_2^- relative to the parent anion and its dehydrogenated anion. This indicates that a direct and unilateral comparison with either free electron attachment or alkali atom collisions is not sufficient to explain the results. Indeed, the fact that the NO_2^- yield is very low appears to indicate that NO_2^- formation both through initial capture into $^2B_1$ (free electron attachment pathway) or into $^2A_1$ (electron transfer pathway) states are either suppressed or results mostly in auto-detachment.

As mentioned above, the formation of NO_2^- from a vertical transition to the $^2A_1$ dissociative curve can only occur if dissociation successfully competes with auto-detachment. The presence of the potassium cation in alkali atom collisions accomplishes this suppression [2]. However, since we do not obtain a significant yield of NO_2^- in the present measurements, the presence of the hydrogen radical does not appear to provide stabilization with respect to a vertical transition to the $^2A_1$ curve. Hence this suggests that auto-detachment suppression in alkali atom-molecule collisions is indeed due to a coulombic interaction between the electron donor and the target molecule. This lends support to the rationale of considering an ionic (K^++$CH_3NO_2^-$) transient complex during the collision time for potassium-nitromethane collisions.

On the other hand, the inability to produce NO_2^- from an initial capture to the $^2B_1$ state can imply that the tunnelling mechanism shown to explain the NO_2^- formation with free electrons is somehow suppressed [2,31,32]. Indeed, if the asymptotic value of the $^2A_1$ curve is higher than the final vibrational state of the $(CH_3NO_2^-)^{\#}$ transient anion, no such tunnelling effect is possible. This interpretation suggests that, whereas with free electrons the transition to the anionic state can be

considered vertical (Franck-Condon), this is not necessarily the case for electron transfer mechanisms, neither for ion-pair formation nor in the present experiments.

As can be seen in Fig. 5.6, higher projectile energies seem to favour formation of higher mass fragments, namely NO_2^-. Fig. 5.7 presents spectra with the same collision energies but different projectiles. A direct comparison shows that higher mass projectiles favour dissociation.

Methanol (CH_3OH)

As the simplest methyl alcohol, free electron attachment studies of methanol have been extensively performed [33,35,36]. In these studies, O^-, OH^- and the dehydrogenated parent anion (CH_3O^-) are the main fragments [33] and the hydride anion was also found to be a major fragmentation product [35,36], sharing the same resonances as CH_3O^-. All of the fragments have been attributed to core-excited resonances since their energetic thresholds (2.1, 2.4 and 2.9 eV for O^-, OH^- and CH_3O^-, respectively) [33] are much lower than the obtained resonance profiles.

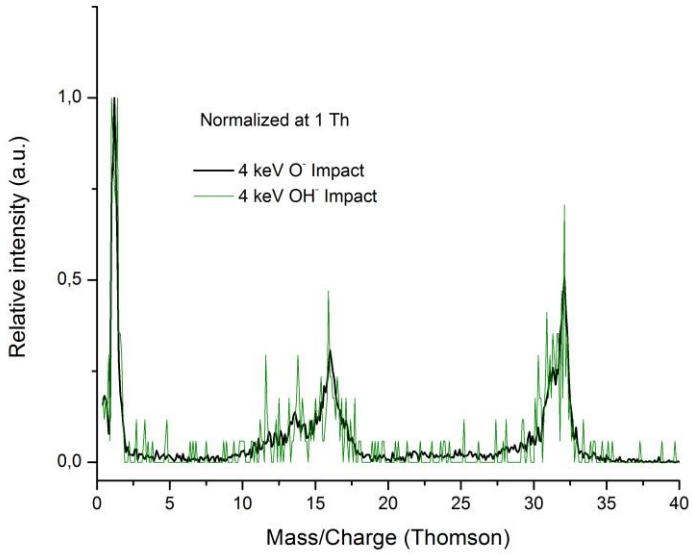

Figure 5. 8 Mass spectra of anions produced in 4 keV O^- and OH^- collisions with gas-phase methanol. The data has been normalized to 1 Th.

As in the free electron attachment studies, the main fragments in the present O^- and OH^- impact experiments on methanol are H^-, O^-, OH^- and CH_3O^- (Fig. 5.8). As for the 32 Th signal that may correspond to the parent anion (CH_3OH^-), this has neither been detected in free electron attachment studies nor in any other previous negative ion studies [33,35]. This is reminiscent of the rather small vertical electron affinity (~ 0 eV) of methanol. Though, we do not discard the possibility of an O_2^- contribution. In any case electron transfer experiments (e.g., with alkalis) will be shortly performed in our laboratory in order to further investigate the presence of this anion in the context of atom-molecule collisions.

Ethanol (C_2H_5OH)

The main fragments produced in recent free electron attachment experiments are O^-, OH^- and the dehydrogenated parent anion $CH_3CH_2O^-$, with no detection of the parent anion $CH_3CH_2OH^-$ [34]. These studies report that the resonances for those fragments are lower in energy but still well above the energy thresholds, similar to the methanol results [33,34].

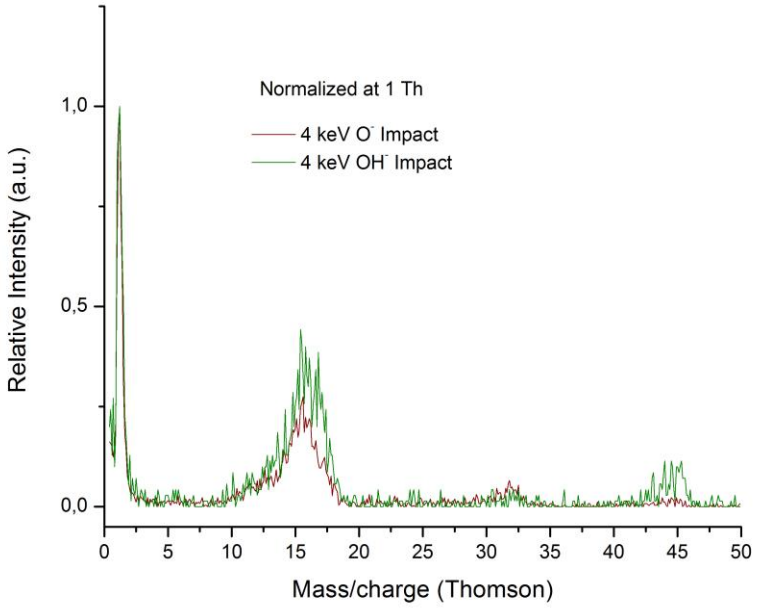

Figure 5. 9 Mass spectra of anions produced in 4 keV O^- and OH^- collisions with gas-phase ethanol. The data has been normalized to 1 Th.

The present OH^- and O^- impact experiments on ethanol produced H^-, O^-, OH^- and $CH_3CH_2O^-$ fragments (Fig. 5.9). Comparing the relative anion yields of O^-, OH^- and $CH_3CH_2O^-$ in free electron attachment studies with the relative intensities in this work reveals that they have approximately similar values. Furthermore, as in the case of methanol, H^- formation is obtained in the present studies but no information regarding the accessible resonant states through free electron attachment is available. Finally, a small but rather clear structure appears at 32 Th, which can be attributed to methanol anion (CH_3OH^-). The exact origin of this anion cannot be unambiguously determined. One possibility is the formation of this anion by abstraction of the methyl together with a hydrogen transfer. However, another more straightforward explanation is the presence of methanol as an impurity in the sample or in the sample admission system. As in methanol, the possibility of O_2^- contribution should also be considered. Further studies in the future will help clarifying this issue.

Water (H_2O)

Studies of electron attachment in water have been quite extensively performed. An extensive review on this ubiquitous molecule has been published recently [37]. The reported fragmentation consists of H^-, O^- and OH^- [37,38]. H^- formation is predominantly from a rather broad resonance at 6.4 eV and another less broad resonance at 8.24 eV, which is shared with formation of O^- and OH^-. The formation of these two anions share the same resonances (at 6.4, 8.24 and ~11.5 eV), though with different cross sections [37,38].

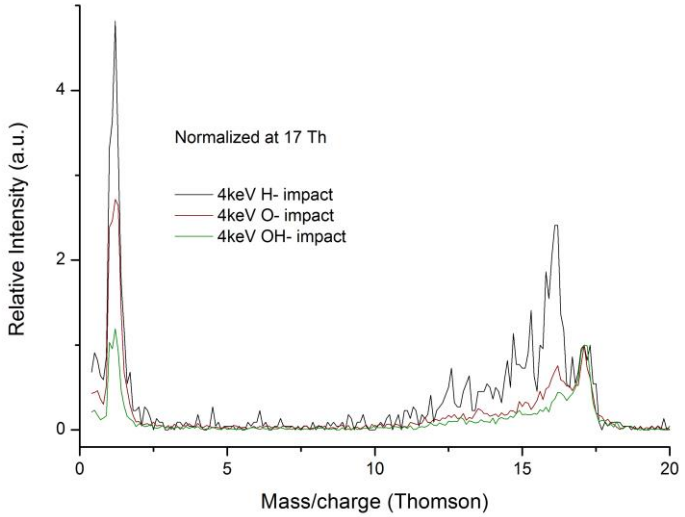

Figure 5. 10 Mass spectra of anions produced in 4 keV H^-, O^- and OH^- collisions with gas-phase water. The data has been normalized to 17 Th.

Compared with the pseudo-free electron energy (2.2 eV) for a 4 keV H^- projectile, the free electron attachment resonance energies are all high even when the velocity of the bound electron in the ion frame is taken into account, giving the range 0.38 - 5.58 eV (see section 1). Therefore, the pseudo-free electron analogy would lead us to expect negligible formation of any of these product anions. However, these free electron attachment profiles are reminiscent to core-excited resonances and so their contributions may deviate from the assumptions drawn for low energy resonances (typically below 3-4 eV) in the model. At this point, it is quite interesting to note that, in H^- collision studies with N_2, a higher energy structure in the H energy loss spectra appears around the 10 eV region, which the authors attribute to "collisional excitation" [7]. Water, methanol and ethanol share the fact that their fragmentation stems from core-excited resonances. Furthermore, electron transmission spectroscopy studies performed on N_2 show the presence of core-excited resonances within the 8-11 eV energy range [39] thereby indicating that the "collisional excitation" brought forward in the anion collision studies may indeed be due to core-excited resonances. The quasi-free electron attachment model developed in the aforementioned studies [8-10] most likely does not encompass these core-excited resonances.

We report the formation of 1, 16 and 17 Th fragments, as shown in Fig. 5.10, assigning them to H^-, O^- and OH^-, respectively. Similarly to free electron attachment, H^- formation is the dominant fragment for all projectiles, although its yield is comparable to the other fragments, which is not in agreement with the ionic yields in free electron attachment, where H^- is one order of magnitude higher than O^- and two orders of magnitude higher than OH^- [37,38].

The most interesting fragment however is OH^-. As can be seen in Fig. 5.10, OH^- yield increases significantly for increasing mass of the projectile. For H^- collisions, the OH^- yield is distinctly lower than the yield for O^- formation. In O^- collisions, the O^- and OH– yields are approximately the same and finally, for OH^- collisions, OH^- yield is significantly higher than the O^- yield.

For H^- collisions, the OH^- yield is low compared with its yield for O^- and H^- formation with this projectile. Hence the present H^- impact data is more similar to the free electron attachment data [38] than the OH^- and the O^- impact data, as generally expected on the basis of the pseudo-free electron rationale. Further investigations are necessary to identify the mechanisms leading to the strong OH^- and O^- product ion channels in the present heavier anion projectile data. It is worth noting that the timescale of the present collisions (tens of femtoseconds) is too short for proton transfer processes to take place.

5.1.5. Conclusions

In this work we have measured mass spectra for both anion and cation production for anion collisions (H^-, O^- and OH^-) with several organic compounds. For all the molecules studied (nitromethane, methanol, and ethanol) the product cations were consistent with mass spectra observed using alternative energy deposition mechanisms (notably electron impact ionisation), however differences were observed in terms of the relative intensities. The relative production of fragment cations/parent cations from nitromethane in collisions with H^- increased as a function of impact velocity in the range 0.01-0.40 v_{Bohr}. At constant anion impact energy (4 keV), fragmentation increased with the mass of the projectile anion in the sequence ($OH^- > O^- > H^-$). A possible common interpretation for both these results is to associate higher projectile momentum with increased energy deposition in the collisions. No clear evidence was observed for effects on the mass spectra due to the binding energy of the projectile anion's outermost electron. However, it has to be noted that some of the fragments not observed in this study may simply be due to the poor statistics and resolution of the quadrupole system, rather than to suppression of the fragmentation pathway.

In the case of negative ion formation, both methanol and ethanol show fragmentation patterns that closely resemble free electron attachment, although a significant signal of the parent anion in methanol is also observed. In the case of nitromethane, the fragmentation is significantly different from that obtained both in free electron attachment and in alkali atom-molecule collisions. It is quite

interesting to note that the low yield of NO_2^- lends credibility to the assumption that the stabilizing effect produced by the potassium cation in alkali atom collisions [2,32] stems from the electrostatic interaction between the potassium cation and the molecular TNI [2]. This mechanism has also been reported with biological molecules elsewhere [3,4]. As far as water is concerned, the reason for the increased yield of OH^- for higher mass projectiles is still not clear.

Finally, one of the main issues surrounding the analysis of the presented spectra pertained to inability of the quasi-free electron model to explain the appearance of fragments that require energies significantly above the ones obtained through it. By analysing data regarding N_2 [7,39], it was proposed in this study that the processes of collisional excitation described in ref. 7 can actually correspond to core-excited resonances. By extending this rationale to the molecules studied herein, the formation of the fragments that show thresholds higher than the energy range allowed by the classical quasi-free electron model can also be explained through the access to core-excited resonances.

In summary, the present spectra show that the fragmentation channels of these anion-molecule collisions can be very different from those obtained both in free electron attachment and in electron transfer. However, as expected from the pseudo-free electron approximation, the H^- projectile anion mass spectra from nitromethane and water better resemble the previous free electron attachment data than the mass spectra for OH^- and O^- projectiles. It is worth noting that the fragmentation of water, ethanol and methanol has previously been shown to stem from core-excited resonances [33,34,36,38]. Future work exploring these mechanisms in anion-molecule collisions may provide some answers regarding the limitations of the quasi-free electron model.

Acknowledgements

The authors wish to acknowledge the ITS-LEIF network, Ion Technology and Spectroscopy with Low Energy Ion beam Facilities, Transnational Access, Integrating Activities and Accompanying Measures, Integrated Infrastructure Initiative – I3, 6th FP, ITS LEIF-BH-2005-003, 2006–2009. D.A. and R.A. wish to acknowledge the Portuguese Foundation for Science and Technology (FCT-MCTES) for post-graduate scholarships SFRH/BD/61645/2009 and SFRH/BD/32271/2006, respectively. S.E. acknowledges the exchange visit to the Universidade Nova de Lisboa during the analytical stage of this research. S.E. and P.L.V. acknowledge the support from the British Council for the Portuguese-English joint collaboration. S.E. acknowledges the support of the British EPSRC through the Life Sciences Interface Fellowship program and of the European Commission through a Marie Curie Intra-European Reintegration Grant. We also acknowledge Professor Michael Probst from the University of Innsbruck for providing his DFT calculations on the vertical electron affinities. PLV acknowledges the visiting fellow position at the Department of Physics and Astronomy, The Open University, UK. This work forms part of EU COST Action CM0601 and CM0805 programmes “ECCL” and “The Chemical Cosmos”, respectively.

References:

[1]. V. Vuitton, P. Lavvas, R. V. Yelle, M. Galand, A. Wellbrock, G. R. Lewis, A. J. Coates and J. E. Wahlund, *Planet. Space Sci.*, **57**, 1558-1572, (2009).

[2]. R. Antunes, D. Almeida, G. Martins, N. J. Mason, G. Garcia, M. J. P. Maneira, Y. Nunes and P. Limao-Vieira, *Phys. Chem. Chem. Phys.*, **12**, 12513-12519, (2010).

[3]. F. Ferreira da Silva, D. Almeida, R. Antunes, G. Martins, Y. Nunes, S. Eden, G. Garcia, and P. Limão-Vieira, Phys. Chem. Chem. Phys., 13, 21621–9, (2011).

[4]. D. Almeida, R. Antunes, G. Martins, S. Eden, G. Garcia, F. Ferreira da Silva, Y. Nunes and P. Limao-Vieira, *Phys. Chem. Chem. Phys.*, **13**,15657-15665, (2011).

[5]. T. Okamoto, Y. Sato and H. Inouye, *Phys. Rev. Lett.*, **52**, 184-187, (1984).

[6]. V. N. Tuan, J. P. Gauyacq and V. A. Esaulov, *J. Phys. B-At. Mol. Opt.*, **16**, L95-L98, (1983).

[7]. V. N. Tuan and V. A. Esaulov, *J. Phys. B-At. Mol. Opt.*, **15**, L95-L100, (1982).

[8]. V. N. Tuan, V. Esaulov, J. P. Gauyacq and A. Herzenberg, *J. Phys. B-At. Mol. Opt.*, **18**, 721-735, (1985).

[9]. V. N. Tuan, V. Esaulov and J. P. Guayacq, *J. Phys. B-At. Mol. Opt.*, **17**, L133-L137, (1984).

[10]. V. N. Tuan, V. A. Esaulov, J. P. Grouard, R. I. Hall and J. L. Montmagnon, *J. Phys. B-At. Mol. Opt.*, **17**, 2897-2912, (1984).

[11]. NIST, NIST Chemistry WebBook, http://webbook.nist.gov.

[12]. J. Sorensen, L. H. Andersen and L. B. Nielsen, *J. Phys. B-At. Mol. Opt.*, **21**, 847-858, (1988).

[13]. J. P. Giese and E. Horsdal, *Nucl. Instrum. Meth. B*, **40-1**, 201-204, (1989).

[14]. F. Zappa, A. L. F. de Barros, L. F. S. Coelho, G. Jalbert, S. D. Magalhaes and N. V. D. Faria, *Phys. Rev. A*, **70, (**2004).

[15]. A. L. F. de Barros, S. Martinez, F. Zappa, S. Suarez, G. Bernardi, G. Jalbert, L. F. S. Coelho and N. V. D. Faria, *Phys. Rev. A*, **72, (**2005).

[16]. M. M. Sant'Anna, *Braz. J. Phys.*, **36**, 518-521, (2006).

[17]. M. Harnois, R. A. Falk, R. Geballe and J. Risley, *Phys. Rev. A*, **16**, 2256-2263, (1977).

[18]. J. Geddes, J. Hill and H. B. Gilbody, *J. Phys. B-At. Mol. Opt.*, **14**, 4837-4846, (1981).

[19]. J. A. Stone and T. J. Morgan, *Phys. Rev. A*, **31**, 3612-3619, (1985).

[20]. M. W. Gealy and B. Vanzyl, *Phys. Rev. A*, **36**, 3091-3099, (1987).

[21]. R. Cabrera-Trujillo, J. R. Sabin, Y. Ohrn and E. Deumens, *Phys. Rev. Lett.*, **84**, 5300-5303, (2000).

[22]. R. Cabrera-Trujillo, Y. Ohrn, E. Deumens and S. Jr, *Phys Rev A*, **62, (**2000).

[23]. S. G. Lias, in *NIST Chemistry WebBook*, NIST, 2009.

[24]. W. Sailer, A. Pelc, S. Matejcik, E. Illenberger, P. Scheier and T. D. Mark, *J. Chem. Phys.*, **117**, 7989-7994 (2002).

[25]. E. Alizadeh, F. F. da Silva, F. Zappa, A. Mauracher, M. Probst, S. Denifl, A. Bacher, T. D. Mark, P. Limao-Vieira and P. Scheier, *Int. J. Mass Spectrom.*, **271**, 15-21 (2008).

[26]. R. N. Compton, H. S. Carman, C. Desfrancois, H. AbdoulCarmine, J. P. Schermann, J. H. Hendricks, S. A. Lyapustina and K. H. Bowen, *J. Chem. Phys.*, **105**, 3472-3478 (1996).

[27]. D. C. Clary, *J. Phys. Chem.*, **92**, 3173-3181 (1988).

[28]. E. Fermi and E. Teller, *Phys. Rev.*, **72**, 399-408 (1947).

[29]. T. Sommerfeld, *Phys. Chem. Chem. Phys.*, **4**, 2511-2516 (2002).

[30]. G. L. Gutsev and R. J. Bartlett, *J. Chem. Phys.*, **105**, 8785-8792 (1996).

[31]. R. F. M. Lobo, A. M. C. Moutinho, K. Lacmann and J. Los, *J. Chem. Phys.*, **95**, 166-175 (1991).

[32]. I. C. Walker and M. A. D. Fluendy, *Int. J. Mass Spectrom.*, **205**, 171-182 (2001).

[33]. A. Kuhn, H. P. Fenzlaff and E. Illenberger, *J. Chem. Phys.*, **88**, 7453-7458 (1988).

[34]. M. Orzol, I. Martin, J. Kocisek, I. Dabkowska, J. Langer and E. Illenberger, *Phys. Chem. Chem. Phys.*, **9**, 3424-3431 (2007).

[35]. L. V. Trepka and H. Neuert, *Z. Naturforsch. Pt. A*, **A 18**, 1295 (1963).

[36]. M. G. Curtis and I. C. Walker, *J. Chem. Soc. Faraday T.*, **88**, 2805-2810 (1992).

[37]. Y. Itikawa and N. Mason, *J. Phys. Chem. Ref. Data*, **34**, 1-22 (2005).

[38]. J. Fedor, P. Cicman, B. Coupier, S. Feil, M. Winkler, K. Gluch, J. Husarik, D. Jaksch, B. Farizon, N. J. Mason, P. Scheier and T. D. Mark, *J. Phys. B-At. Mol. Opt.*, **39**, 3935-3944 (2006).

[39]. L. Sanche and G. J. Schulz, *Phys. Rev. A*, **6**, 69 (1972).

[40]. S. Pilling, H. M. Boechat-Roberty, A. C. F. Santos and G. G. B. de Souza, *J. Electron Spectrosc.*, **155**, 70-76 (2007).

[41]. J. Berkowitz, G. B. Ellison and D. Gutman, *J. Phys. Chem.*, **98**, 2744-2765 (1994).

[42]. P. Warneck, *Z. Naturforsch. Pt. A*, **A 26**, 2047 (1971).

[43]. L. Friedman, F. A. Long and M. Wolfsberg, *J. Chem. Phys.*, **27**, 613-622 (1957).

[44]. H. S. Kilic, K. W. D. Ledingham, C. Kosmidis, T. McCanny, R. P. Singhal, S. L. Wang, D. J. Smith, A. J. Langley and W. Shaikh, *J. Phys. Chem. A*, **101**, 817-823 (1997).

[45]. C. Lifshitz, M. Rejwan, I. Levin and T. Peres, *Int. J. Mass Spectrom. Ion Proc.*, **84**, 271-282 (1988).

[46]. R. J. Kandel, *J. Chem. Phys.*, **23**, 84-87 (1955).

[47]. S. Tsuda, C. E. Melton and W. H. Hamill, *J. Chem. Phys.*, **41**, 689 (1964).

[48]. B. Ruscic and J. Berkowitz, *J. Chem. Phys.*, **101**, 10936-10946 (1994).

[49]. J. L. Holmes, J. K. Terlouw and F. P. Lossing, *J. Phys. Chem.*, **80**, 2860-2862 (1976).

[50]. R. D. Bowen and A. Maccoll, *Org. Mass Spectrom.*, **19**, 379-384 (1984).

[51]. K. M. A. Refaey and W. A. Chupka, *J. Chem. Phys.*, **48**, 5205 (1968).

[52]. Y. Niwa, T. Nishimura, H. Nozoye and T. Tsuchiya, *Int. J. Mass Spectrom. Ion Proc.*, **30**, 63-73 (1979).

[53]. M. A. Haney and J. L. Franklin, *J. Chem. Phys.*, **50**, 2028 (1969).

[54]. A. N. Stepanov, A. A. Perov, S. P. Kabanov and A. P. Simonov, *High. Energ. Chem.*, **22**, 81-85 (1988).

[55]. V. H. Dibeler, J. A. Walker, H. M. Rosenstock, *Journal of Research of the National Bureau of Standards - A. Physics and Chemistry*, 70, 459-463 (1966).

Chapter 6

6. Electron transfer to DNA/RNA sugar unit surrogates: THF vs D-Ribose

In order to graduate to the study of more complex biological relevant molecules, namely uridine, one first has to study its parts separately. The knowledge of the parts may allow for a better understanding of the complex molecular structure of some parts of DNA/RNAas a whole. This chapter focuses on the study of two molecules which have been proposed as possible surrogates for the DNA/RNA sugar unit: tetrahydrofuran (THF) and D-Ribose.

The first part of this chapter pertains to the study of electron transfer in potassium collisions with D-Ribose. The main emphasis is given to the discrepancy between electron transfer and DEA measurements, namely the dominance of OH^- formation in electron transfer measurements. A rationale involving the presence of the potassium cation near the TNI was developed in order to explain this discrepancy.

In the second part of the chapter, the fragmentation patterns of THF when subjected to electron transfer by collisions with potassium atoms is presented. It was shown in this study that, although the accessed resonances in DEA and electron transfer are most likely the same, the fragmentation patterns may be quite different. In other words, when comparing DEA and electron transfer, the initially accessed TNI state may be the same, however, it can decay through different fragmentation pathways. The main difference between electron transfer and DEA is the dominance of the O^- channel, which is indicative of cyclic esther ring breaking .

Dynamic of negative ions in potassium-D-Ribose collisions

D. Almeida [1],F. Ferreira da Silva [1], G. García [2,3] and P. Limão-Vieira [1,4*]

[1] Laboratório de Colisões Atómicas e Moleculares, CEFITEC, Departamento de Física, Faculdade de Ciências e Tecnologia, Universidade Nova de Lisboa, 2829-516 Caparica, Portugal
[2] Instituto de Física Fundamental, Consejo Superior de Investigaciones Científicas, Serrano 113-bis, 28006 Madrid, Spain
[3] Centre for Medical Radiation Physics, University of Wollongong, NSW2522, Australia
[4] Centre for Earth, Planetary, Space and Astronomical Research, Department of Physical Sciences, The Open University, Walton Hall, MK7 6AA, United Kingdom

Published in J. Chem. Phys., **139**, 114304 (2013).

Abstract

We present negative ion formation from collisions of neutral potassium atoms with D-Ribose ($C_5H_{10}O_5$), the sugar unit in the DNA/RNA molecule. From the negative ion time-of-flight (TOF) mass spectra, OH^- is the main fragment detected in the collision range 50 to 100 eV accounting on average for 50% of the total anion yield. Prominence is also given to the rich fragmentation pattern observed with special attention to O^- (16 m/z) formation. These results are in sharp contrast to dissociative electron attachment (DEA) experiments. The TOF mass spectra assignments show that these channels are also observed, albeit with a much lower relative intensity. Branching ratios of the most abundant fragment anions as a function of the collision energy are obtained, allowing to establish a rationale on the collision dynamics.

6.1.1. Introduction:

Further to the recent studies on the damaging capability of low energy electrons (LEEs) to decompose DNA [1], studying electron interactions with its constituents provides valuable insight into the fundamental mechanisms underlying such damage. A recent study has shown that electron-driven reactions to DNA yielding single, double and clustered lesions, can be explained through damage to its building blocks, i.e. the nucleobases, the sugar unit and the phosphate groups [1,2]. In the light of these ground-breaking studies, an increased attention to low energy electron interactions with DNA/RNA subunits has been observed. As such, studying chemical reactions for biomolecular systems is relevant to understand radiation induced damage at the molecular level. Recent developments of Monte Carlo-based empirical simulations on pseudo-physiological environment allow us to model electron (and positron) tracks that result from the interaction of high energy quanta through a given tissue-equivalent material (TEM) [3-7]. At the moment, however, the simulations are restricted to rather simplistic TEMs [6-8], owing to the empirical nature of these models requiring information on the cross sections and dynamics of the underlying physicochemical processes.

Therefore, the study of fundamental molecular mechanisms is of particular relevance to allow for these models to encompass increasingly (and therefore more accurate) descriptions of the physiological environment's response to radiation-induced changes. In the particular case of the DNA/RNA sugar unit or a given substitute, knowledge on electron elastic and inelastic scattering is quite well established (see e.g. [9]), which is also the case of DEA processes [1,10-17]. However, data on the interaction with electron-donating projectiles, i.e. electron transfer processes in potassium-molecule collisions is, as far as authors are aware, absent. As such, studying the processes that occur in the context of electron transfer in atom-molecule collisions can be a stepping stone in our understanding of some of the molecular mechanisms that can happen in non-gas-phase environments. In particular, studying the role of the sugar unit is critical, as it is now well established that one of the main sources of possible damage to DNA/RNA stems from changes in the D-Ribose unit [18].

Recently, we have pursued in our laboratory a series of detailed studies on negative ion formation in collisions of potassium atoms with several bio-related molecular targets [19-25]. Further to the studies of atomic collisions with nucleobases [23], herein we present the negative ion fragmentation pattern from collisions of potassium atoms with the D-Ribose molecule ($C_5H_{10}O_5$), the monosaccharide pentose ring in the DNA/RNA structure. The mechanism studied in these collisions is the transfer of the unpaired valence electron of a neutral hyperthermal potassium atom (K) to a target molecule (AB). The electron transfer mechanism is only possible at particular potassium-molecule distances, the crossing radius, R_c, with a rough estimate of ~3.2Å for the present case. Briefly, in atom-molecule collisions, where an adiabatic electron transfer occurs, a negative ion is formed as part of an intermediate step or as a final product. The electron transfer process happens when electrons follow adiabatically the nuclear motion in the vicinity of the crossing of the stationary non-perturbed states, i.e. the covalent and the ionic diabatic states (from the crossing of the covalent and the ionic diabatic potential surfaces) at large atom-molecule distances. The ionic surface lies above the covalent surface, the endoergicity being $\Delta E=IE(K)–EA(AB)$, where IE stands for the ionisation energy of the potassium atom and EA the electron affinity of the target molecule. However, due to the coulombic interaction, there is a crossing seam for which both stationary non-adiabatic potential energy surfaces have the same value. During the collision process and near that crossing, there can be a perturbation of the stationary states induced by the projectile/target nuclear motion leading to a coupling. This leads after the collision path to the formation of a positive ion K^+ and a molecular anion, which may even allow access to parent molecular states that are otherwise not accessible in free electron attachment experiments [22,23,26]. In particular, states with a positive electron affinity can be formed, and the role of vibrational excitation of the parent neutral molecule can be studied [27] by the collision dynamics [19].

Another consequence of the K^+ presence is that, even if the free negative molecular ion is unstable with respect to autodetachment, in the collision complex it can be stabilized at distances shorter than the crossing between the two potential energy surfaces. This is due to the attractive

interaction with the positive ion, K^+ [26]. Indeed, recent measurements of anion collisions (H^-, O^- and OH^-) with nitromethane (CH_3NO_2) indicate that the autodetachment suppression mechanism is not as efficient as in neutral atom-molecule collisions [28], which can be rationalized as the interaction between the resulting molecular anion and neutral projectile being much weaker than the coulombic interaction that persists in neutral atom-molecule collisions.

As far as DEA is concerned, several studies have been already performed on the D-Ribose (DR) molecule [1,10,11,13] and its substitutes [15], particularly using isotopic labelling, which showed a remarkable site selectivity in the fragmentation channels yielding $(DR\text{-}H_2O)^-$ formation [10]. The water abstraction sites were explored in more detail in this study, and a tentative identification of some sequential reaction channels was performed[10].

Another interesting study using a Fourier transform ion cyclotron resonance mass spectrometer and density functional theory (DFT) calculations [29] concluded that, upon heating in the gas-phase D-Ribose, the molecule changes its geometry to form a pyranose structure (six-membered ring) rather than keeping its furanose form (five-membered ring), the latter present in the DNA/RNA framework [29]. As such, this study concludes that the dominant conformer in gas-phase D-Ribose is the pyranose form.

In this work we focus our attention on the negative ion formation in collisions of neutral potassium atoms (50-100 eV lab frame) with D-Ribose molecules. In the next section, we provide a brief summary of the experimental setup. In Section 3 we present and discuss the negative ion mass spectra. Where and when possible, comparisons with available DEA data will provide relevant information of the electronic structure of the target molecule. Finally, in Section 4, some conclusions will be drawn regarding the importance of these studies as far as state of the art electron-driven DNA/RNA damage is concerned.

6.1.2. Experimental details:

The experimental setup used to obtain the negative ion TOF mass spectra has been described elsewhere [23,26]. Briefly, an effusive molecular beam crosses a primary beam of fast neutral potassium (K) atoms. K^+ ions produced in a potassium ion source were accelerated to 50-100 eV, before passing through an oven where they resonantly charge exchange with neutral potassium to produce a beam of fast (hyperthermal) atoms. Residual ions from the primary beam are removed by electrostatic deflecting plates outside the oven. The intensity of the neutral potassium beam was monitored using a Langmuir-Taylor ionisation detector, before and after the TOF mass spectra collection. The effusive beam of D-Ribose (DR) was then introduced into a 1 mm diameter source where it was crossed with the neutral hyperthermal potassium beam between two parallel plates at 1.2 cm mutual separation. The anions produced were extracted by a 220 Vcm^{-1} pulsed electrostatic field. The typical base pressure in the collision chamber was 8×10^{-5} Pa and the working pressure upon

heating the powder samples was 2×10^{-4} Pa. Mass spectra were obtained by subtracting the background signal from the sample measurements. TOF mass spectra calibration was carried out on the basis of the well-known anionic species formed after potassium collisions with the nitromethane molecule [23,26]. This allows for safe mass assignment, even when the width of the peaks is larger than 1 m/z.
The solid sample used in the present experiment was purchased from Sigma-Aldrich with a minimum purity of ≥ 99%. It was used as delivered. The sample was heated up to 373K. In order to test for any thermal decomposition, the spectra were recorded at different temperatures (up to ~ 400K). No differences were observed in the relative peak intensities as a function of the heating temperature. The extraction region and the TOF system were heated throughout measurements in order to prevent any sample condensation and thence charge accumulation on the electrodes. It is worth noting that the width of the mass peaks may give information on the kinetic energy release distribution of the fragment. However such approach would require a substantially different treatment of the experimental data, which is not within the scope of the present study.

6.1.3. Results and Discussion:

The negative ion TOF mass spectra obtained for 50, 75 and 100 eV potassium collision energies in the lab frame are presented in Fig. 6.1(a-c) and peak assignments in Table 6.1. Additionally, branching ratios for the major fragments as a function of the collision energy are shown in Fig. 6.2. A brief analysis of these data shows that the most abundant fragments are assigned to OH^- (17 m/z), followed by O^- (16 m/z) and $C_3H_6OH^-/CH_3COO^-$ (59 m/z). One can clearly see that there is evidence of neither the parent or its dehydrogenated anion formation, where the latter was only reported in previous DEA studies [10,11,13,15]. A close inspection of Table 6.1 reveals that fragment anions m/z 25, 41, 43 and 45 were not reported in DEA experiments. Regarding the absence of the dehydrogenated parent anion $(DR\text{-}H)^-$ formation, it is interesting to note that in DEA its resonance profile (shape and energy position) is similar to other fragments [13]. This implies that, while the initial accessed state may be the same, it then opens up different fragmentation pathways. In this context, it is plausible to reason that the pathway resulting in $(DR\text{-}H)^-$ formation will not be able to compete with the other fragmentation pathways. Since the main difference between DEA and electron transfer lies on the presence of the potassium cation post-collision, it stands to reason that the potassium cation may indeed be the cause for this discrepancy. Another possible rationale for such absent channel may reside on the fact that upon electron capture, the sugar ring may pucker, which will lead to an increased chance of overlapping between molecular orbitals. This in turn may enhance intramolecular electron transfer between π^* and σ^* orbitals. This then leads to an inability of the electron to stay in a less anti-bonding orbital, which in turn may result in prompt dissociation.

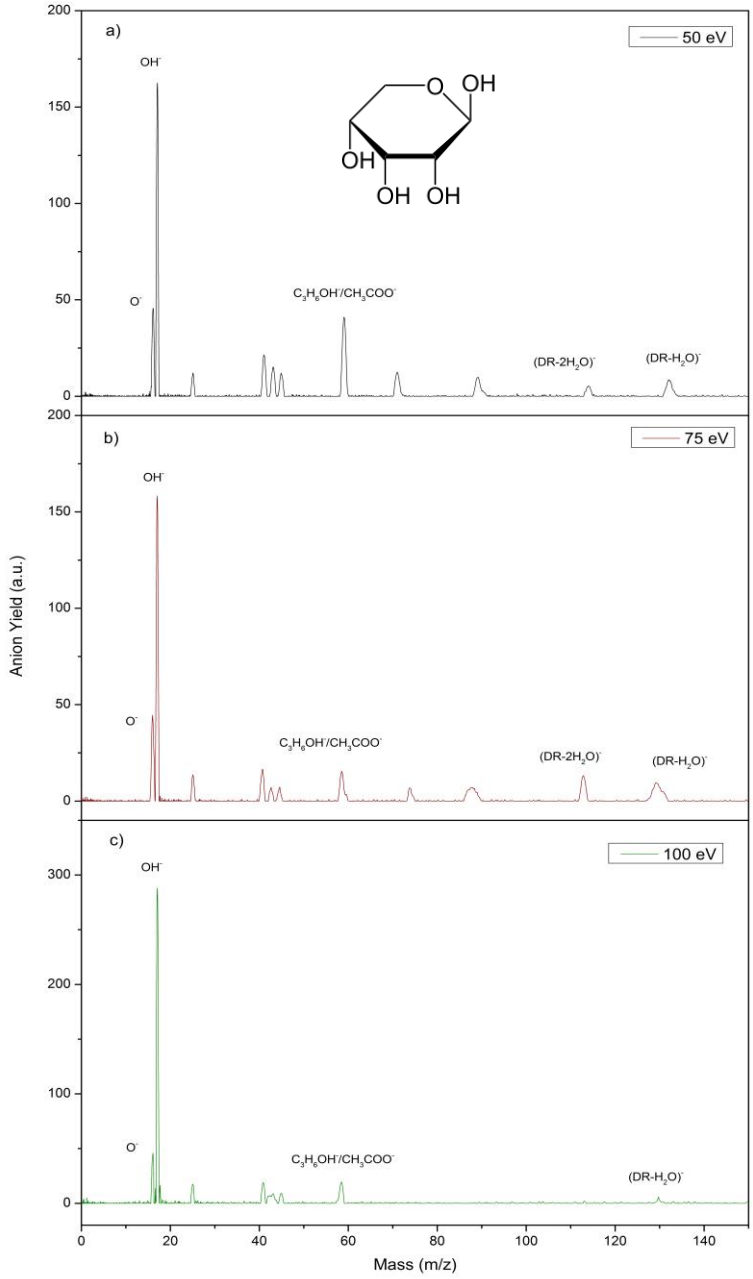

Figure 6. 1 Negative TOF mass spectra in potassium-D-Ribose collisions at: a) 50 eV; b) 75 eV; and c) at 100 eV collision energy in the lab frame. An insert with the dominant conformer is added[29].

As mentioned before, the dominant conformer in gas-phase D-Ribose is the six-membered pyranose form ring, which is structurally analogous to fructose. Additionally it is worth noting that a theoretical study has determined that the dipole moment for such conformers lies between 3 and 4 D,

which has been shown to be enough to support dipole-bound anion states. We now discuss the majority of the anions formed in such potassium-molecule collisions.

Proposed anion assignment	This work	DEA studies	
		Deoxyribose[10,11,13]	Fructose[15]
H^-	×	×	✓
O^-	✓	✓	✓
OH^-	✓	✓	✓
C_2H^-	✓	×	×
C_2HO^-	✓	×	×
$C_2H_3O^-$	✓	×	×
$HCOO^-$	✓	×	✓
$C_3H_6OH^-/CH_3COO^-$	✓	✓	×
$C_3H_4O_2^-$	✓	✓	✓
$C_3H_5O_3^-$	✓	✓	×
$(M\text{-}2H_2O)^-$	✓	✓	✓
$(M\text{-}H_2O)^-$	✓	✓	✓
$(M\text{-}H)^-$	×	✓	×

Table 6. 1 Assignment of TOF mass spectrum anions in collisions of potassium atoms with D-Ribose. Comparisons are made with the available DEA studies to deoxyribose and fructose molecules. M means parent.

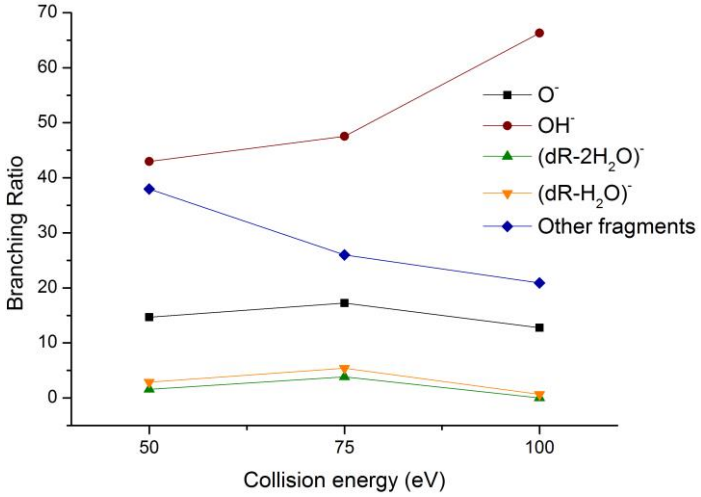

Figure 6. 2 Branching ratios for the anions as a function of the collision energy. Error bars are within the data points and so not visible.

(DR-H_2O)$^-$ & (DR-$2H_2O$)$^-$

The fragment anion m/z 132 can be assigned to the loss of one hydroxyl and hydrogen group, whereas m/z 114 to the abstraction of two hydroxyl and hydrogen radicals. An ensuing discussion of certain aspects of these fragmentation channels leads to the following questions: 1) do hydrogen and hydroxyl excision lead to a water molecule formation?; 2) from which positions do the fragments stem from?; and 3) given that some of the neutral fragments do not require ring breaking, does the molecular anion remain in its ring form? Regarding the first, such fragment anions have been also reported in DEA studies [10,11,13,15]. In the case of fructose, it was shown that formation of a water molecule is exothermic by - 242 kJ.mol^{-1} (-2.51 eV). Furthermore, positive ion spectra in electron interactions with D-Ribose report the presence of H_2O^+ [13,15]. This therefore leads to the conclusion that the abstraction of the hydrogen and hydroxyl radicals will result in the formation of one (or two) water molecule(s).

The second question pertains to site selectivity in the formation of these fragments. Indeed, as was shown in DEA studies that make a criterion use of isotope-labelled ribose rings, formation of water molecules does not appear to stem from the C_1-H bond [10].

Regarding the third question, it is known that (DR-H_2O)$^-$ and (DR-$2H_2O$)$^-$ formation stems from accessing the same initial state. According to DEA experiments [13], these fragments show near-0 eV resonances reminiscent of dissociation mechanisms present in other molecules, such as the well-explored case of uracil/thymine [30-32]. Some studies have indeed shown that dissociation through near-0 eV resonances pertains to a molecular mechanism in which an incident electron is capture into a diffuse dipole-bound state (DBS), followed by an intramolecular electron transfer to a valence state that subsequently leads to fragmentation [30-32]. This "doorway" mechanism is indeed somewhat pervasive, namely appearing in molecules such as nitromethane[33] and uracil/thymine [30]. Indeed, a theoretical study on fructose [14] shows that it is possible for the pyranose conformer of D-Ribose to undergo such mechanism. As such, the discussion is centred on the basis of an initial capture of the incoming electron into a dipole-bound state, due to the molecule's considerable average dipole moment (3.2 D [14] depending on the conformer). Such value is more than enough to warrant the presence of a stable DBS. Subsequently, a transfer of the extra electron to one of the valence states may be possible, but only through an opening of the ring, which in turn will result in fragmentation. This therefore leads to the abstraction of an H and OH, with the molecular anion becoming acyclical, i.e. losing its ring structure. This study therefore lends support to the conclusion that capture of virtually no-energy electrons will result in formation of an acyclic form of the molecular anion [14]. As such, in the case of the present study, it can be assumed that the resonance enhanced mechanisms governing such fragmentation channels are the same as in DEA.

A detailed analysis of Fig. 6.2 shows that, with the exception of OH^- and other fragments, O^-, (DR-H_2O)$^-$ and (DR-$2H_2O$)$^-$ branching ratios do not change appreciably with the collision energy, and

so do not depend on the collision time. This means that the channels yielding these fragments are not affected by the type of atomic scattering process, i.e. either covalent or ionic (a more concise discussion on the relevance of these scattering processes can be found in refs. [20,34]). As such, for those fragments, their branching ratios show the same trend, which is indicative that both dissociative channels are a result of similar collision dynamics.

Finally, owing to the width of the mass peak, it is not possible to unambiguously discard the possibility of sole formation of OH radicals (either in detriment or in conjunction with), for both m/z 114 and 132 peaks. However, several mass calibrations point towards the aforementioned assignments. Additionally, it is important to note that, given the symmetry between the flanks of the peak, formation of OH radicals is, at best, negligible at 50 and 100 eV collision energy. In other words, formation of the OH radical would entail, at least, a difference in the right flank of the TOF mass peak, which may be the case at 75 eV (Fig. 6.1b)). However due to the present mass resolution limitation no further discussion will be added on this issue.

OH^-

OH^- is the most abundant fragment ion for all collision energies, amounting for 43% at 50 eV of the total anion yield and increasing up to 66% at 100 eV collision energy. Moreover, by gleaning at Fig. 6.2, OH^- relative yield further increases with increasing collision energy. This fact is in sharp contrast with the branching ratios for the other fragments, where for energies higher than 75 eV, their relative yields decrease. With such high yield (> 60%), the dissociation mechanism is indicative of a diatomic-like behaviour along the C-OH coordinate(s), which is particularly interesting since such is prevalent in halogenated species such as C_6H_5F [19].

The dominance of this fragmentation channel in the present study is in sharp contrast with DEA experiments, in which while present, but at much lower yield than the dominant water-abstraction channels [13,15]. Such discrepancies between DEA and electron transfer experiments have already been detected in other molecules, most notably regarding the CNO^- yield in uracil and thymine [23]. Briefly, it was shown that, owing to the presence of the potassium cation in the vicinity of the molecular anion, a delay in the autodetachment process of the extra electron occurs, allowing π^* orbitals to be populated long enough for the electron to be transferred to a highly dissociative σ^* orbital [23,35], which will subsequently lead to fragmentation. Indeed, a recent DEA study to D-Ribose shows a resonance profile for OH^- formation consisting of one dominant peak at near-zero energy and a weak wider structure at around 7 eV, the latter assigned to a shape resonance [11]. The OH^- signal appears as not the main dominant signal in DEA experiments, in contrast with the present experiments. Additionally, the DEA study presents quantum chemical calculations that provide an assignment of a π^* anionic state to a shape resonance with a lifetime of ~ 3.1 fs [11]. This, therefore, can lead one to propose a OH^- formation mechanism similar to that responsible for CNO^- as in uracil

and thymine [23], i.e. the potassium cation will, in effect, increase the lifetime of the anionic state formed at 7 eV, therefore allowing for fragmentation to successfully compete with autodetachment, thereby leading to an enhancement of the OH^- yield. Considering that in electron transfer, autodetachment suppression is much more efficient in the case of ionic scattering, the collision dynamics for OH^- formation may be reasonably described by the major contribution of this type of scattering. It is critical to note that higher collision energies imply a smaller probability of ionic scattering [20,34]. Nevertheless, such assumption seems to be inconsistent with the significant rise of OH^- branching ratio, where for higher collision energies a covalent scattering should prevail. However, it is important to stress that the branching ratio does not provide information about the absolute rate of formation, but limited to information about the relative yield. As such, one can rationalize by stating that, while a gradual increase of covalent scattering does indeed happen, and therefore a decrease in the probability of OH^- formation occurs, it does not necessarily mean that the branching ratio for this fragment decreases. This is even true because such behaviour may be expected for the other fragment anions, and the branching ratio is always obtained by the summation of the total anion yield. Assuming the mechanism proposed above, an interesting discussion that can follow would be to determine if site and bond selectivity mechanisms yielding OH^- formation play an important role in the dissociation process. Such selectivity has already been shown in other molecules, both in DEA [36,37] and in atom-molecule collision experiments [24,25]. However for D-Ribose there is no data to sustain such mechanism and due to the fact that OH^- appears to stem from only one anionic state (as discussed before), site selectivity in the electron transfer process most likely does not play a relevant role.

O^-

O^- (16 m/z) presents itself as one of the most intense fragments in the TOF mass spectra, which contrasts with DEA experiments where its yield is only marginal. The O^- branching ratio shows a small increase from 15% (at 50 eV) to 17% (at 75 eV), followed by a small decrease to 13% (at 100 eV), (Fig. 6.2). Further to the discussion above on OH^- formation, and given that the energy resonance profile of O^- in DEA shows only high energy resonances (> 6 eV), it is plausible to attribute O^- to a competition with OH^- formation through those high-lying resonances. However, in order to further discard O^- formation from ring breaking, studies are needed and at present we are performing electron transfer studies to tetrahydrofuran (THF) in order to specifically address this issue.

Other fragments

From Figs. 6.1(a-c), apart from the major anions, the fragmentation pattern is quite rich in other anionic species. In Table 6.1 assignments of the several fragment anions are proposed, where not

only the results from DEA experiments to D-Ribose studies are considered [10,11,13], but, and perhaps more interestingly, results from DEA studies to sugar substitutes [15] are also reported for comparison. The similarity between the fragmentation patterns in DEA and electron transfer experiments is quite significant, with the main differences lying on the relative yields. From the comparison between D-Ribose electron transfer and DEA data on fructose [15] (one of the sugar substitutes) we also note a similarity between some of the fragmentation patterns, mainly the water abstraction channels, 72 ($C_3H_4O_2^-$), 45 ($HCOO^-$) and 16 (O^-) m/z. Fructose is most likely to be the closest substitute to gas-phase D-Ribose, owing to the pyranose form in the gas-phase upon heating the sample [29]. A more thorough study on sugar substitutes in the context of neutral atom collisions would be of great interest and we are currently pursuing such investigations in our laboratory. Finally, of particular relevance we note C_2H^- formation in the present experiments, which was not reported in DEA studies to deoxyribose and fructose (see Table 1). The C_2H^- formation requires multiple bond breaking in the precursor anion. However, C_2H has a considerable high electron affinity (2.969 eV) [38], which can explain being observed at all collision energies.

6.1.4. Conclusions:

The present work provides the first study on negative ion formation in collisions of potassium atoms with D-Ribose, the DNA/RNA sugar unit. The fragmentation pattern is similar to recent DEA studies. However, the relative yields of several fragments are significantly different when compared to DEA, in particular for OH^-, which is here the dominant ion detected in the TOF mass spectra. The enhancement in the formation of this fragment is proposed to be due to the ability of potassium cation to suppress and/or even delay efficiently autodetachment, an effect that has been increasingly observed as pervasive in the context of atom-molecule collision studies [21-23,28]. Noteworthy is the fact that neither the parent nor its dehydrogenated negative ions are reported. Finding out if water abstraction channels result indeed in the formation of a water molecule, rather than an abstraction of H and OH radicals, remains critical. Due to their quite high reactivity, the efficiency of these radicals as a damaging agent on the surrounding molecules in the biological environment may be quite significant. However, the presence of H_2O^+ in the positive ion mass spectra studies to D-Ribose [13,15], lends support to the possibility of a concerted mechanism where an H and OH are abstracted, resulting in a water molecule formation. Such, can be regarded as a non-harmful agent to the surrounding molecular framework of the DNA/RNA.

In DEA studies to several (bio)molecular targets, the dominant fragmentation channels result from very low energy resonances (often as low as ~0 eV) consisting of vibrational Feshbach resonances [32]. This can be rationalized by the fact that, in DEA, accessing high-energy resonances (such as formation of CNO^- in uracil/thymine [38]) will mostly result in autodetachment, rather than

in fragmentation. However, in atom-molecule collisions, there are strong evidences that autodetachment is significantly suppressed, enhancing fragment formation. Such is the case for uracil and thymine and is also the case for D-Ribose. As far as authors are aware, electron transfer studies to D-Ribose are completely unprecedented, with the most similar technique with which to compare being DEA studies. DEA studies on D-Ribose show that the main fragmentation channels consist of near-0 eV shape resonances that result in abstraction of one or more H and OH radicals, thereby not causing break of the sugar ring [13]. However, less intense fragmentation channels at higher electron energies (5-10 eV) do result in ring-breaking [13]. We notice that extended DEA studies will be of particular relevance in order to attempt a more thorough knowledge of the mechanisms behind the fragmentation pathways, in particular unreported anionic fragments. This may eventually lead to the understanding of possible damage mechanisms that this entails to the DNA molecule as a whole. However, it is interesting to mention the analogy that can be made between electron transfer and the presence of electron-donating elements in the vicinity of the DNA molecule. While this is an admittedly gross approximation, we suggest that it can be viewed as means to study molecule(atom)-molecule interactions between radicals (e.g. $O^{\bullet}$ and $OH^{\bullet}$ are formed from the water radiolysis) and the various components of the DNA macromolecule. Interestingly, higher-energy shape resonances in D-Ribose have been identified [11] but are, owing to their low lifetimes, generally ignored as not being very important in the context of low-energy electron damage to DNA. Though, the present results highlight that this may not be the case. We have shown that the presence of a third body near the TNI can greatly affect its fragmentation pathways and as such, formation of TNIs through the aforementioned resonances cannot, and should not, be disregarded.

However, it is known that the sugar unit in DNA has a furanosic form. As such, studies with furanosic sugars, namely THF (which is an ether but is a known sugar surrogate), need to be performed in order to ascertain how important this characteristic is in the discussion of DNA/RNA sugar substitutes. Indeed, it has been shown that, for both THF and furan, no low-energy resonances (< 5 eV) appear [15]. This is in contrast to deoxyribose, D-Ribose and fructose.

Acknowledgements

D.A. and F.F S. acknowledge the Portuguese Foundation for Science and Technology (FCT-MEC) for a post-graduate Grant No. SFRH/BD/61645/2009 and post-doctoral Grant No. SFRH/BPD/68979/2010, respectively. We are also grateful to the partial funding from the Portuguese research Grants PEst-OE/FIS/UI0068/2011 and PTDC/FIS-ATO/1832/2012 through FCT-MEC. PL-V acknowledges his visiting Professor position at The Open University, UK. The Spanish Ministerio de Economía y Competitividad (Project No. FIS 2009-10245) is also acknowledged. Some of this work forms part of the EU/ESF COST Actions Nano-IBCT-MP1002 and The Chemical Cosmos-CM0805.

References

[1]. B. Boudaïffa, P. Cloutier, D. Hunting, M.A. Huels, and L. Sanche, Science **287**, 1999 (2000).

[2]. F. Martin, P. Burrow, Z. Cai, P. Cloutier, D. Hunting, and L. Sanche, Phys. Rev. Lett. **93**, 6 (2004).

[3]. A.G. Sanz, M.C. Fuss, A. Munoz, F. Blanco, P. Limão-Vieira, M.J. Brunger, S.J. Buckman, and G. Garcia, Int. J. Rad. Bio. **88**, 71 (2012).

[4]. M.C. Fuss, A. Muñoz, J.C. Oller, F. Blanco, A. Williart, P. Limão-Vieira, M.J.G. Borge, O. Tengblad, C. Huerga, M. Téllez, and G. García, App. Rad. Isotop. **69**, 1198 (2011).

[5]. M.C. Fuss, A. Muñoz, J.C. Oller, F. Blanco, P. Limão-Vieira, A. Williart, C. Huerga, M. Téllez, and G. García, Eur. Phys. J. D **60**, 203 (2010).

[6]. J.C. Oller, A. Muñoz, J.M. Pérez, F. Blanco, P. Limão-Vieira, and G. García, Chem. Phys. Lett. **421**, 439 (2006).

[7]. M.C. Fuss, A.G. Sanz, A. Muñoz, T.P.D. Do, K. Nixon, M.J. Brunger, M.-J. Hubin-Franskin, J.C. Oller, F. Blanco, and G. García, Chem. Phys. Lett. **560**, 22 (2013).

[8]. M.C. Fuss, A. Muñoz, J.C. Oller, F. Blanco, M.-J. Hubin-Franskin, D. Almeida, P. Limão-Vieira, and G. García, Chem. Phys. Lett. **486**, 110 (2010).

[9]. M. Fuss, A. Muñoz, J.C. Oller, F. Blanco, D. Almeida, P. Limão-Vieira, T.P.D. Do, M.J. Brunger, and G. García, Phys. Rev. A **80**, 052709 (2009).

[10]. I. Bald, J. Kopyra, and E. Illenberger, Angew. Chem., Int. Ed. Engl. **45**, 4851 (2006).

[11]. I. Baccarelli, F.A. Gianturco, A. Grandi, N. Sanna, R.R. Lucchese, I. Bald, J. Kopyra, and E. Illenberger, J. Am. Chem. Soc. **129**, 6269 (2007).

[12]. C. Wang, J. Nguyen, and Q. Lu, J. Am. Chem. Soc. **131**, 11320 (2009).

[13]. S. Ptasińska, S. Denifl, P. Scheier, and T.D. Märk, J. Chem. Phys. **120**, 8505 (2004).

[14]. T. Sommerfeld, J. Chem. Phys. **126**, 124301 (2007).

[15]. P. Sulzer, S. Ptasinska, F. Zappa, B. Mielewska, A.R. Milosavljevic, P. Scheier, T.D. Märk, I. Bald, S. Gohlke, M.A. Huels, and E. Illenberger, J. Chem. Phys. **125**, 44304 (2006).

[16]. I. Bald, J. Kopyra, I. Dabkowska, E. Antonsson, and E. Illenberger, J. Chem. Phys. **126**, 074308 (2007).

[17]. L. Sanche, Nature **461**, 358 (2009).

[18]. K. Miaskiewicz and R. Osman, J. Am. Chem. Soc. **116**, 232 (1994).

[19]. P. Limão-Vieira, A.M.C. Moutinho, and J. Los, J. Chem. Phys. **124**, 054306 (2006).

[20]. A.W. Kleyn and A.M.C. Moutinho, J. Phys. B: At. Mol. Opt. Phys. **4075**, R1 (2001).

[21]. F. Ferreira da Silva, M. Lança, D. Almeida, G. García, and P. Limão-Vieira, Eur. Phys. J. D **66**, 78 (2012).

[22]. F. Ferreira da Silva, D. Almeida, R. Antunes, G. Martins, Y. Nunes, S. Eden, G. Garcia, and P. Limão-Vieira, Phys. Chem. Chem. Phys. **13**, 21621 (2011).

[23]. D. Almeida, R. Antunes, G. Martins, S. Eden, F. Ferreira da Silva, Y. Nunes, G. Garcia, and P. Limão-Vieira, Phys. Chem. Chem. Phys. **13**, 15657 (2011).

[24]. D. Almeida, F. Ferreira da Silva, G. García, and P. Limão-Vieira, Phys. Rev. Lett. **110**, 023201 (2013).

[25]. F. Ferreira da Silva, C. Matias, D. Almeida, G. García, O. Ingólfsson, H.D. Flosadottir, S. Ptasińska, B. Puschnigg, P. Scheier, P. Limão-Vieira, and S. Denifl, J. Am. Soc. Mass Spectrom. (2013) DOI: 10.1007/s13361-013-0715-9.

[26]. R. Antunes, D. Almeida, G. Martins, N.J. Mason, G. Garcia, M.J.P. Maneira, Y. Nunes, and P. Limão-Vieira, Phys. Chem. Chem. Phys. **12**, 12513 (2010).

[27]. H.P. Fenzlaff and E. Illenberger, Int. J. Mass Spectrom. Ion Proc. **59**, 185 (1984).

[28]. D. Almeida, R. Antunes, G. Martins, G. Garcia, R.W. McCullough, S. Eden, and P. Limão-Vieira, Int. J. Mass Spectrom. **311**, 7 (2012).

[29]. L.P. Guler, Y. Yu, and H. Kentta, J. Phys. Chem. A **106**, 6754 (2002).

[30]. T. Sommerfeld, J. Phys. Chem. A **108**, 9150 (2004).

[31]. A.M. Scheer, K. Aflatooni, G. Gallup, and P. Burrow, Phys. Rev. Lett. **92**, 3 (2004).

[32]. P.D. Burrow, G.A. Gallup, A.M. Scheer, S. Denifl, S. Ptasinska, T. Märk, and P. Scheier, J. Chem. Phys. **124**, 124310 (2006).

[33]. T. Sommerfeld, Phys. Chem. Chem. Phys. **4**, 2511 (2002).

[34]. A.W. Kleyn, J. Los, and E.A. Gislason, Phys. Rep. **90**, 1 (1982).

[35]. F.A. Gianturco, F. Sebastianelli, R.R. Lucchese, I. Baccarelli, and N. Sanna, J. Chem. Phys. **128**, 174302 (2008).

[36]. S. Ptasińska, S. Denifl, V. Grill, T.D. Märk, P. Scheier, S. Gohlke, M.A. Huels, and E. Illenberger, Angew. Chem., Int. Ed. Engl. **44**, 1647 (2005).

[37]. S. Ptasińska, S. Denifl, V. Grill, T.D. Märk, E. Illenberger, and P. Scheier, Phys. Rev. Lett. **95,** 1 (2005).

[38]. S. Denifl, S. Ptasińska, G. Hanel, B. Gstir, M. Probst, P. Scheier, and T.D. Märk, J. Chem. Phys. **120**, 6557 (2004).

New fragmentation pathways in K-THF collisions as studied by electron transfer experiments: negative ion formation

D. Almeida [1], F. Ferreira da Silva [1], S. Eden [2], G. García [3,4] and P. Limão-Vieira [1,2,*]

[1] Laboratório de Colisões Atómicas e Moleculares, CEFITEC, Departamento de Física, Faculdade de Ciências e Tecnologia, Universidade Nova de Lisboa, 2829-516 Caparica, Portugal
[2] Department of Physical Sciences, The Open University, Walton Hall, Milton Keynes, MK7 6AA, UK
[3] Instituto de Física Fundamental, Consejo Superior de Investigaciones Científicas, Serrano 113-bis, 28006 Madrid, Spain
[4] Departamento de Física de los Materiales, UNED, Senda del Rey 9, 28040 Madrid, Spain

Accepted for publication in J. Phys. Chem. A (2013)

Abstract

Time-of-flight (TOF) negative ion mass spectra have been obtained in collisions of 30-100 eV neutral potassium atoms with tetrahydrofuran (C_4H_8O), an analogue for the sugar unit in DNA/RNA. The dominant fragment anions were assigned to O^- and $C_2H_3O^-$ and are indicative of ring breaking. Other less intense anionic fragments such as m/z = 13, 14, 25, and 41 have been also detected and assigned to CH^-, CH_2^-, C_2H^- and $C_3H_5^-$, respectively. In contrast with dissociative electron attachment (DEA), no evidence was observed for non-dissociated or dehydrogenated parent anions. Ring cleavage enhancement in O^- and $C_2H_3O^-$ formation in electron transfer compared with DEA experiments highlights the significant differences in the fragmentation pathways obtained through both techniques.

6.2.1. Introduction:

Further to its applications as a solvent in chemical industries, tetrahydrofuran (THF) has attracted considerable interest as a model for the sugar unit in DNA/RNA. Electron-induced processes in THF and other molecules analogising parts of key biological macromolecules have received particular attention due to evidence that sub-ionisation energy electrons can cause efficient damage in DNA subunits through dissociative electron attachment (DEA) [1,2]. As low energy electrons are the most abundant products of ionising radiation in the biological environment, detailed understanding electron attachment and transfer processes is essential to characterise and model radiation damage mechanisms at the nanoscale level [3]. This can have significant impact on radiotherapy developments, notably in the emerging field of nano-dosimetry [4].

Previous theoretical [5–7] and experimental [8–17] gas-phase studies have quite thoroughly described the molecular chemistry of gas-phase THF under low-energy (< 20 eV) electron interactions. We also note a set of studies in the condensed phase [2,18–21] and in cluster environments [22,23], as well total cross section measurements for electron scattering in the incident energy range 50 - 5000 eV

[24]. Dissociative electron attachment (DEA) experiments have shown that the main resonance structures are at ~ 6 - 11 eV [12,13,15,17], although some studies report fragmentation and electron interaction at ~1 eV [10,17]. The different fragmentation channels were also assigned to their respective resonances [10]. In order to clarify the nature of these resonances, as well as the fragmentation pathways, Ibanescu *et al* [13,14] performed electron interaction studies with alcohols and ethers using photoelectron spectroscopy and supported by theoretical calculations. It was shown that the DEA profiles consist of Feshbach resonances where the parent neutral is in a Rydberg (excited) state, highly correlated with the lowest ionisation energies obtained through photoelectron spectroscopy.

The electronic state spectroscopy of THF has been explored by photoelectron and VUV photoabsorption experiments together with quantum chemical calculations. These studies determined that C_s and C_2 conformers (see Fig. 6.3 [25])coexist (55% vs 45%) in the gas-phase at room temperature, although C_s was found to be energetically more stable [25]. However, in the case of electron scattering cross sections it was shown that there is significant difference between planar and non-planar conformers, but not much difference between the dominant C_s and C_2 conformers [6]. It is interesting to note that the C_s conformer possesses a more similar geometry to deoxyribose than the C_2 conformer. One would therefore expect the former to be a better approximation to the sugar unit within the DNA/RNA frame [6].

In this work, we report negative ion formation from electron transfer in collisions of neutral hyperthermal potassium atoms with THF in the 30-100 eV collision energy range. Similarities with previous electron transfer studies to D-Ribose [26] are discussed together with thresholds for the formation of particular fragments. Briefly, transfer of the potassium valence electron to the target moleculeoccurs in a collision when there is a non-adiabatic coupling of the ionic and covalent states of K + THF at a particular distance, R_c. The resulting negative ionis formed in a metastable anionic state, which is unstable towards dissociation through different fragmentation pathways. In most cases, like the previously studied pyrimidine bases [27], glycine [28] and D-Ribose [26], the internal excess energy cannot be efficiently dissipated and the molecular anion undergoes fragmentation, either through direct or statistical dissociation depending on the collision energy.

This work is part of an on-going effort in using atomic collisions to better understand low-energy electron damage to DNA/RNA-constituent molecules and their derivatives [29]. Some previous studies on pyrimidine bases have shown significant differences in the fragmentation patterns between dissociative electron attachment and electron transfer experiments [27,30], which have been attributed primarily to delayed autodetachment due to the presence of the potassium cation post-collisions. As was already mentioned, THF shares its cyclic esther ring geometry with deoxyribose, the sugar unit in DNA/RNA, which lends support to consider THF as a possible surrogate candidate for the DNA/RNA sugar unit. This fact is even more critical since it was recently shown that the dominant conformer of deoxyribose in the gas-phase is the pyranosic ring form, in contrast to the furanosic form in which the

latter exists in the DNA frame [31]. As such, the molecular geometry of THF in the gas-phase is more similar to the DNA sugar unit geometry than the deoxyribose molecule itself.

6.2.2. Experiment:

The experimental setup used to obtain the anionic time-of-flight (TOF) mass spectra has been described in detail previously [30]. Briefly, a neutral hyperthermal potassium beam crosses an effusive molecular beam and the anionic products are extracted into a TOF mass spectrometer. Potassium cations are produced in an ionic source and accelerated by an electric potential to the entrance of a charge exchange chamber containing potassium vapour. The incoming hyperthermal potassium cations resonantly charge exchange in collisions with the neutral thermal potassium atoms, resulting in a neutral hyperthermal potassium beam. A set of deflecting plates outside the oven ensures the removal of the remaining potassium cations in the beam. In the present measurements, the neutral potassium energy is varied between 30 and 100 eV in the lab frame. The calculated energy resolution of the potassium beam is approximately 0.5 eV.

Owing to THF's relatively high vapour pressure, the effusive molecular beam is obtained through a sample admission system at room temperature. By contrast, previous experiments on deoxyribose required heating to 383K or higher [32], which may affect isomer ratios in the effusive beam targets. The TOF mass spectrometer is of a Wiley-McClaren type operating at ~1μs width pulsed extraction voltage of ~242 $V.cm^{-1}$. The mass resolution is 125. Systematic background spectra enabled residual gas contributions to be subtracted from the sample spectra. Owing to the high extraction voltage in comparison to the expected kinetic energy of the fragments, the transmission of the TOF spectrometer should be mass independent.

6.2.3. Results and Discussion:

The negative ion TOF mass spectra obtained for 30, 70 and 100 eV potassium energies in the lab frame are presented in Fig. 6.4 and peak assignments in Table 6.2. Branching ratios (BR) for the major fragments as a function of the collision energy are presented in Fig. 6.5. For all collision energies, the most abundant fragments are O^- (16 m/z) and $C_2H_3O^-$ (43 m/z), followed closely by CH^- (13 m/z), CH_2^- (14 m/z), C_2^- (24 m/z) and C_2H^- (25 m/z). It is worth noting that no parent anion is formed, nor its dehydrogenated analogue. As far as DEA is concerned, there is still no agreement on the parent and dehydrogenated anions formation. Indeed, we notice some studies showing weak signals for these fragments with resonances at ~1 eV [10,17], whereas others report no signal and offering a rationale to their absence [12]. However, the DEA cross section for accessing this resonance is much lower than the cross section for the higher energy states. This is discussed below in the context of the resonance structure obtained in DEA experiments [12]. Herein we do not report the

presence of both these fragments but we cannot exclude de possibility of a very low signal that does rise above the noise level. It is worth noting that no dehydrogenated parent anion is obtained in similar studies with D-Ribose [26].

Total DEA cross section measurements show an absence of significant resonance structures with maxima below 6 eV [12,17], while DEA studies report peaks attributed to core-excited resonancesat ~ 6.7, ~ 7.6 and ~ 8.5 eV[12,14]. It is interesting to compare the present spectra at different collision energies in the context of these resonances. Fig. 6.4 provides information on the minimum energy responsible for the formation of particular fragment anions and on the collision dynamics. Potassium impact energies in the lab frame of 30, 70 and 100 eV correspond to available energies in the K-THF centre-of-mass frame of 13.0, 24.5 and 36.1 eV, respectively [33].The mass spectrum obtained at 20 eV (inset in 6.4.a)), for which the available energy is 7.2 eV, shows very weak signals for several of the fragment anions, assigned to H^-, O^-, OH^-, C_2^-, C_2H^- and $C_2H_3O^-$. These signals are barely discernible from the noise baseline, which means that only a small portion of theresonance profile is accessed in electron transfer experiments. This is consistent with the previous theoretical and experimental DEA studies [10,12].We now discuss the majority of the anions formed in such potassium-molecule collisions.

$C_3H_5^-$ & $C_2H_3O^-$

The peak at 43 m/z can be assigned to $C_2H_3O^-$, in agreement with recent DEA studies [10,12]. However, 41 m/z, which was initially attributed to C_2HO^-, has been shown to actually be $C_3H_5^-$. This assignment was due to recent measurements on deuterated THF [34].

Both peaks are present in the mass spectra shown in Fig. 6.4; the 43 m/z is the second highest for 30 and 70 eV collision energy and the fourth highest for 100 eV. In the 20 eV measurement, there is no evidence for $C_3H_5^-$ production and only a very weak signal for $C_2H_3O^-$ is noticeable. As the available energy for 20 eV potassium-THF collisions system is 7.2 eV, this indicates a slightly higher threshold for the channel through which $C_3H_5^-$ is formed, while the threshold for $C_2H_3O^-$ formation is slightly lower. This is consistent with DEA experiments showing that the thresholds for $C_3H_5^-$ and $C_2H_3O^-$ formation are ~7.0 and ~6.0 eV, respectively [12]. One can therefore conclude that the accessible resonances in the present experiment are the same as in DEA. As such, since these fragments are formed through different resonances, it is unlikely that they compete with each other. However, the $C_3H_5^-/C_2H_3O^-$ ratio in DEA is strongly different fromthe present measurements, i.e., while in the former accounts for ~15/1 [12], for the latter the ratio is, at best, 0.4/1 for 100 eV collision energy. This discrepancy can be explained by the presence of the potassium cation, which may effectively preclude autodetachment in the resonances yielding $C_2H_3O^-$ formation. This mechanism has been thoroughly discussed in the context of other molecular targets [27,30]. Another rationale lies on considering the nature of the resonances involved. Indeed, a remarkable set of studies by Allan's

group [13,14] concluded that the Feshbach resonances that occur in a wide variety of alcohol and amine derivative molecules can be associated with the corresponding Rydberg states of the neutral. As such, owing to the low perturbation of the positive ion core by the Rydberg electron, it is argued that the energy difference between the cationic state (i.e., the grand-parent ion) and the anionic state depends dominantly on the type of the Rydberg state, i.e. ~4.5 eV for ns and ~1.8 eV for np states [14]. An extension of this rationale to THF, a cyclic ether, is therefore attempted here. As the general shape of the first ionisation band [6,25] and the DEA band with a maximum at 7.65 eV [12] are similar in shape, we can tentatively attribute this resonance (responsible for the formation of anions with m/z = 41) to an initial occupation of an np Rydberg state associated with the first ionisation energy. At this point, it is interesting to note that recent high-resolution photoelectron and photoabsorption spectroscopic studies have shown that the first ionisation band is characterised by a set of vibrational progressionsassigned to the cation in its electronic ground state [25].

The resonance with a maximum at 6.7 eV [12] can be tentatively attributed to an initial excitation into a ns Rydberg state, stemming from the second ionisation limit. It is also noteworthy that according to this study [25], Rydberg series converging to the second ionisation limit are exclusive of THF C_2 isomer (note the expected presence of C_2 and C_s conformers in the gas-phase [25]). Hence it is plausible to state that the perturbation of the potassium cation on the ns and np Rydberg states may be responsible for the contrasting $C_3H_5^-/C_2H_3O^-$ ratios in DEA and electron transfer experiments.

Another issue pertains to the fragmentation pathways undertaken in the formation of each of these fragments. The most recent study of DEA to THF proposes that the first step following electron capture is ring opening via C-O bond breakage [12], with the electron mostly localized in the vicinity of the oxygen atom. The high internal energy of the resulting metastable intermediate anion will lead to fragmentation or autodetachment [12]. Fragmentation can occur in different parts of the alkyl chain. Cleavage of the C_2-C_3 bond, together with additional hydrogen abstractions, will result in fragment anions discussed in this section. Given that the accessed resonances in DEA and in electron transfer appear to be the same, the above rationale should also apply to the case of electron transfer.

Finally, an analysis of the branching ratios (Fig. 6.5) shows a major change in the relative yields of both the fragments, $C_3H_5^-$ and $C_2H_3O^-$, as a function of collision energy. The ratio of $C_3H_5^-$ production / total anion production decreases from 30 to 70 eV collision energy but slightly increases from 70 to 100 eV. Conversely, $C_2H_3O^-$ branching ratio remains constant from 30 to 70 eV, but falls significantly from 70 to 100 eV.

O^-

The fragment at 16 m/z (O^-) is the most abundant anion. As with the fragments discussed above, an analysis of the 20 eV collision energy spectrum (Fig. 6.3) shows a very weak O^- signal,

suggesting that the threshold for its formation is only slightly below ~7.2 eV. This most likely means that O^- is obtained through accessing the same states as in DEA, but following a different dissociation pathway. Indeed, it is surprising that DEA studies do not report O^-formation at this energy and as such, it is not possible to ascertain which of the anionic states are playing a role in yielding this fragment. However, it is interesting to look once again at the proposed intermediate anion state in Fig. 3 of ref. [12]. As mentioned, the initial step in fragmentation of THF upon electron capture consists on the cleavage of the C-O bond, thereby resulting in a linear esther molecule, with the extra electron residing near the oxygen [12,13]. Owing to the localization of the extra electron, it is quite plausible to suggest thatthis intermediate state may also have an anti-bonding character along the C-O bond, eventually leading bond breakage and O^- formation.

An interesting issue is the absence of O^- in DEA experiments. Given that it is reasonable to assume that the initially accessed states in DEA and in electron transfer are the same, the reason for this fact will most likely be due to autodetachment competingin one of the intermediate anions that give rise to O^-, or alternatively, a competition between O^- formation and formation of some other fragment (either neutral or anionic). In the former case, the presence of the potassium cation can be seen as efficiently suppressing autodetachment long enough for fragmentation to successfully compete with re-ejection of the extra electron. In the latter case, the potassium cation could be seen as a perturbing third-body that changes the probability for the extra electron to undergo intramolecular transfer, thereby allowing different fragmentation channels.

Finally, an interesting remark pertains to the comparison of THF with deoxyribose in the context of electron transfer collisions. Both these molecules undergo fragmentation resulting in the formation of O^-. However, in the case of deoxyribose, it was not possible to unambiguously determine whether formation of O^- stemmed from the oxygen of the ether ring, or from one of the hydroxyl groups bonded to the ring. The fact that O^- formation is possible in THF supports attributing O^- formation in deoxyribose to the breaking of the ring. It is however important to note that there are some differences between the gas-phase ring structures of THF and deoxyribose (see ref. [31]). According to the branching ratios in Fig. 6.5, the relative yield of O^- increases significantly from 30 to 70 eV, further followed by a smaller increase towards 100 eV. Interestingly, this branching ratio change is shared with CH^- and CH_2^- formation.

Other fragments

The remaining anionic fragments include m/z 13, 14, 24 and 25, which are assigned to CH^-, CH_2^-, C_2^- and C_2H^-, respectively (see Table 6.2). Similarly to the previous discussion, only a residual presence of these fragments appears in the 20 eV spectrum. This then implies that the threshold values for the formation of these anions is very close to 7.2 eV available energy. As such, it is reasonable to assume that the formation of these fragments will also occur through access of the same resonant

states as in DEA experiments. However, despite their significant presence for all collision energies (> 20 eV) these fragments are, to the best of the authors' knowledge, unreported in previous DEA studies. It therefore stands to reason that, much like in the case of O^-, the presence of the potassium cation post-collision will influence the dissociation mechanisms, namely by promoting competition between otherwise dominant states. In other words, while in DEA the dominant fragmentation channel appears to be $C_2H_3O^-$, in the present studies the potassium cation appears to allow for other dissociation channels to successfully compete with this channel. It therefore bears mentioning that, not only is the potassium cation responsible for mitigating autodetachment, as was already proposed in other molecular targets [27,30], it also apparently affects the way the fragmentation channels progress. Indeed, it is tempting to rationalize this mechanism as an initial cleavage of the C-O bond, followed by a cleavage on the alkyl carbons of the no-longer furanosic intermediate esther anion. These fragmentation possibilities can be perceived as complementing channels to $C_3H_5^-$ and $C_2H_3O^-$ formation, insofar as the cleaved C-C bonds are concerned since formation of all these fragments requires only cleavage of different C-C bonds. The difference will therefore mainly lie on where the extra electron remains, i.e. either at the end of the alky group or at the esther.

Another discrepancy when comparing the electron transfer technique with DEA is the presence of OH^-. The formation of this anionrequires some rearrangement during the fragmentation process. However, such rearrangement seems quite plausible since there are hydrogen atoms bonded to the adjacent carbon and as such, a tautomeric transition can occur and eventually evolve into an abstraction of an hydroxyl anion from the chain esther. Finally, we also notice H^- formation, albeit with a very low anionic yield at lower collision energies. This is in contrast with the significant yield obtained in one of the DEA studies[12]. The relative yield of this fragment is quite small in electron transfer measurements, which can be explained through competition with other fragments such as $C_2H_3O^-$, which can be seen to possess resonances at similar energies [12]. However, we note that C_2H_3O has a considerable higher electron affinity (1.82 eV) than H (0.75 eV) [36].

6.1.4. Conclusions:

The present work provides novel data on low-energy neutral atom collisions to THF, a possible surrogate for the DNA/RNA sugar unit. This data strongly highlights the major differences in the fragmentation dynamics between capture of a free electron (DEA) and electron donation (as in electron transfer experiments). The difference between these two mechanisms is attributed to the presence of the potassium cation *post collision*, which can affect the decaying process of the TNI. Within this context, it is clear that the study of different electron delivery mechanisms can greatly increase our understanding of electron-driven processes in DNA/RNA damage. Indeed, it is worth noting that the DEA and electron transfer fragmentation patterns for THF are the most dissimilar for all the already-studied molecular targets with these types of collisions. More specifically, some DEA

studies report the formation of the parent anion and dehydrogenated version [10], which are absent in the present study. This point highlights a tendency to observe an enhancement of ring breaking in electron transfer, as opposed to DEA, where the dominant fragmentation normally does not proceed through loss of ring integrity.

Indeed, the near-absence formation of the several fragments in the 20 eV spectrum supports the claim that the formation thresholds are similar to DEA. Indeed, the presence of the main fragmentation products at 20 eV collision energy (7.2 eV available energy) is, at best, only slightly above the noise level since the available energy is only marginally higher than the threshold values of the resonances and as such, a significant amount of the total width of the resonance is not accessed. This lends support to assuming that the initially accessed states in DEA and electron transfer are the same. Indeed, a recent DEA study assigns such profiles to Feshbach Resonances in which the neutral parent state is a Rydberg excitation [12,14]. However, it is clear that, while the initial states are the same, these (states) can decay into different fragments, presumably due to the presence of the potassium cation. Indeed, it is proposed that the fragmentation of this molecule is sequential whereupon a chain esther anion is initially formed by C-O bond cleavage. This is followed by a subsequent break along the different parts of the alkyl chain. Depending on the site of bond cleavage, different fragments are to be formed . For example, a bond break of the remaining C-O bond will most likely lead to O^- formation, whereas cleavages of the various C-C bonds will entail the formation of all other fragments (with the exception of $OH^-$and H^-). The selective nature of these cleavages remains somewhat elusive but the present data clearly points towards the rationale presented above. We then tentatively suggest that fragmentation will most likely consist of an intramolecular electron transfer from the initial intermediate state into different highly anti-bonding valence states along the C-C bonds. In other words, bond cleavage in the C1-C2 bond will most likely result in formation of CH^-, CH_2^- and $C_3H_5^-$, whereas in the C2-C3 bond leads to formation of C_2^- and C_2H^- fragments. As for $C_2H_3O^-$ and O^-, a similar mechanism also seems plausible but with the electron remaining on the esther side of the chain.

It is quite surprising that the fragmentation pattern in electron transfer is significantly richer than the reported in DEA experiments. Furthermore, the strongest of the fragment anions is O^-, which was until now un-reported in electron capture to THF.

Finally, from a more general point of view, these results highlight the frailty of the esther ring in regard to low-energy electron interactions. However, the sugar unit in DNA/RNA does not seem to behave as so in both DEA and in potassium-molecule experiments, where the main fragmentation channels consist of OH abstraction and not ring breaking. Therefore, the hydroxyl groups, apart from their other functional roles, can be also argued to provide structural protection to the sugar unit ring. This can be important since it is known that significant DNA damage by low energy electrons stems from bond breaks in the sugar unit [35]. Notwithstanding, this data once shows the significant

difference underlying electron donating mechanisms against free electron attachment, which was less evident from previous studies.

Owing to the similar ring structure, THF was initially proposed to be a good substitute for deoxyribose as the DNA/RNA sugar unit. However, both experimental [10] and theoretical [6] studies have concluded that THF is not a good surrogate model for the DNA/RNA sugar unit owing to, unlike deoxyribose, not being a good electron scavenger. In the context of the present study, it stands to note that accessing low energy resonances (<3 eV) in deoxyribose and the absence of similar resonances in THF point towards the same inability of THF to be a proper sugar unit surrogate.

Acknowledgements

D.A. and F.F.S. acknowledge the Portuguese Foundation for Science and Technology (FCT-MEC) for a post-graduate SFRH/BD/61645/2009 and post-doctoral grants SFRH/BPD/68979/2010, respectively. We also acknowledge partial funding from the Portuguese research Grants PEst-OE/FIS/UI0068/2011 and PTDC/FIS-ATO/1832/2012 through FCT-MEC, and from the Spanish Ministerio de Economía y Competitividad (Project No. FIS 2009-10245). S.E. acknowledges the financial support of the British EPSRC (CAF fellowship). P.L.V. acknowledges his visiting Professor position at The Open University, UK. Some of this work forms part of the EU/ESF COST Actions Nano-IBCT-MP1002.

References

[1]. B. Boudaiffa, P. Cloutier, D. Hunting, M.A. Huels, L. Sanche, Science **287**, 1658(2000).

[2]. D. Antic, L. Parenteau, M. Lepage, L. Sanche, J. Phys. Chem. B **103**, 6611(1999).

[3]. I. Baccarelli, I. Bald, F.A. Gianturco, E. Illenberger, J. Kopyra, Phys. Rep. **508**, 1(2011).

[4]. A.G. Sanz, M.C. Fuss, A. Munoz, F. Blanco, P. Limão-Vieira, M.J. Brunger, S.J. Buckman, G. Garcia, Int. J. Rad. Bio. **88**, 71(2012).

[5]. C. Winstead, V. McKoy, J. Chem. Phys. **125,** 244302(2006).

[6]. C. Winstead, V. McKoy, J. Chem. Phys. **125,** 074302(2006).

[7]. S. Tonzani, C.H. Greene, J. Chem. Phys. **125,** 094504(2006).

[8]. M. Zubek, M. Dampc, I. Linert, T. Neumann, J. Chem. Phys. **135,** 134317(2011).

[9]. A. Zecca, C. Perazzolli, M.J. Brunger, J. Phys. B: At. Mol. Opt. Phys. **38**, 2079(2005).

[10]. P. Sulzer, S. Ptasinska, F. Zappa, B. Mielewska, A.R. Milosavljevic, P. Scheier, T.D. Märk, I. Bald, S. Gohlke, M.A. Huels, E. Illenberger, J. Chem. Phys. **125**, 44304(2006).

[11]. P. Możejko, E. Ptasińska-Denga, A. Domaracka, C. Szmytkowski, Phys. Rev. A **74**, 012708(2006).

[12]. B.C. Ibănescu, O. May, M. Allan, Phys. Chem. Chem. Phys. **10,** 1507(2008).

[13]. B.C. Ibănescu, M. Allan, Phys. Chem. Chem. Phys. **11**, 7640(2009).

[14]. B.C. Ibănescu, M. Allan, Phys. Chem. Chem. Phys. **10**, 5232(2008).

[15]. M. Dampc, E. Szymańska, B. Mielewska, M. Zubek, J. Phys. B: At. Mol. Opt. Phys. **44**, 055206(2011).

[16]. C.J. Colyer, V. Vizcaino, J.P. Sullivan, M.J. Brunger, S.J. Buckman, New J. Phys. **9**, 41(2007).

[17]. K. Aflatooni, A.M. Scheer, P.D. Burrow, J. Chem. Phys. **125**, 054301(2006).

[18]. M. Lepage, S. Letarte, M. Michaud, F. Motte-Tollet, M.-J. Hubin-Franskin, D. Roy, L. Sanche, J. Chem. Phys. **109**, 5980(1998).

[19]. C. Jäggle, P. Swiderek, S.-P. Breton, M. Michaud, L. Sanche, J. Phys. Chem. B **110**, 12512(2006).

[20]. S.-P. Breton, M. Michaud, C. Jäggle, P. Swiderek, L. Sanche, J. Chem. Phys. **121**, 11240(2004).

[21]. D. Antic, L. Parenteau, L. Sanche, J. Phys. Chem. B **104**, 4711(2000).

[22]. R.M. Young, M.A. Yandell, M. Niemeyer, D.M. Neumark, J. Chem. Phys. **133,** 154312(2010).

[23]. Y.S. Park, H. Cho, L. Parenteau, A.D. Bass, L. Sanche, J. Chem. Phys. **125**, 074714(2006).

[24]. M. Fuss, a. Muñoz, J.C. Oller, F. Blanco, D. Almeida, P. Limão-Vieira, T.P.D. Do, M.J. Brunger, G. García, Phys. Rev. A **80**, 052709(2009).

[25]. A. Giuliani, P. Limão-Vieira, D. Duflot, A.R. Milosavljevic, B.P. Marinkovic, S. V. Hoffmann, N. Mason, J. Delwiche, M.-J. Hubin-Franskin, Eur. Phys. J. D **51**, 97(2008).

[26]. D. Almeida, F. Ferreira da Silva, G. Garcia, P. Limao-Vieira, J. Chem. Phys., **139**, 114304 (2013)..

[27]. D. Almeida, R. Antunes, G. Martins, S. Eden, F. Ferreira da Silva, Y. Nunes, G. Garcia, P. Limão-Vieira, Phys. Chem. Chem. Phys. **13**, 15657(2011).

[28]. F. Ferreira da Silva, M. Lança, D. Almeida, G. García, P. Limão-Vieira, Eur. Phys. J. D **66**, 78(2012).

[29]. D. Almeida, F. Ferreira da Silva, G. García, P. Limão-Vieira, Phys. Rev. Lett. **110**, 023201 (2013).

[30]. R. Antunes, D. Almeida, G. Martins, N.J. Mason, G. Garcia, M.J.P. Maneira, Y. Nunes, P. Limão-Vieira, Phys. Chem. Chem. Phys. **12**, 12513(2010).

[31]. L.P. Guler, Y. Yu, H. Kentta, J. Phys. Chem. A **106**, 6754(2002).

[32]. S. Ptasińska, S. Denifl, P. Scheier, T.D. Märk, J. Chem. Phys. **120,** 8505(2004).

[33]. A.W. Kleyn, A.M.C. Moutinho, J. Phys. B: At. Mol. Opt. Phys. **4075,** R1(2001).

[34]. R. Janecková, O. May, A.R. Milosavljevic, J. Fedor, Private Communication (2013).

[35]. K. Miaskiewicz, R. Osman, J. Am. Chem. Soc. **116**, 232(1994).

[36]. NIST Chemistry WebBook, http://www.nist.gov

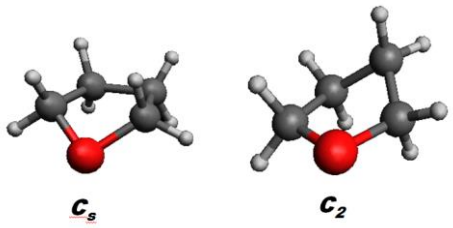

Figure 6. 3 Structure of gas-phase dominant C_s and C_2 conformers of THF, according to proposed geometries as in refs. [6,25].

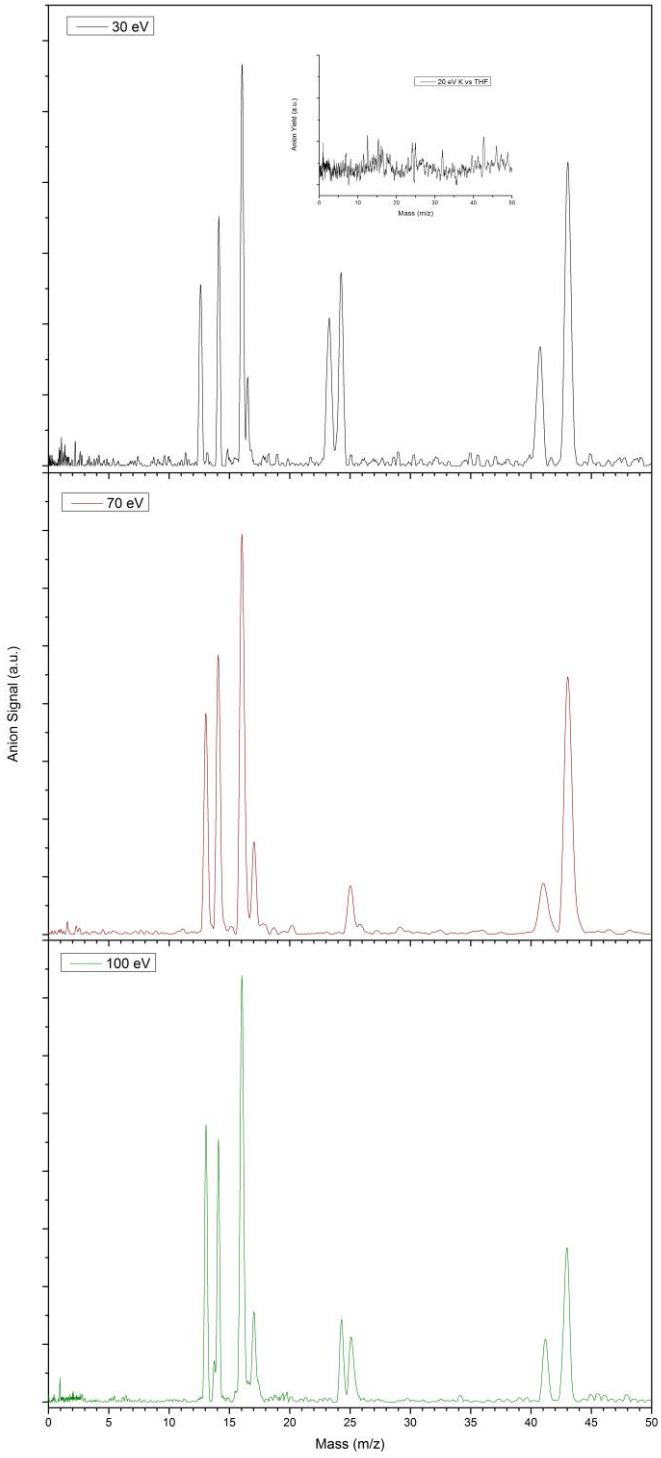

Figure 6. 4 TOF negative ions mass spectra from collisions of potassium atoms with THF at: a) 30 eV; b) 70 eV and c) 100 eV. An inset of a spectra at 20 eV is presented in a) in order to show the absence of the fragmentation channels at the corresponding available energy.

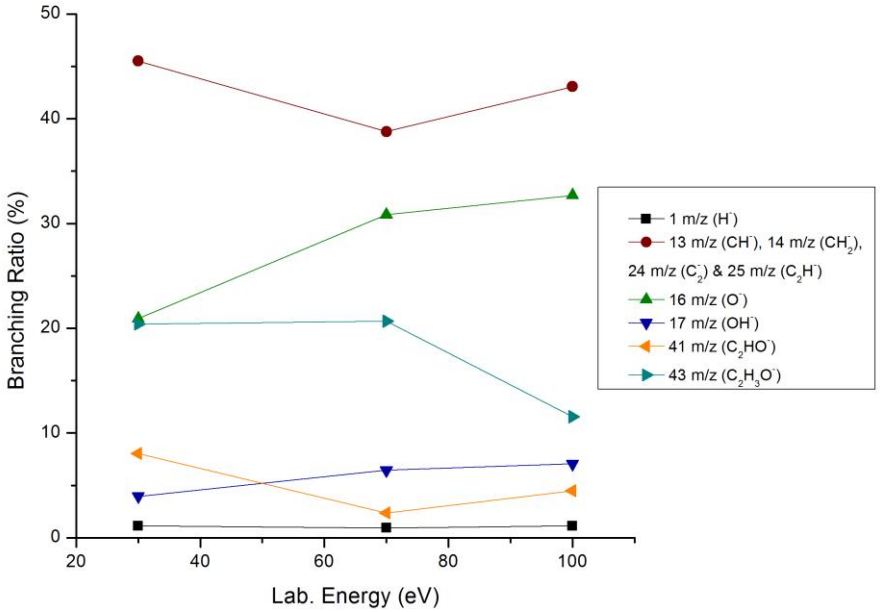

Figure 6. 5 Branching ratios (fragment anion yield / total anion yield) as a function of the collision energy in the lab frame.

Mass peak (m/z)	Proposed assignment	This work	DEA studies
1	H^-	✓	✓
13	CH^-	✓	×
14	CH_2^-	✓	✓†
16	O^-	✓	✓†‡
17	OH^-	✓	✓†
24	C_2^-	✓*	×
25	C_2H^-	✓	×
41	$C_3H_5^-$	✓	✓†
43	$C_2H_3O^-$	✓	✓

Table 6. 2 Assignment of the anions produced by potassium impact on THF (C_4H_8O, m/z = 72). Comparisons are made with the available DEA studies. * Only observed at 30 and 100 eV; no signal was observed above the background level at 70 eV; † From ref. [33]; ‡ A possible water contribution from the background (ref. [33]).

7. Conclusions

7.1. Concluding remarks:

The main emphasis of this thesis was to study negative ion formation triggered by electron transfer in collisions of atoms, most importantly neutral potassium atoms, with molecules of biological relevance. The initial stage of the work revolved around measurements of methylated derivatives of pyrimidine bases, in an attempt to understand the underlying molecular mechanisms during and after the collision. Most notably, these studies showed for the first time site and bond selectivity yielding H^- formation in atom-molecule collisions; a novel contribution to the field of low energy atomic collisions. This work was achieved by measuring negative ion mass spectra that result from collisions of site specific methylated and deuterated derivatives of pyrimidine with potassium atoms at different projectile collision energies. These energies were chosen according to the information provided on the resonances by previous DEA experiments [8,9]. Indeed, it was shown, that in electron transfer mechanisms, abstraction of H^- from a given site of the pyrimidine base is exclusively associated with the access to a specific initial TNI resonant state. On top of these unprecedented results, we have also performed a series of extensive studies for other fragment anions, namely CNO^- (see e.g. [27]). A second feature that was brought up by these sets of studies pertains to the de-methylation reaction pathway that, in electron transfer, results is one of the main species. At the time, DEA measurements presented no such anionic channel, however, later studies showed its presence and with the help of theoretical support, reaction pathways for both electron transfer and DEA channels were tentatively proposed [18]. Both of these studies highlight the present need to further investigate at a more fundamental level the physico-chemical processes that occur during these collisions.

At the same time, a close collaboration with Queen's University Belfast allowed to experimentally investigate positive and negative ion fragmentation patterns in collisions of H^-, O^- and OH^- with several simple organic molecules. These have included nitromethane, water, methanol and ethanol. In this study, a particular emphasis was given on nitromethane, since it was a molecule that had already been measured in the context of potassium-molecule collisions, thereby allowing some comparisons between neutral and anionic projectile systems to be established. Indeed, a comparison between the negative ion fragmentation patterns in potassium-nitromethane collisions and anion-nitromethane collisions revealed the importance of the coulombic interaction within the collision complex.

Finally, , studies of two possible sugar surrogates: THF and D-Ribose were performed at different projectile kinetic energies. In the case of D-Ribose, two main issues are to be noted: 1) the dominant conformer of this molecule in the gas-phase is in the form of a pyranose ring, rather than in the DNA/RNA furanose ring form. This geometric difference can greatly influence the fragmentation patterns upon electron transfer in atom-molecule collisions; 2) for all studied collision energies, OH^-

was observed to be the dominant fragment anion. This is in sharp contrast with previously observed measurements of DEA. However, a rationale on the formation of a temporary coulombic complex between the potassium cation and the temporary molecular anion was developed to explain this discrepancy, by making use of some theoretically-supported DEA studies[28].

Another molecular system investigated in order to clarify some of the fragmentation pathways of D-Ribose wasTHF. Tetrahydrofuran, unlike D-Ribose, is a liquid and retains his furanosic form when brought to the gas-phase. As such, the fundamental structural difference between this molecule and the sugar unit is the presence of the hydroxyl groups in the ring carbons, whereas THF only has hydrogens attached to the ring carbons. The main focus of this particular study led to the conclusion that the accessed initial resonant states in electron transfer and in DEA are most likely the same, however, the reaction pathways will decay differently. In particular, it is suggested that the initial common stage amongst all the accessed resonant states is the breaking of the C-O bond, after which each state will decay into different fragments. Significant differences between DEA and electron transfer fragmentation yields are attributed to the perturbing presence of the potassium cation *post collision*.

From a general point of view, two general goals were achieved during the work presented in this thesis. On one hand, a significant amount of attention was given in understanding the basic fundamental mechanisms that govern electron transfer in atom-molecule collisions. Site and bond selectivity in bond breaking was shown in these systems and the role of the potassium cation in the collision complex was further explored, both through studying chemical derivatives of some previously studied molecules, and also through the study of slightly different collision systems, i.e. anion-molecule collisions.

Studies on thymine, uracil and glycine have already been reported and, in order to continue in this line of research, sugar unit surrogates D-ribose and THF were studied. The data obtained, has the added value of, together with similar data on pyrimidine bases, being compared to future data on increasingly complex molecules, e.g. uridine or thymidine. This bottom-up approach can lend significant support to better understanding of the basic mechanisms involved in electron transfer as a possible physico-chemical process of indirect radiation-induced DNA damage.

7.2. Future work:

As a result of the work performed throughout this thesis, several suggestions for future investigations can be proposed where improvements to the current experimental system can greatly increase the value of the obtained data, as well as studies with other molecular targets can greatly increase the scientific contribution that this technique can provide not only to the field of radiation-induced DNA damage, but also to other areas such as astrochemistry.

Several improvements can be proposed as far as the experimental setup is concerned. These mostly require implementation of new components, in order to allow for additional information to be obtained. While other spectrometers like a quadrupole can be implemented, TOF mass spectrometers can eventually be tailored to study metastable decay, which seems to play an important role in the fragmentation patterns of these molecules. Another experimental improvement pertains to the optimization of the potassium beam, with the intent of allowing for lower kinetic energies to be used without much loss of beam current. This can be relevant to allow for obtaining formation thresholds of the resulting fragments, with particular attention to the resonance profiles < 6 eV. These improvements do not entail a significant change in the system.

Another very important information from these studies is the knowledge of the kinetic energy loss of the potassium beam after electron transfer. This would directly give information regarding the accessed resonant states of the molecular target. In order to obtain this information, it is possible to implement a retarding potential energy analyser after the collision region. However, it would also be necessary to optimize the beam current in order to have a reasonably enough beam signal (~1 μA). Finally, absolute cross section values for these processes can be extremely important, not only from a more fundamental point of view, but also since they can be used as input data in recently developed radiotherapy simulation models that, by doing so, are able to take into account these nanoscopic processes.

From a scientific perspective, two main points can be made. The first pertains to the current lack of theoretical support to the reported studies. As far as we are aware, no studies on electron transfer in atom-molecule collisions are being performed in this range of collision energies. Apparently, the complexity of the required dynamical calculations is the main factor for the absence of such studies. Regardless, calculations that account for presence of a third body during the collision would be critical as a way to not only confirm the proposed rationales in the already published studies, but also as a possible way to more precisely understand the dynamics of the collision itself and help point the experimental studies in new directions allowing also to compare these with electron scattering calculations.

The second point pertains to the choice of molecular targets. At this point, two paths can be taken. One is to continue performing studies in biologically relevant molecules, in particular nucleotides. However, it is known that these bigger molecules tend to be thermally decomposed when brought to the gas-phase upon heating the sample's powder, some other method of bringing them to the gas-phase is required, e.g, Laser-Induced Acoustic Desorption (LIAD). In spite of this, many biologically relevant molecules still remain unmeasured. Some examples are the other nucleobases adenine and cytosine, other sugar unit surrogates, namely substituted versions of THF, e.g. substitution with phosphate groups in order to simulate the presence of the phosphate in the DNA/RNA framework. On another approach, measurement of aminoacids is also quite important and is currently being performed. The second path pertains to choosing smaller molecular targets. This choice brings up

several advantages, one of the main ones being that smaller molecules imply that the available energy will be smaller and hence easier to perform measurements at lower collision energies.

Finally, it is worth noting that water has still not been completely measured. Some measurements were already performed but much more detail is required to better understand this ubiquitous molecule when subjected to electron transfer. Other notable examples of yet-unmeasured molecules are simple alcohols and other small organic molecules, which have been shown to be extremely important in other fields of research, such as the aforementioned case of astrochemistry.

References

[1] H. Varmus, Science **312**, 1162(2006).

[2] C. von Sonntag, The Chemical Basis for Radiation Biology, Taylor and Francis, London, 1987.

[3] K. Miaskiewicz, R. Osman, J. Am. Chem. Soc. **116**, 232(1994).

[4] F. Martin, P. Burrow, Z. Cai, P. Cloutier, D. Hunting, L. Sanche, Phys. Rev. Lett. **93**, 6 (2004).

[5] B. Boudaïffa, P. Cloutier, D. Hunting, M.A. Huels, L. Sanche, Science **287**, 1999 (2000).

[6] G. Hanel, B. Gstir, S. Denifl, P. Scheier, M. Probst, B. Farizon, M. Farizon, E. Illenberger, T. Märk, Phys. Rev. Lett. **90**, 188104(2003).

[7] V. Cobut, Y. Frongillo, J.P. Patau, T. Goulet, Radiat. Phys. Chem. **3**, 229(1998).

[8] S. Ptasińska, S. Denifl, V. Grill, T.D. Märk, E. Illenberger, P. Scheier, Phys. Rev. Lett. **95**, 1(2005).

[9] S. Ptasińska, S. Denifl, V. Grill, T.D. Märk, P. Scheier, S. Gohlke, M.A. Huels, E. Illenberger, Angew. Chem., Int. Ed. Engl. **44**, 1647(2005).

[10] S. Ptasinska, S. Denifl, P. Scheier, E. Illenberger, T.D. Märk, Angew. Chem., Int. Ed. Engl. **44**, 6941(2005).

[11] L. Sanche, Nature **461**, 358(2009).

[12] R. N. Compton, H. S. Carman Jr, C. Desfrancois, H. Abdoul-Carime, J. P. Schermann, J. H. Hendricks, S. A. Lyapustina, K. H. Bowen J. Chem. Phys. **105**, 3472 (1996).

[13] I.C. Walker, M.A.D. Fluendy, Int. J. Mass Spectrom. **205**, 171(2001).

[14] A. Kühn, H. Fenzlaff, E. Illenberger, J. Chem. Phys. **88**, 7453(1988).

[15] R. Antunes, D. Almeida, G. Martins, N.J. Mason, G. Garcia, M.J.P. Maneira, Y. Nunes, P. Limão-Vieira, Phys. Chem. Chem. Phys. **12**, 12513(2010).

[16] D. Almeida, R. Antunes, G. Martins, S. Eden, F. Ferreira da Silva, Y. Nunes, G. Garcia, P. Limão-Vieira, Phys. Chem. Chem. Phys. **13**, 15657(2011).

[17] D. Almeida, F. Ferreira da Silva, G. García, P. Limão-Vieira, Phys. Rev. Lett. **110**, 023201(2013).

[18] D. Almeida, D. Kinzel, B. Puschnigg, D. Gschliesser, P. Limao-Vieira, L. Gonzalez, P. Scheier, S. Denifl, Phys. Chem. Chem. Phys. **15**, 11431(2013).

[19] D. Almeida, R. Antunes, G. Martins, G. Garcia, R.W. McCullough, S. Eden, P. Limão-Vieira, Int. J. Mass Spectrom. **311**, 7(2012).

[20] M.J.P. Maneira, Formação de Pares de Iões Em Colisões Entre Átomos e Moléculas Tetraédricas, New University of Lisbon, 1984.

[21] A.W. Kleyn, J. Los, E.A. Gislason, Phys. Rep. **90**, (1982).

[22] A.W. Kleyn, Vibronic Excitation in Atom Molecule Collisions, University of Amsterdam, 1980.

[23] A.W. Kleyn, A.M.C. Moutinho, J. Phys. B: At. Mol. Opt. Phys. **4075**, R1(2001).

[24] R. Antunes, The Role of Halouracils in Radiotherapy Studied by Electron Transfer in Atom-Molecule Collision Experiments The Role of Halouracils in Radiotherapy Studied by Electron Transfer in Atom-Molecule Collision Experiments, New University of Lisbon, 2011.

[25] J.A. Aten, J. Los, J. Phys. E: Sc. Inst. **8**, 408(1975).

[26] W.C. Wiley, I.H. McLaren, Rev. Sci. Inst. **26**, 1150(1955).

[27] F. Ferreira da Silva, C. Matias, D. Almeida, G. Garcia, O. Ingolfsson, H. D. Flosadottir, B. Omarsson, S. Patsinska, B. Puschnigg, P. Scheier, P. Limão-Vieira, S. Denifl, J. Am. Soc. Mass Spectrom., (2013).

[28] I. Baccareli, F. Gianturco, A. Grandi, N. Sanna, R. R. Lucchese, I. Bald, J. Kopyra, E. Illenberger, J. Am. Chem. Soc., **129**,6269(2007).